HYPERSPECTRAL REMOTE SENSING AS A MONITORING TOOL FOR GEOLOGIC CARBON SEQUESTRATION

by

Gabriel John Bellante

A thesis submitted in partial fulfillment
of the requirements for the degree

of

Master of Science

in

Land Resources and Environmental Sciences

MONTANA STATE UNIVERSITY

Bozeman, Montana

August 2011

APPROVAL

of a thesis submitted by

Gabriel John Bellante

This thesis has been read by each member of the thesis committee and has been found to be satisfactory regarding content, English usage, format, citation, bibliographic style, and consistency, and is ready for submission to The Graduate School.

Dr. Scott Powell and Dr. Rick Lawrence

Approved for the Department of Land Resources and Environmental Sciences

Dr. Tracy Sterling

Approved for The Graduate School

Dr. Carl A. Fox

STATEMENT OF PERMISSION TO USE

In presenting this thesis in partial fulfillment of the requirements for a master's degree at Montana State University, I agree that the Library shall make it available to borrowers under rules of the Library.

If I have indicated my intention to copyright this thesis by including a copyright notice page, copying is allowable only for scholarly purposes, consistent with "fair use" as prescribed in the U.S. Copyright Law. Requests for permission for extended quotation from or reproduction of this thesis in whole or in parts may be granted only by the copyright holder.

Gabriel John Bellante

August, 2011

DEDICATION

For my family, who has provided me with invaluable support during my graduate education. Without their encouragement my achievement would have seemed unattainable.

ACKNOWLEDGEMENTS

I would like to thank Scott Powell and Rick Lawrence for their mentorship and guidance. Thanks to my other committee members, Kevin Repasky and Tracy Dougher, for their assistance throughout my graduate education. Thanks to Rand Swanson and Casey Smith of Resonon Inc., without their technical support on the operation of the Pika II sensor and their assistance in geometric and radiometric image corrections this would not have been possible. A big thanks to Chris Boyer at Kestrel Aerial Services for providing the airplane platform for imaging over the Zero Emissions Research and Technology (ZERT) site, and for his willingness to push the limits of my motion sickness for good quality data. Diana Cooksey deserves thanks for her help with GPS surveying equipment. Thanks to Jamie Barr for her computer programming skills and assistance with the CO_2 probes. I would like to thank David Baumbauer for his assistance in killing pests that threatened my greenhouse study plants. A shout out to Kevin Shields for his willingness to help with a greenhouse study that never came easy. Laura Dobeck deserves recognition for her assistance at ZERT. Thanks to Mark Greenwood for his statistical advice. I would like to acknowledge my lab mates Jennifer Watts and Steven Jay for their support and entertainment. Thanks to Anne Loi who provided instant computer technical support whenever I needed it—which was too much—and for her great stories. Thanks to all my friends and family for their continued support over the past two years. Finally, thanks to the US Department of Energy (DOE) for their financial support of this project.

TABLE OF CONTENTS

TABLE OF CONTENTS - CONTINUED

LIST OF TABLES

LIST OF FIGURES

LIST OF FIGURES - CONTINUED

LIST OF EQUATIONS

ABSTRACT

The contemporary global climate crisis demands mitigation technologies to curb atmospheric greenhouse gas emissions, principally carbon dioxide (CO_2). Geologic carbon sequestration (GCS) is a method by which point source CO_2 emissions are purified and deposited in subsurface geologic formations for long-term storage. Accompanying this technology is the inherent responsibility to monitor these large-scale subsurface reservoirs for CO_2 leaks to ensure safety to local environments and inhabitants, as well as to alleviate global warming.

Elevated CO_2 levels in soil are known to cause anoxic conditions in plant roots, thereby interfering with plant respiration and inducing a stress response that could possibly be remotely sensed using aerial imagery. Airborne remote sensing technology has the potential to monitor large land areas at a relatively small cost compared to alternative methods. In 2010, an aerial campaign was conducted during the height of the growing season to obtain an image time series that could be used to identify and characterize CO_2 stress in vegetation from a simulated CO_2 leak. An unsupervised classification was performed to classify CO_2 stressed vegetation as a result of the subsurface injection. Furthermore, a spectral index was derived to amplify the CO_2 stress signal and chart vegetation health trajectories for pixels affected by the CO_2 release. A theoretical framework was developed for analysis strategies that could be implemented to detect a CO_2 leak using aerial hyperspectral imagery with minimal *a priori* knowledge.

Although aerial detection of CO_2 stressed vegetation was possible while no other physiological plant stressors were present, the spectral distinction between vegetation stress agents would have important implications for the appropriate timing that GCS monitoring using remote sensing data could commence. A greenhouse experiment was devised to compare the spectral responses of alfalfa plants to CO_2 and water stress in order to reveal whether CO_2 leak detection is possible when soil water availability is highly variable or during periods of drought. Spectral discernment of a CO_2 leak appears to be possible when soil water is spatially variable and during moderate drought conditions with remote sensing instruments that are sensitive to reflectance in the short wave infrared, where water absorption features related to leaf water content occur.

CHAPTER 1

INTRODUCTION

The focus of this study is to examine the viability of using hyperspectral remote sensing to monitor large land areas for surface carbon dioxide (CO_2) leakage over subsurface storage reservoirs. In an attempt to mitigate greenhouse gas emissions from stationary point sources, geologic carbon sequestration (GCS) is on the brink of broad-scale, commercial implementation. Inherent risks to people and the environment exist with the storage of large amounts of CO_2 in deep, subsurface reservoirs, and successful geologic storage of CO_2 requires sequestration for long periods of time with little or no leakage to the land surface (Hepple and Benson 2005; Oldenburg et al. 2009; Pruess 2008; Wilson et al. 2007). Therefore, surface monitoring of GCS sites becomes critical when assessing the effectiveness of this carbon capture and storage technique. It has been proposed that aerial remote sensing could image relatively large tracts of land over GCS sites to monitor for surface CO_2 leaks through the detection of plant stress caused by the adverse effects of elevated soil CO_2 concentrations (Keith et al. 2009; Male et al. 2010; Noomen and Skidmore 2009). But little is known about the aerial detection of CO_2 leaks and the seasonal extent that vegetation stress could be used as a bio-indicator of a CO_2 leak from a GCS site.

CO_2 is the most critical of the greenhouse gasses due to its overall relative abundance as an insulating gas in our atmosphere. Furthermore, CO_2 pollution is of utmost importance because of its production as an industrial bi-product from human source emissions (Pacala and Socolow 2004). The primary anthropogenic source of CO_2

results from the combustion of fossil fuels for energy production in transportation and industrial activities (IPCC AR4 2007; Joos and Spahni 2008). Since greenhouse gasses trap radiant heat from the sun within the earth's atmosphere, the threat of global climate change requires the accounting of greenhouse gas emissions and demands a strategy to reduce emissions.

The carbon capture and storage strategy of GCS takes point source CO_2 emissions, captured from stationary sources (e.g. power plants, industrial and agricultural processing factories etc.), for storage in deep subsurface geologic formations (Hepple and Benson 2005; LBNL 2000; Wilson et al. 2007; Carbon Sequestration Atlas 2008; Pruess 2008; Oldenburg et al. 2009). GCS is a promising technology that has the potential to store enormous amounts of CO_2 that would otherwise escape to the atmosphere and exacerbate global warming (Pacala and Socolow 2004; Hepple and Benson 2005; Wilson et al. 2007; Pruess 2008).

Cost-effective, periodic, large-area monitoring of GCS sites for surface CO_2 leaks will be required to ensure site safety, as well as to verify successful sequestration of CO_2 for economic and climatic reasons (Cortis et al. 2008; Hepple and Benson 2005; Oldenburg et al. 2009; Wilson et al. 2007). Aerial remote sensing (e.g., from airplanes, satellites, balloons, unmanned aerial vehicles) has often been used to provide timely, near instantaneous data at broad spatial scales in a wide range of real world investigations. The high spectral resolution data afforded by hyperspectral remote sensing is different from conventional multi-spectral instruments in that they contain a wealth of spectral data in nearly continuous, discrete, narrow bandwidths gathered throughout the visible and

infrared portions of the electromagnetic spectrum. Hyperspectral data allows for more rigorous Earth object differentiation through the characterization of physical and chemical attributes of those objects (Goetz et al. 1985). Although past experiments have demonstrated that hyperspectral remote sensing can detect plant stress caused by elevated soil CO_2 (Keith et al. 2009; Male et al. 2010; Noomen and Skidmore 2009), the temporal and spatial extent to which a CO_2 leak could be detected remains relatively unknown.

Two distinct experiments were conducted to elucidate the timing and detection capabilities of hyperspectral remote sensing to monitor GCS sites for CO_2 leaks: (1) A time series analysis was conducted with aerial imagery collected with a hyperspectral sensor over an outdoor experimental CO_2 release site to examine the timing and degree to which a CO_2 leak is detectable; and (2) A greenhouse experiment was conducted to determine whether plant physiological responses to elevated soil CO_2 concentrations and water stress can be spectrally distinguished. The 2010 aerial imaging campaign was conducted over a buried release pipe at the Zero Emissions Research and Technology (ZERT) site in Bozeman, MT, designed to emulate a CO_2 leak from a GCS site. Never before has an image time series been acquired from an airborne platform to evaluate vegetation spectral response to elevated soil CO_2 concentrations during an extensive CO_2 release experiment. Although this experiment provided a framework for the aerial detection of a CO_2 leak from a GCS site during the height of the growing season (the month of June), it also raised interesting questions regarding the timing in which remote sensing is an appropriate tool for the detection of stress caused by elevated soil CO_2. Soil water availability is known to be spatially variable and dependent on soil type, vegetation

cover, and meteorological conditions (Baier 1969; Denmead and Shaw 1962), therefore patches of vegetation around a GCS site could likely be water stressed due to landscape heterogeneity. Drought is another common environmental condition that could cause water stress in large areas of vegetation and might limit the applicability of remote sensing to monitor GCS sites. A greenhouse experiment was designed to test if the physiological response of plants to elevated soil CO_2 was spectrally distinguishable from water stress in order to examine potential limitations of remote sensing data to be used for GCS monitoring.

References

Baier, W. 1969. Concepts of soil moisture availability and their effect on soil moisture estimates from a meteorological budget. *Agricultural Meteorology*. 6: 165-178.

Cortis, A., Oldenburg, C.M., Benson, S.M. 2008. The role of optimality in characterizing CO_2 seepage from geologic carbon sequestration sites. *International Journal of Greenhouse Gas Control*. 2: 640-652.

Denmead, O, T, Shaw, R.H. 1962. Availability of soil water to plants as affected by soil moisture content and meteorological conditions. *Agronomy Journal*. 54: 385-390.

Goetz, A.F.H., Vane, G., Solomon, J.E., Rock, B.N. 1985. Imaging spectrometry for Earth Remote Sensing. *Science*. 228 (4704): 1147-1153.

Hepple, R.P., Benson, S.M. 2005. Geologic storage of carbon dioxide as a climate change mitigation strategy: performance requirements and the implications of surface seepage. *Environmental Geology*. 47: 576-585.

IPCC Fourth Assessment Report (AR4), 2007. *IPCC Fourth Assessment Report on Climate Change*. Cambridge University Press, Cambridge, UK.

Joos, F., Spahni, R. 2008. Rates of change in natural and anthropogenic radiative forcing over the past 20,000 years. *Proceedings of the National Academy of Sciences (PNAS)*. 105: 1425-1430.

Keith, C.J., Repasky, K.S., Lawrence, R.L., Jay, S.C., Carlsten, J.L. 2009. Monitoring effects of a controlled subsurface carbon dioxide release on vegetation using a hyperspectral imager. *International Journal of Greenhouse Gas Control*. 3: 626-632.

Lawrence Berkeley National Laboratory (LBNL), 2000. An overview of geologic sequestration of CO_2. In: *ENERGEX'2000: Proceedings of the 8th International Energy Forum*, Las Vegas, NV.

Male, E.J., Pickles, W.L., Silver, E.A., Hoffmann, G.D., Lewicki, J.L., Apple, M., Repasky, K., Burton, E.A. 2010. Using hyperspectral plant signatures for CO_2 leak detection during the 2008 ZERT CO_2 sequestration field experiment in Bozeman, Montana. *Environmental Earth Sciences*. 60: 251-261.

National Energy Technology Laboratory (NETL). 2008. *Carbon Sequestration Atlas of the United States and Canada*.

Noomen, M.F., Skidmore, A.K. 2009. The effects of high soil CO_2 concentrations on leaf reflectance of maize plants. *International Journal of Remote Sensing*. 30: 481-497.

Oldenburg, C.M., Bryant, S.L., Nicot, J.P. 2009. Certification framework based on effective trapping for geologic carbon sequestration. *International Journal of Greenhouse Gas Control*. 3: 444-457.

Pruess, K. 2008. On CO_2 fluid flow and heat transfer behavior in the subsurface, following leakage from a geologic storage reservoir. *Environmental Geology*. 54: 1677-1686.

Thoning, K.W., Tans, P.P., Komhyr, W.D. 1989. Atmospheric carbon dioxide at Mauna Loa Observatory 2. Analysis of the NOAA GMCC data, 1974-1985. *J. Geophys. Research*. 94: 8549-8565.

Wilson, E.J., Friedmann, S.J., Pollak, M.F. 2007. Research for deployment: Incorporating risk, regulation, and liability for carbon capture and sequestration. *Environmental Science & Technology*. 41: 5945-5952.

CHAPTER 2

LITERATURE REVIEW

Geologic Carbon Sequestration

Climate Change

Paleoclimate records derived from ice cores obtained from Greenland and Antarctica, and current air samples collected from eddy covariance towers at the Mauna Loa observatory have indicated that the atmospheric concentration of CO_2 has increased from the pre-industrial level of 280 ppm to > 380 ppm—the highest level in 600,000 years (Cuffey and Vimeux 2001; Masarie and Tans 1995; Monnin et al. 2001; Petit et al. 1999; Scripps 2007; Seigenthaler et al. 2005; Thoning et al. 1989). The current trends of atmospheric CO_2 concentration correspond with unprecedented global temperature increases (Joos and Spahni 2008). Global surface temperature increased 0.74° ± 0.18°C (1.33° ± 0.32° F) from 1906 to 2005 (IPCC AR4 2007). Growing international concern speculates that these changes could alter our earth's climate, resulting in devastating effects to the environment and the planet's inhabitants (Parmesan 2006; Hansen et al. 2008; Norby and Luo 2006; Shackleton 2000; Vinnikov and Grody 2003). Efforts to curb greenhouse gas emissions focus on the sequestration of carbon dioxide (CO_2) because of its overall abundance in the earth's atmosphere and its prevalence as a combustion byproduct.

In 2007, the United States produced 7,150 Gt (billion metric tons) of CO_2 equivalent, with more than half the emissions coming from stationary sources (NETL

2008; Joos and Spahni 2008; US EPA 2009). The DOE has identified subsurface geologic formations that have the potential storage capacity to sequester 100's to 1000's of billion metric tons of captured CO_2 (NETL 2008; IPCC 2005). Therefore, geologic sequestration of CO_2 is considered to be one of the primary strategies to be utilized to limit future atmospheric emissions, and facilitate the continued use of fossil fuels during the transitional period to more renewable and sustainable energy technologies (Hepple and Benson 2005; Oldenburg et al. 2009; Pacala and Socolow 2004; Wilson et al. 2007). In 1997, the Kyoto Protocol was developed and proposed by the United Nations Framework Convention on Climate Change (UNFCCC) in an attempt to solidify a united global effort to effectively thwart global warming. As stated by the UNFCC, the objective of the Kyoto Protocol is the "stabilization and reconstruction of greenhouse gas concentrations in the atmosphere at a level that would prevent dangerous anthropogenic interference with the climate system" (UNFCC 2009). More recently the United Nations deliberated at the 2009 Climate Change Conference in Copenhagen Denmark, and the urgency of curbing greenhouse gas emissions, principally CO_2, was top priority.

Geologic Carbon Sequestration as a Climate Mitigation Strategy

Geologic carbon sequestration (GCS) has been posed as a carbon capture and storage technique that could play a major role as a climate mitigation strategy to remove large amounts of CO_2 from our atmosphere (Hepple and Benson 2005; Hepple 2002; Herzog 2001; IPCC 2005; LLNL 2000; Pacala and Socolow 2004; Wilson et al. 2007). GCS captures point source emissions from manufacturing plants and power stations, then stores them as a condensed super critical fluid in large subsurface reservoirs (Figure 1).

The National Carbon Sequestration Database and Geographic Information System (NATCARB) estimates annual point source emissions to be over 3,800 $MtCO_2$ for North America (NETL 2007). Reconnaissance has identified North American basalts, deep saline formations, underground coal seams, and depleted oil wells as geologic regions that have the potential storage capacity of over 3,500 $GtCO_2$ (NETL 2008; IPCC 2005; LBNL 2000; Mingzhe et al. 2006; Xu 2004).

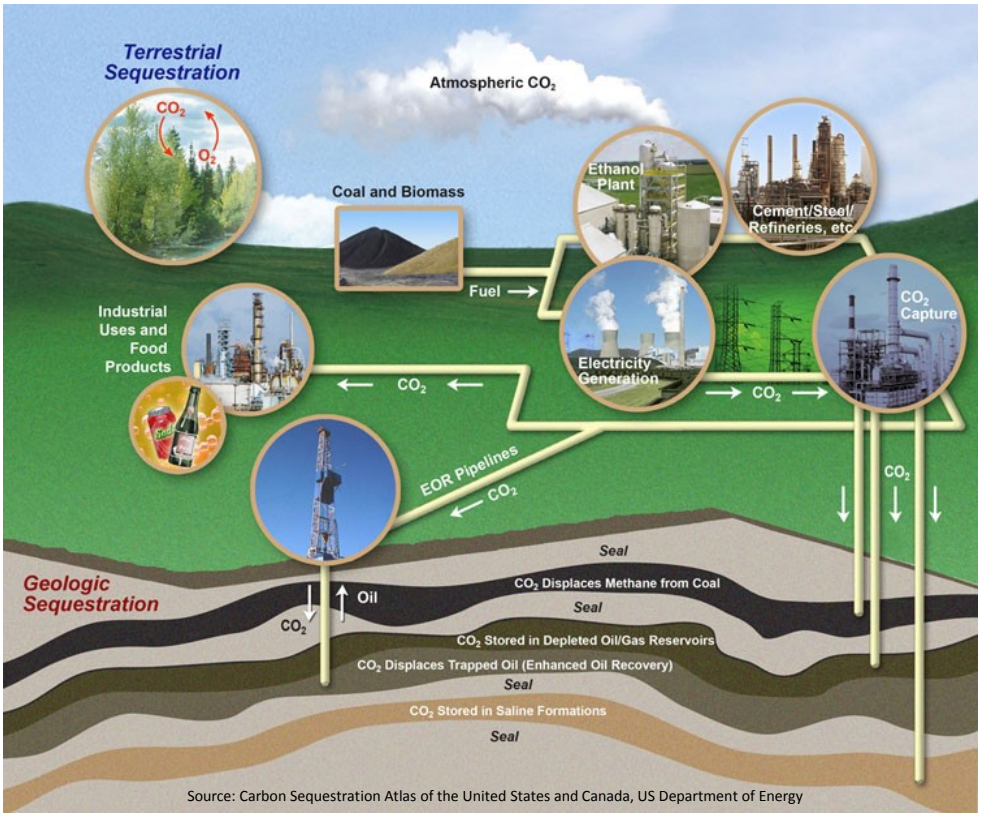

Figure 2.1: Overview of the GCS process.

The U.S. Department of Energy (DOE) is investigating a variety of avenues to sequester atmospheric CO_2 for long periods of time. A network of seven regional carbon sequestration partnerships was created by the DOE to solidify research and development within carbon sequestration science and technology. Several types of geologic

formations have been identified with certain characteristics to effectively sequester CO_2 in the subsurface environment. They include: current and abandoned oil and gas reservoirs; unmineable coal seams; deep saline formations; and, potentially, basalt and shale formations (Carbon Atlas 2008; Hepple and Benson 2005; IPCC 2005; Wilson et al. 2007). Injection of CO_2 into both subsurface coal beds and oil and gas reservoirs has the additional benefit of enhanced oil and coal bed methane recovery. Therefore, the economic tradeoff of carbon sequestration is more advantageous in these geologic regions. Deep saline formations are characterized as containing the greatest subsurface volume capacity because of their abundant distribution in worldwide sedimentary basins. All of these geologic formations are characterized by a relatively permeable mineral layer overtopped by a denser, impermeable cap rock that will trap and store injected target emissions. Sources of leakage will be confined to abandoned or improperly sealed wellbores, fault zones, and geologic inconsistencies (Cortis et al. 2008; LLNL 2005; Oldenburg et al. 2009; Pruess 2008).

Storage of CO_2 within the subsurface environment involves processes that capture target emissions from stationary sources and convert the gas into a supercritical fluid that is less mobile and more condensed for better storage. However, supercritical CO_2 is more buoyant than groundwater, therefore, its tendency for upward migration is more likely than other traditional forms of liquid injection processes, such as groundwater recharge, solution mining, and hazardous liquid and gas disposal (LLNL 2005; Oldenburg et al. 2009; Wilson et al. 2007). Also, because the large volumes of

supercritical CO_2 will be pressurized when injected into confined underground reservoirs, the possibility of CO_2 and brine leakage through upward migration will increase.

Currently, there are four active, industrial-scale GCS projects in the world. The largest is the Weyburn-Midale CO_2 Project (Saskatchewan, Canada) where approximately 1.5 $MtCO_2$/year is stored by enhanced oil recovery (Whittaker 2004); Second, the Sleipner Project in the North Sea, has been storing approximately 1$MtCO_2$/year of stripped CO_2 from extracted natural gas since 1996 (Korbol and Kaddour 1995); Third, a project in the Snøhvit gas field injects about 0.7 $MtCO_2$ /year into a deep saline aquifer within a sandstone formation that is 2,600 m underneath the seabed (Maldal and Tappel 2004); and Fourth, approximately 1 $MtCO_2$/year is captured annually and re-injected into the desert floor in Salah, Algeria (Knott 2008). Also, the United States DOE has been exploring GCS options with numerous pilot projects (Figure 2).

GCS is still in its experimental phase with small-scale projects being conducted in North America, Europe, and Africa. While injection of relatively small amounts of CO_2 into the subsurface has been successful in enhanced oil and coalbed methane recovery efforts, relatively little is known about injecting large amounts of CO_2 for the purpose of long-term storage in deep underground reservoirs. Commercial implementation of GCS will not only require scientific validation, but also public endorsement of this capture and storage technology. Large-scale deployment will mandate monitoring these sites to ensure both the safety of the environment and local inhabitants, as well as to confirm the adequate sequestration of CO_2 for long periods of time (Hepple and Benson 2005; Oldenburg et al. 2009; Pruess 2008; Wilson et al. 2007).

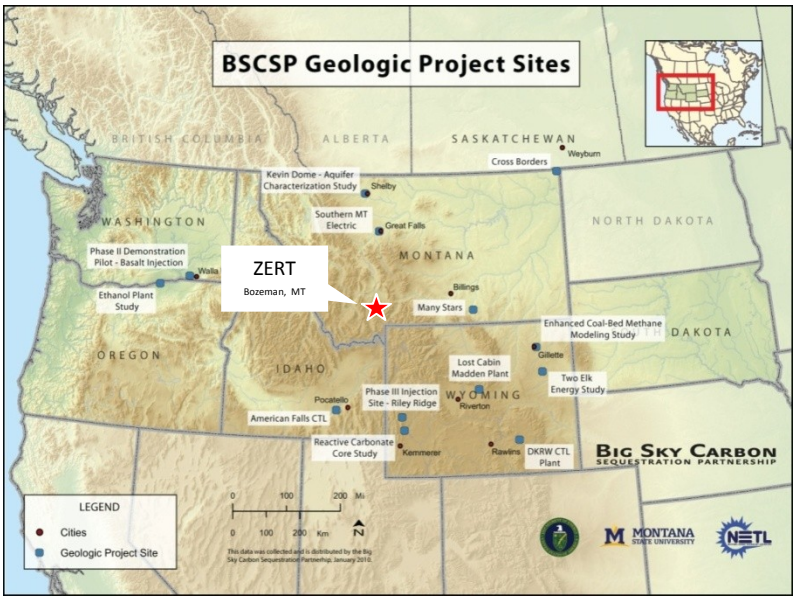

Figure 2.2: Location of current and proposed Big Sky Carbon Sequestration Partnership (BSCSP) and Department of Energy (DOE) carbon projects. My 2010 aerial hyperspectral imaging campaign at the Zero Emissions and Research Technology (ZERT) site, Montana State University, Bozeman, MT is but a part of a whole suite of research being conducted. (modified from LBNL 2000).

Risks from Geologic Carbon Sequestration

The risks associated with leaks from geologic reservoirs include: 1) acidification and contamination of underground drinking water; 2) asphyxiation at the near-surface or surface environment from CO_2 discharge; and 3) compromising emission credits and undermining the goal of GCS (Oldenburg et al. 2009; Pruess 2008; Wilson et al. 2007). Evidence of the potential damage and hazard accompanying a leak scenario from a GCS site can be understood by examining natural surface leaks of CO_2 via volcanic and geothermal vents. In 1986, a CO_2 gas bubble exploded in Lake Nyos in Western Cameroon resulting in over 1,700 human deaths (Kling et al. 2005). On Mammoth Mountain, CA, a snow cavern collapsed around a volcanic vent during the 2006 ski season, killing three ski patrollers from asphyxiation (UCSB—Office of Public Affairs

2006). Additionally, the Long Valley Caldera has caused widespread forest mortality due to elevated soil CO_2 levels surrounding Mammoth Mountain, CA (Jong 1998). These are evidence of the potential hazard that accompanies storing large quantities of CO_2 deep in subsurface reservoirs within the context of hypothetical surface leakage scenarios.

Monitoring Geologic Carbon Sequestration Sites Using Hyperspectral Data

There are numerous methods by which a CO_2 leak from a GCS site could be detected, however, most are time consuming, resource intensive, and have limited spatial coverage. Methods that have been employed for CO_2 leakage detection include: CO_2 flux measurements recorded by an accumulation chamber; the use of perfluorocarbon tracers to monitor CO_2 movement; differential absorption detection using laser-based instruments; CO_2 concentration measurements using non-dispersive infrared sensors; inelastic neutron scattering; eddy covariance station measurements; water chemistry analysis; and resistivity/conductivity surveys (Spangler et al. 2009; Strazisar et al. 2009). All of these techniques require expensive equipment that can cause destruction to the surface environment, as well as require large amounts of time for instrumentation setup and data acquisition. Foremost, these methods could only monitor small areas for CO_2 leakage without an impractical amount of labor and equipment resources. Aerial remote sensing, alternatively, could provide large land area monitoring at a relatively low-cost and minimal resource requirement.

It has been postulated that remote sensing could indirectly identify a CO_2 leak from a GCS site covered by vegetation through the detection of plant stress caused by

elevated soil CO_2. Underground gas leaks have been shown to displace soil oxygen, resulting in discernable plant-stress spectral response in multiple plant species (Smith et al. 2004a; Smith et al. 2004b). Additionally, CO_2 leaks have also caused adverse effects in maize plants by causing anoxic conditions, whereby oxygen is displaced at the roots, disrupting plant respiration and causing acidification of the ground water (Noomen and Skidmore 2007).

Hyperspectral Imaging for Detection of Surface CO_2 Leakage

Periodic airborne imaging campaigns could potentially provide GCS monitoring of large land areas to detect CO_2leaks expressed as plant stress at the surface (Keith et al. 2009). Hyperspectral remote sensing offers the advantage of high spectral resolution data that is collected within numerous, continuous, narrow reflectance bands. This allows not only for Earth object identification, but also for the characterization of the physical and chemical attributes of those objects (Goetz 1985). Thus, pre-visual detection of plant stress using hyperspectral imaging has been possible (Carter and Miller 1994; Lawrence and Labus 2003; Rock et al. 1988; Sampson et al. 2003). Perhaps, even plant stress induced by elevated soil CO_2 concentrations could be spectrally discerned from other physiological stressors given the highly dimensional nature of hyperspectral data. Early CO_2 leak detection would allow site managers to take immediate remediation measures to prevent further leakage, while minimizing safety risk and economic loss. However, the extent and effectiveness of remote sensing to monitor GCS sites and detect surface CO_2 leaks is still unknown.

Chlorophyll Content: Plant stress detection evaluates spectral data in regions that are either sensitive to plant photosynthetic efficiency by detecting changes in absorption and reflectance determined by plant pigment levels, or through the detection of changes to physical plant structure. Chlorophyll is the most influential plant pigment because of its ability to harness the Sun's radiative light to convert CO_2 into organic compounds, especially sugars, and obtain energy (Smith 1997). Plant spectral characteristics within the visible blue region are determined by heavy absorption by chlorophyll *a* and *b*, as well as other carotenoids, whereas the visible red is characterized by chlorophyll *a* and *b* absorption only (Jensen 2004). Chlorophyll *a* and *b* absorption is highest in the blue (400 – 500 nm) and middle-red (near 680 nm) portions of the electromagnetic (EM) spectrum and lowest in the visible green wavelengths, thus giving plants their green appearance. Heavy chlorophyll absorption within these spectral regions prevents early plant stress detection because they are not sensitive to small changes in chlorophyll content due to the strong activity of chlorophyll and accessory pigments that saturates the signal (Carter and Knapp 2001; Lichtenthaler 1987; Merzlyak et al. 1999). Contrarily, decreases to chlorophyll content in response to plant stress in order to down regulate photosynthesis is expressed where chlorophyll absorption is weakest in the visible green and far red portion of the spectrum (Carter and Knapp 2001; Buschmann and Nagel 1993). It has been demonstrated that the far red wavelengths near 700 nm are the most reliable spectral indicator for stress (Carter et al. 1996; Cibula and Carter 1992).

The most commonly studied spectral region for detection of plant stress occurs on the boundary of the late visible red and early near infrared portion of the EM spectrum,

thus termed the “red edge”. The red edge is a reflectance spike in plant spectra associated with heavy chlorophyll *a* and *b* absorption in the visible light wavelengths (400 nm - 700 nm), and high reflectance in the near infrared (750 nm -900 nm) due to the spongy leaf mesophyll (Carter and Knapp 2001; Smith et al. 1997; Zarco-Tejada et al. 2000). Plant stress is known to degrade chlorophyll pigment absorption, increasing the reflectance of photosynthetically active radiation in the visible region of the EM spectrum. Analysis of the red edge can detect plant stress by tracking changes in the peak and trough inflection points or changes in the derivatives of the reflectance spike responses. Narrow-band red edge spectral indices, in the form of ratios or derivatives, have been used repeatedly as proxy measures of chlorophyll content in plants (Carter and Miller 1994; Buschmann and Nagel 1993; Demetriades-Shah et al. 1990; Gitelson and Merzylak 1996; Gitelson and Merzylak 1997; Strachan et al. 2002; Vogelmann et al. 1993). These hyperspectral indices have the distinct advantage of being more sensitive to smaller, more subtle spectral changes as compared to traditional broadband indices, such as the Normalized Difference Vegetation Index NDVI or Simple Ratio (SR). Chlorophyll content is directly related to the photosynthetic activity and efficiency in plants, and therefore, changes to chlorophyll content (observed as changes in chlorophyll light absorption) can be used to detect plant stress.

Additionally, the red edge reflectance spike has been observed to move 5-10 nm towards shorter wavelengths when a plant is stressed, termed the “blue shift” (Carter and Miller 1994; Carter and Knapp 2001; Demetriades-Shah et al. 1990; Rock et al. 1988; Smith et al. 2004; Vogelmann et al. 1993). There has been evidence that this blue shift is

associated with the pre-visual detection of plant stress, which would allow for hyperspectral instruments to remotely sense changes to plant health even before they could be perceived by the human eye. Land managers view this as an important attribute of monitoring technologies because it would allow for the early detection of target plant stress and a quick response for ameliorative action that would limit resource and economic loss.

Xanthophyll Cycle: Although the majority of plant stress spectral investigations have examined chlorophyll absorption within the visible red and near infrared portion of the spectrum, numerous studies have also utilized absorption patterns of other pigments in the blue and green portion of the spectrum. Notably, the xanthophyll cycle pigments contained within the palisade mesophyll have been associated with photosynthetic radiation use efficiency (Gamon et al. 1997), and therefore have been used in the Photochemical Reflectance Index (PRI) to relate levels of photoprotective pigments as an indicator of plant stress (Meroni et al. 2008; Peguero-Pina et al. 2008; Rascher and Pieruschka 2008; Suarez et al. 2008). Stressed plants will down regulate photosynthetic activity, thus lowering photosynthetic-radiation-use-efficiency and increasing the reflectance of leaves within the visible green spectrum.

Water Stress: Water stress has also been detected in specific water absorption features that are directly related to water spectral properties in the infrared portion of the EM spectrum. Absorption features near 1400, 1900, and 2500 nm have been identified as regions that are most sensitive and best correlated to moisture content in plant leaves

(Carter 1991). However, influences of solar irradiance properties, atmospheric transmissivity, and the scale (leaf-level versus canopy-level and ground-based versus aircraft or space platforms) at which spectral information is collected restrict the size of spectral regions that are sensitive to leaf water content. Solar radiation output drops off beyond 2500 nm, while absorption and attenuated light transmission by atmospheric water vapor has limited the ideal sensitivity of hyperspectral instrumentation to the dehydration of leaves to the range of 1480 nm to 1750 nm for ground-based remote sensing and 1550 nm to 1630 nm for space platforms (Tucker 1980a). Detection of the water stress signal within the visible red wavelengths is considered a secondary plant response, in which chlorophyll pigment concentration decreases as a mechanism of down regulating photosynthesis (Tucker 1980b; Carter 1991). Alternatively, spectral measurements of leaf moisture content directly monitors for water deficits and hypothetically would offer a more immediate plant response to water stress, as well as look spectrally distinct compared to other types of physiological stressors.

Modeling Approaches

Hyperspectral imagery has been used for modeling plant stress for the detection of heavy metal soil contamination (Schuerger et al. 2002); salinity stress (Naumann et al. 2009); water stress (Peguero-Pina et al. 2008; Penuelas et al. 1997; Suarez et al. 2008); nutrient levels and crop status (Gamon et al. 1997; Strachan et al. 2002); ozone exposure (Meroni et al. 2008); and for mapping the pattern of ecosystem water and carbon flux (Fuentes 2006). All of these models used vegetation indices as surrogates for plant response, despite the diverse applications of hyperspectral data. Arguably, these models

were not fully utilizing the high spectral dimensionality of hyperspectral imaging. Conversely, bandwise regression is a method by which numerous bands can be used as explanatory variables in a linear regression model versus that of a simplified vegetation index (Lawrence and Ripple 1998; Maynard et al. 2006), thus utilizing the wealth of spectral information available with hyperspectral imaging.

The random forest classifier (a.k.a. Breiman Cutler Classifications) is another method by which all of the possible spectral information is utilized to model a categorical response. This classification method has been used to model hyperspectral data to obtain high accuracy classifications that discern between subtle vegetation characteristics (Lawrence et al. 2005). Random forest is an ensemble classifier that consists of numerous individual decision trees that use a random subset of observational data for each single tree's construction (Breiman 2001). A randomly selected subset of explanatory variables is used to determine each split (or node) within each individual classification tree. Subsequently, final class distinctions are made based on the plurality vote among the ensemble of decision trees. This technique is a powerful tool to classify high dimensional hyperspectral data, in which there are potentially many explanatory variables (spectral bands) that relate to a response variable (Lawrence et al. 2006; Gislason et al. 2006). However, model interpretation is ambiguous because of the "black box" nature of the random forest algorithm, which outputs variable importance that provides only a general sense of which explanatory variables were relatively important in the determination of the response (Prasad et al. 2006).

Alternatively, classification tree analysis is a non-parametric technique which uses only a single decision tree to model data, unlike the ensemble random forest classifier. Classification trees use decision based rules that lower deviance between samples and allows for analyst interpretation. Classification trees have been used to model remote sensing data with high classification accuracy and have provided insight into spectral investigations by clearly identifying the precise wavelengths or bands used to distinguish between classes (Lawrence and Labus 2003; Lawrence and Wright 2001).

References

Breiman, L. 2001. Random forests. *Machine Learning*. 45: 5-32

Buschmann, C., Nagel, E. 1993. In vivo spectroscopy and internal optics of leaves as basis for remotes sensing of vegetation. *International Journal of Remote Sensing*. 14 (4): 711-722.

Carter, G.A. 1993. Response of leaf spectral reflectance to plant stress. *American Journal of Botany*. 80: 239-243.

Carter, G. A., Knapp, A.K. 2001. Leaf optical properties in higher plants: linking spectral characteristics to stress and chlorophyll concentration. *American Journal of Botany*. 88: 677-684.

Carter, G.A., Miller, R.L. 1994. Early detection of plant stress by digital imaging within narrow stress-sensitive wavebands. *Remote Sensing of Environment*. 50: 295-302.

Cibula, W.G., Carter, G.A. 1992. Identification of a far-red reflectance response to ectomycorrhizae in slash pine. *International Journal of Remote Sensing*. 13: 925-932.

Cortis, A., Oldenburg, C.M., Benson, S.M. 2008. The role of optimality in characterizing CO_2 seepage from GCS sites. *International Journal of Greenhouse Gas Control*. 2: 640-652.

Cuffey, K.M., Vimeux, F. 2001. Covariation of carbon dioxide and temperature from the Vostok ice core after deuterium-excess correction. *Nature*. 412: 523-527.

Demetriades-Shah, T.H., Steven, M.D., Clark, J. A. 1990. High resolution derivative spectra in remote sensing. *Remote Sensing of Environment*. 33: 55-64.

Fuentes, D.A., Gamon, J.A., Cheng, Y.F., Claudio, H.C., Qiu, H.L., Mao, Z.Y., Sims, D.A., Rahman, A.F., Oechel, W., Luo, H.Y. 2006. Mapping carbon and water vapor fluxes in a chaparral ecosystem using vegetation indices derived from AVIRIS. *Remote Sensing of Environment*. 103: 312-323.

Gamon, J.A., Serrano, L., Surfus, J.S. 1997. The photochemical reflectance index: an optical indicator of photosynthetic radiation use efficiency across species, functional types, and nutrient levels. *Oecologia*. 112: 492-501.

Gislason, P.O., Benediktsson, J.A., Sveinsson, J.R. 2006. Random Forests for land cover classification. *Pattern Recognition Letters*. 27: 294-300.

Gitelson, A.A., Buschmann, C., Lichtenthaler, H.K. 1999. The chlorophyll fluorescence ratio F-735/F-700 as an accurate measure of the chlorophyll content in plants. *Remote Sensing of Environment*. 69: 296-302.

Gitelson, A.A., Merzlyak, M.N. 1997. Remote estimation of chlorophyll content in higher plant leaves. *International Journal of Remote Sensing*. 18: 2691-2697.

Gitelson, A.A., Merzlyak, M.N. 1996. Signature analysis of leaf reflectance spectra: Algorithm development for remote sensing of chlorophyll. *Journal of Plant Physiology*. 148: 494-500.

Goetz, A.F.H., Vane, G., Solomon, J.E., Rock, B.N. 1985. Imaging spectrometry for Earth Remote Sensing. *Science*. 228 (4704): 1147-1153.

Hansen, J., Sato, M., Kharecha, P., Beerling, D., Masson-Delmotte, V., Pagani, M., Raymo, M., Royer, D.L., Zachos, J.C. 2008. Target atmospheric CO_2: where should humanity aim? *Open Atmospheric Science Journal*. 2: 217-231.

Hepple, R.P. 2002. Implications of surface seepage on the effectiveness of geologic storage of carbon dioxide as a climate change mitigation strategy. *Lawrence Berkeley National Laboratory (LBNL)*, Paper LBNL-51267.

Hepple, R.P., Benson, S.M. 2005. Geologic storage of carbon dioxide as a climate change mitigation strategy: performance requirements and the implications of surface seepage. *Environmental Geology*. 47: 576-585.

Herzog, H.J. 2001. What future for carbon capture and sequestration? *American Chemical Society.* 35 (7): 148A–153A.

Intergovernmental Panel on Climate Change (IPCC). 2005. In: Metz, B., Davidson, O., de Coninck, H., Loos, M., Meyer, L. (Eds.), Intergovernmental Panel on Climate Change Special Report on Carbon Capture and Storage. Cambridge University Press, Cambridge, UK.

IPCC Fourth Assessment Report (AR4), 2007. *IPCC Fourth Assessment Report on Climate Change*. Cambridge University Press, Cambridge, UK.

Jensen, J.R. 2004. *Introductory Digital Image Processing, 3rd Edition*. Pearson Prentice Hall.

Jong, S.M.d. 1998. Imaging spectrometry for monitoring tree damage caused by volcanic activity in the Long Valley caldera, California. *ITC Journal*. 1-10.

Joos, F., Spahni, R. 2008. Rates of change in natural and anthropogenic radiative forcing over the past 20,000 years. *Proceedings of the National Academy of Sciences (PNAS)*. 105: 1425-1430.

Keith, C.J., Repasky, K.S., Lawrence, R.L., Jay, S.C., Carlsten, J.L. 2009. Monitoring effects of a controlled subsurface carbon dioxide release on vegetation using a hyperspectral imager. *International Journal of Greenhouse Gas Control*. 3: 626-632.

Kling, G.W., Evans, W.C., Tanyileke, G., Kusakabe, M., Ohba, T., Yoshida, Y., Hell, J.V. 2005. Degassing Lakes Nyos and Monoun: Defusing certain disaster. *Proceedings of the National Academy of Sciences of the United States of America*. 102: 14185-14190.

Knott, T. 2008. Capturing carbon dioxide. *Frontiers the BP magazine of technology and innovation*. April: 16-24.

Korbol, R., Kaddour, A. 1995. Sleipner vest CO_2 disposal-injection of removed into the Utsira formation. *Energy Conversion and Management*. 36: 509–512.

Lawrence Berkeley National Laboratory (LBNL), 2000. An overview of geologic sequestration of CO_2. In: *ENERGEX'2000: Proceedings of the 8th International Energy Forum*, Las Vegas, NV.

Lawrence Livermore National Library (LLNL). 2005. Locked in rock sequestering carbon. *S& TR*. 12-19.

Lawrence, R.L., Labus, M. 2003. Early detection of Douglas-fir beetle infestation with subcanopy resolution hyperspectral imagery. *Western Journal of Applied Forestry*. 18: 202-206.

Lawrence, R.L., Ripple, W.J. 1998. Comparisons among vegetation indices and bandwise regression in a highly disturbed, heterogeneous landscape: Mount St. Helens, Washington. *Remote Sensing of Environment*. 64: 91-102.

Lawrence, R.L., Wood, S.D., Sheley, R.L. 2006. Mapping invasive plants using hyperspectral imagery and Breiman Cutler classifications (RandomForest). *Remote Sensing of Environment*. 100: 356-362.

Lichtenthaler, H.K. 1987. Chlorophylls and carotenoids: pigments of photosynthetic biomembranes. *Methods in Enzymology*. 148: 350-382.

Lillesand, T. M., Kiefer, R. W., Chipman, J. W. 2008. *Remote Sensing and Image Interpretation 6th Edition*. John Wiley & Sons.

Maldal, T., Tappel, I.M. 2004. CO_2 underground storage for Snøhvit gas field development. *Energy*. 29: 1403–1411.

Masarie, K., Tans, P.T. 1995. Extension and integration of atmosphere carbon dioxide data into a globally consistent measurement record. *Journal of Geophysical Research*. 100: 11593-11610.

Maynard, C.L., Lawrence, R.L., Nielsen, G.A., Decker, G. 2007. Modeling vegetation amount using bandwise regression and ecological site descriptions as an alternative to vegetation indices. *GIScience & Remote Sensing*. 44: 68-81.

Meroni, M., Rossini, M., Picchi, V., Panigada, C., Cogliati, S., Nali, C., Colombo, R. 2008. Assessing steady-state fluorescence and PRI from hyperspectral proximal sensing as early indicators of plant stress: The case of ozone exposure. *Sensors*. 8: 1740-1754.

Merzlyak, M.N., Gitelson, A.A., Chivkunova, O.B., Rakitin, V.Y. 1999. Non-destructive optical changes during leaf senescence and fruit ripening. *Physiologia Plantarum*. 106: 135-141.

Mingzhe, D., Zhaowen, L., Shuliang, L., Huang, S. 2006. CO_2 sequestration in depleted oil and gas reservoirs-caprock characterization and storage capacity. *Energy Conservation and Management*. 47: 1372–1382.

Monnin, E., Indermühle, A., Dällenbach, A., Flückiger, J., Stauffer, B., Stocker, T.F.,Raynaud, D., Barnola, J.-M. 2001. Atmospheric CO_2 concentrations over the last glacial termination. *Science.* 291 (5501): 112–114.

Naumann, J.C., Young, D.R., Anderson, J.E. 2009. Spatial variations in salinity stress across a coastal landscape using vegetation indices derived from hyperspectral imagery. *Plant Ecology*. 202: 285-297.

National Energy Technology Laboratory (NETL). 2007. *Carbon Sequestration Atlas of the United States and Canada*.

National Energy Technology Laboratory (NETL). 2008. *Carbon Sequestration Atlas of the United States and Canada*.

Noomen, M.F., Skidmore, A.K. 2009. The effects of high soil CO_2 concentrations on leaf reflectance of maize plants. *International Journal of Remote Sensing*. 30: 481-497.

Noomen, M.F., Smith, K.L., Colls, J.J., Steven, M.D., Skidmore, A.K., Van der Meer, F.D. 2008. Hyperspectral indices for detecting changes in canopy reflectance as a result of underground natural gas leakage. *International Journal of Remote Sensing*. 29: 5987-6008.

Norby, R.J., Luo, Y. 2006. Evaluating ecosystem responses to rising atmospheric CO_2 and global warming in a multi-factor world. *New Phytologist*. 162 (2): 281–293.

Oldenburg, C.M., Bryant, S.L., Nicot, J.P. 2009. Certification framework based on effective trapping for geologic carbon sequestration. *International Journal of Greenhouse Gas Control*. 3: 444-457.

Pacala, S., Socolow, R. 2004. Stabilization wedges: solving the climate problem for the next 50 years with current technologies. *Science*. 305: 968-972.

Parmeson, C., 2006. Ecological and evolutionary responses to recent climate change. *Annual Review of Ecology, Evolution , and Systematics*. 37: 637-669.

Peguero-Pina, J.J., Morales, F., Flexas, J., Gil-Pelegrin, E., Moya, I. 2008. Photochemistry, remotely sensed physiological reflectance index and de-epoxidation state of the xanthophyll cycle in Quercus coccifera under intense drought. *Oecologia*. 156: 1-11.

Penuelas, J., Llusia, J., Pinol, J., Filella, I. 1997. Photochemical reflectance index and leaf photosynthetic radiation-use-efficiency assessment in Mediterranean trees. *International Journal of Remote Sensing*. 18: 2863-2868.

Petit, J.R., Jouzel, J., Raynaud, D., Barkov, N.I., Barnola, J.-M., Basile, I., Bender, M., Chappellaz, J., Davis, M., Delaygue, G., Delmotte, M., Kotlyakov, V.M., Legrand, M., Lipenkov, V.Y., Lorius, C., Pepin, L., Ritz, C., Saltzman, E., Stievenard, M. 1999. Climate and atmospheric history of the past 420,000 years from the Vostok ice core, Antarctica. *Nature*. 399: 429-436.

Prasad, A.M., Iverson, L.R., Liaw, A. 2006. Newer classification and regression tree techniques: Bagging and random forests for ecological prediction. *Ecosystems*. 9: 181-199.

Pruess, K. 2008. On CO2 fluid flow and heat transfer behavior in the subsurface, following leakage from a geologic storage reservoir. *Environmental Geology*. 54: 1677-1686.

Rascher, U., Pieruschka, R. 2008. Spatio-temporal variations of photosynthesis: the potential of optical remote sensing to better understand and scale light use efficiency and stresses of plant ecosystems. *Precision Agriculture*. 9: 355-366.

Rock, B.N., Hoshizaki, T., Miller, J.R. 1988. Comparison of *in situ* and airborne spectral measurements of the blue shift associated with forest decline. *Remote Sensing of Environment*. 24: 109-127.

Sampson, P.H., Zarco-Tejada, P.J., Mohammed, G.H., Miller, J.R., Noland, T.L. 2003. Hyperspectral remote sensing of forest condition: Estimating chlorophyll content in tolerant hardwoods. *Forest Science*. 49: 381-391.

Schuerger, A.C., Capelle, G.A., Di Benedetto, J.A., Mao, C.Y., Thai, C.N., Evans, M.D., Richards, J.T., Blank, T.A., Stryjewski, E.C. 2003. Comparison of two hyperspectral imaging and two laser-induced fluorescence instruments for the detection of zinc stress and chlorophyll concentration in bahia grass (Paspalum notatum Flugge.). *Remote Sensing of Environment*. 84: 572-588.

Scripps CO_2 program (Scripps). 2007. Monthly average carbon dioxide concentration. http://scrippsco2.ucsd.edu/graphics_gallery/mauna_loa_record/mauna_loa_record.html, Scripps Institute of Oceanography.

Seigenthaler, U., Stocker, T.F., Monnin, E., Lüthi, D., Schwander, J., Stauffer, B., Raynaud, D., Barnola, J.-M., Fischer, H., Masson-Delmotte, V., Jouzel, J. 2005. Stable carbon cycle-climate relationship during the Late Pleistocene. *Science*. 310: 1313-1317.

Shackleton, N.J. 2000. The 100,000-year ice-age cycle identified and found to lag temperature, carbon dioxide, and orbital eccentricity. *Science.* 289: 1897–1902.

Smith, A. L. 1997. ISBN 0-19-854768-4. Photosynthesis – the synthesis by organisms of organic chemical compounds, esp. carbohydrates, from carbon dioxide using energy obtained from light rather than the oxidation of chemical compounds. *Oxford dictionary of biochemistry and molecular biology*. Oxford University Press. p. 508.

Smith, K.L., Steven, M.D., Colls, J.J. 2004a. Use of hyperspectral derivative ratios in the red-edge region to identify plant stress responses to gas leaks. *Remote Sensing of Environment*. 92: 207-217.

Smith, K.L., Steven, M.D., Colls, J.J. 2004b. Spectral responses of pot-grown plants to displacement of soil oxygen. *International Journal of Remote Sensing*. 25: 4395-4410.

Spangler, L.H., Dobeck, L.M., Repasky, K.S., Nehrir, A.R., Humphries, S.D., Barr, J.L., Keith, C.J., Shaw, J.A., Rouse, J.H., Cunningham, A.B., Benson, S.M., Oldenburg, C.M., Lewicki, J.L., Wells, A.W., Diehl, J.R., Strazisar, B.R., Fessenden, J.E., Rahn, T.A., Amonette, J.E., Barr, J.L., Pickles, W.L., Jacobson, J.D., Silver, E.A., Male, E.J., Rauch, H.W., Gullickson, K.S., Trautz, R., Kharaka, Y., Birkholzer, J., Wielopolski, L. 2009. A shallow subsurface controlled release facility in Bozeman, Montana, USA, for testing near surface CO_2 detection techniques and transport models. *Environ Earth Sci*. doi:10.1007/s12665-009-0400-2

Strachan, I.B., Pattey, E., Boisvert, J.B. 2002. Impact of nitrogen and environmental conditions on corn as detected by hyperspectral reflectance. *Remote Sensing of Environment*. 80: 213-224.

Strazisar, B.R. , Wells, A.W., Diehl, R.J., Hammack, R.W., Veloski, G.A. 2009. Near-surface monitoring for the ZERT shallow CO_2 injection project. *International Journal of Greenhouse Gas Control*. 3: 736-744.

Suarez, L., Zarco-Tejada, P.J., Sepulcre-Canto, G., Perez-Priego, O., Miller, J.R., Jimenez-Munoz, J.C., Sobrino, J. 2008. Assessing canopy PRI for water stress detection with diurnal airborne imagery. *Remote Sensing of Environment*. 112: 560-575.

Thoning, K.W., Tans, P.P., Komhyr, W.D. 1989. Atmospheric carbon dioxide at Mauna Loa Observatory 2. Analysis of the NOAA GMCC data, 1974-1985. *J. Geophys. Research*. 94: 8549-8565.

Tucker, C.J. 1980a. Remote sensing of leaf water content in the near infrared. *Remote Sens. Environ*. 10: 23-32.

Tucker, C.J., Elgin, J.H., McMurtrey, J.M. 1980b. Relationship of red and photographic infra-red spectral data to alfalfa agronomic values. *International J Remote Sens*.

U.S. Department of Energy (DOE). 2008. Carbon Sequestration Atlas of the United States and Canada. Second Edition.

U.S. Environmental Protection Agency (EPA). 2009. U.S. Greenhouse gas inventory. http://www.epa.gov/climatechange/emissions/usgginventory.html

University of California Santa Barbara (UCSB). 2006. Press release—Office of Public Affairs.

Vinnikov, K.Y., Grody, N.C. 2003. Global warming trend of mean tropospheric temperature observed by satellites. *Science*. 302: 269–272.

Vogelmann, J.E., Rock, B.N., Moss, D.M. 1993. Red edge spectral measurements from sugar maple leaves. *International Journal of Remote Sensing*. 14: 1563-1575.

Whittaker, S.G. 2004. Geological storage of greenhouse gases: the IEA Weyburn CO_2 monitoring and storage project. *Canadian Society of Petroleum and Geologists Reservoir*. 31 (8): 9.

Wilson, E.J., Friedmann, S.J., Pollak, M.F. 2007. Research for deployment: Incorporating risk, regulation, and liability for carbon capture and sequestration. *Environmental Science & Technology*. 41: 5945-5952.

Xu, T. 2004. CO_2 geological sequestration. Lawrence Berkeley National Laboratory, Paper LBNL-56644 JArt.

Yang, C., Everitt, J.H., Bradford, J.M. 2004. Airborne hyperspectral imagery and yield monitor data for estimating grain sorghum yield variability. *Transactions of the Asae*. 47: 915-924.

Zarco-Tejada, P.J., Berni, J.A.J., Suarez, L., Sepulcre-Canto, G., Morales, F., Miller, J.R. 2009. Imaging chlorophyll fluorescence with an airborne narrow-band multispectral camera for vegetation stress detection. *Remote Sensing of Environment*. 113: 1262-1275.

Zarco-Tejada, P.J., Miller, J.R., Mohammed, G.H.; Noland, T.L. 2000. Chlorophyll fluorescence effects on vegetation apparent reflectance: I. leaf-level measurements and model simulation. *Remote Sensing of Environment*. 74 (3): 582-595.

CHAPTER 3

AERIAL DETECTION OF A SIMULATED CO_2 LEAK USING HYPERSPECTRAL IMAGERY

Introduction

Geologic Carbon Sequestration

Global surface temperature increased 0.74° ± 0.18°C from 1906 to 2005 (IPCC AR4 2007). Atmospheric carbon dioxide (CO_2) concentration has risen to over 380 ppm from the pre-industrial level of 280 ppm—the highest level in over 400,000 years (Cuffey and Vimeux 2001; Monnin et al. 2001; Petit et al. 1999; Seigenthaler et al. 2005). The primary source of these trends is due to the anthropogenic forcing of deforestation and the burning of fossil fuels (IPCC AR4 2007; Joos and Spahni 2008). There is growing international concern that these changes could alter the Earth's climate, resulting in devastating effects to the environment and the planet's inhabitants (Hansen et al. 2008; Parmeson 2006; Norby and Luo 2006; Shackleton 2000; Vinnikov and Grody 2003). Efforts to curb greenhouse gas emissions focus on sequestering CO_2 because of its overall abundance in the Earth's atmosphere and its prevalence as a combustion byproduct.

The geologic sequestration of CO_2 has been posed as a carbon capture and storage technique that could play a major role as a climate mitigation strategy to remove large amounts of CO_2 from our atmosphere (Hepple and Benson 2005; Hepple 2002; Herzog 2001; IPCC 2005; LBNL 2000; Pacala and Socolow 2004; Wilson et al. 2007). The National Carbon Sequestration Database and Geographic Information System

(NATCARB) estimates annual point source emissions to be over 3.8 gigatonnes (Gt) CO_2 for North America (NETL 2007). North American basalts, deep saline formations, underground coal seams, and depleted oil wells are geologic regions that are potential storage sites with an estimated total capacity of over 3,500 $GtCO_2$ (NETL 2008; IPCC 2005; LBNL 2000; Mingzhe et al. 2006; Xu 2004). Currently, there are four industrial-scale geologic carbon sequestration (GCS) projects in operation worldwide. Each of these sites is storing approximately 0.001 $GtCO_2$/year in enhanced coal bed methane or oil recovery efforts (Knott 2008; Korbol and Kaddour 1995; Maldal and Tappel 2004; Whittaker 2004).

Safe and efficient GCS must effectively store large amounts of CO_2 underground for extensive periods of time with minimal surface leakage. It has been proposed that a leakage rate of $\leq 0.01\%$ per year would be an appropriate performance requirement to ensure the efficacy of GCS (Benson et al. 2005). Sources of CO_2 leakage from a sequestration site are likely to be confined to improperly sealed well bores, geologic faults, or fractures in the otherwise impermeable cap rock (Benson et al. 2005; Cortis et al. 2008; Knauss et al. 2005; LBNL 2000; IPCC 2005; Oldenburg et al. 2009; Pruess 2008; Wilson et al. 2007).

There is a mandate not only to monitor GCS sites for CO_2 leakage to validate greenhouse gas emission mitigation but also from a safety and environmental standpoint. Natural sources of CO_2 leaks provide examples of the possible consequences of a CO_2 leak from an artificially injected subsurface reservoir. A gas bubble erupted in volcanic Lake Nyos, Western Cameroon, in 1986, for example, killing over 1,700 people and

many more animals from asphyxiation (Kling et al. 2005). Elevated soil CO_2 concentrations due to seeps from the Long Valley Caldera near Mammoth, CA, have caused extensive forest mortality (Bergfeld et al. 2006; Jong 1998; Pickles 2001).

The exact location of a CO_2 surface leak may be unknown to land managers of a GCS site, even though the locations of existing wells and faults will presumably be known. The Department of Energy's (DOE) Regional Carbon Sequestration Partnerships have identified numerous geologic formations as potential GCS sites. These areas are very large and some cover hundreds of square kilometers. Monitoring these sites will require methods that are accurate, practical, economical, and provide adequate spatial coverage (Cortis et al. 2008; Hepple and Benson 2005; Keith et al. 2009; Oldenburg et al. 2009; Schuerger et al. 2003; Wilson et al. 2007). There are numerous methods that a CO_2 leak from a GCS site could be detected, however, most are time consuming, expensive, and resource intensive (Spangler et al. 2009; Strazisar et al. 2009). Ground-based methods could only monitor small areas for CO_2 leakage without an impractical amount of labor resources and equipment. Aerial remote sensing has piqued the interests of managers and researchers because of its potential as a relatively low-cost, practical monitoring tool with large-area coverage capabilities. This study investigated the viability of using airborne hyperspectral remote sensing to detect CO_2 leaks by analyzing imagery collected over a controlled experimental release site.

Hyperspectral Remote Sensing for GCS Monitoring

Vegetation covers a significant portion of the Earth's land surface and is likely to be the predominant land cover at GCS sites, therefore, it has been postulated that remote

sensing could indirectly identify subsurface CO_2 leaks through the detection of plant stress caused by elevated soil CO_2 (Keith et al. 2009). Remote sensing has been used to assess plant stress in a wide range of real world applications. Hyperspectral data have been used in particular because of their wealth of continuous spectral information that is collected in many narrow wavelengths throughout the visible and near infrared portion of the electromagnetic (EM) spectrum to derive spectral signatures to differentiate and characterize vegetation (Goetz et al., 1985). Plant reflectance and absorption features that relate to biochemical processes' found within narrow band spectra of hyperspectral data can be diagnostic of plant health. These spectral characteristics otherwise could be masked out by conventional, broad-band multispectral remote sensing systems (Lillesand et al. 2008).

The Red Edge: Plant stress detection evaluates spectral data in regions that are either sensitive to plant photosynthetic efficiency by detecting changes in absorption and reflectance determined by plant pigment levels or through the detection of changes to physical plant structure. The most commonly studied spectral region to detect plant stress occurs on the boundary of the visible red and near infrared portion of the EM spectrum, termed the "red edge" (~700 nm - 750 nm). The red edge is a reflectance pattern in plant spectra associated with the transition from heavy *chlorophyll a* and *b* absorption in the visible light wavelengths (400 nm - 700 nm) to high reflectance in the near infrared (750 nm - 900 nm) due to the spongy leaf mesophyll (Carter and Knapp, 2001; Smith et al., 1997; Zarco-Tejada et al., 2000). Plant stress is known to degrade chlorophyll pigment absorption, increasing the reflectance of photosynthetically active

radiation in the visible region of the EM spectrum. Analysis of the red edge can detect plant stress by tracking changes in peak and trough reflectance or changes in the slope derivatives. Narrow band red edge spectral indices, in the form of ratios and derivatives, have been used repeatedly as proxy measures of stress in plants (Buschmann and Nagel 1993; Carter and Knapp 2001; Carter and Miller 1994; Demetriades-Shah et al. 1990; Gitelson and Merzylak 1996; Gitelson and Merzylak 1997; Smith et al. 2004; Strachan et al. 2002; Vogelmann et al. 1993). These hyperspectral indices have the distinct advantage of being more sensitive to smaller, subtle spectral changes than traditional broad band indices, such as the Normalized Difference Vegetation Index (NDVI) or Simple Ratio (SR). Hyperspectral techniques that use spectral information in the red edge for the proxy measurement of chlorophyll content and plant structure can therefore be used as a measure of photosynthetic activity and stress in plants.

Plant Response to Elevated Soil CO_2: Elevated soil CO_2 is known to displace oxygen at a plant's roots, causing anoxic conditions that inhibits plant respiration and inducing a stress response (Bergfeld et al. 2006; Maček et al. 2005). Vegetation could act as a "bellwether" for CO_2 leaks at a GCS site if plants exhibit a spectral stress signature in response to elevated soil CO_2. The direct detection of a CO_2 leak by discerning changes in soil CO_2 flux or soil CO_2 concentration within the range of natural background soil CO_2 variability is difficult (Lewicki et al., 2006; Lewicki et al., 2007), however, the indirect identification of CO_2 leaks through the remote detection of plant stress could be an alternative method. Hyperspectral plant signatures obtained by a ground-based field spectrometer were used to assess plant stress caused by elevated soil

CO_2 and detected a plant stress response up to 7.5 m away from a buried release pipe (Male et al. 2010). The most distinguishable plant stress signatures, however, were achieved from plants occurring within a horizontal distance of 2.5 m from a buried CO_2 release pipe (Keith et al. 2009; Male et al. 2010). Another study, investigating the effects of a subsurface natural gas leak, showed that plants within a horizontal distance of 0.5 m from the buried leak source exhibited clear signs of stress due to anoxic soil conditions (Noomen et al. 2008).

Vegetation stress responses to anoxic soil conditions have been expressed as increased reflectance in the visible red and decreased reflectance in near infrared of the red edge (Keith et al. 2009; Male et al. 2010; Noomen et al. 2008; Noomen and Skidmore 2009). The red edge has also been used in the detection of vegetation stress before it is visible to the human eye. A 5 nm – 10 nm shift of the red edge towards shorter wavelengths (called the "blue shift") has been observed and was associated with pre-visual plant stress detection (Carter 1993; Carter and Miller 1994; Rock et al. 1988). Pre-visual stress detection has implications for GCS site monitoring, because it could allow for the early identification of CO_2 leaks with hyperspectral remote sensing.

Airborne Hyperspectral Imaging for Plant Stress Detection: Leaf and canopy-level remote sensing studies have successfully detected plant stress caused by anoxic soil conditions using high spatial resolution data obtained on the ground (Keith et al. 2009; Noomen et al. 2008; Noomen and Skidmore 2009; Rouse et al. 2010). There have been fewer studies using imagery collected from airborne platforms to specifically detect plant stress. Scaling up from ground-based to aerial remote sensing can confound the process

of detecting plant stress due to changes in the illumination characteristics of a scene, the complexity of vegetation structure, and a coarser spatial resolution (Knipling 1970). Leaf-level investigations detect reflectance in the near infrared that is determined by the scattering of light energy within the airy, spongy mesophyll layer within plant leaves. Aerial investigations in contrast, detect reflectance in the near infrared that is sensitive to a wider variety of factors, including vegetation stress, shadowing caused by canopy geometry, leaf area index, plant phenology, and the influence of background reflectance of mixed pixels (e.g., soil and understory vegetation). These additional environmental variables, coupled with imaging geometry, make it difficult to separate the physiological plant stress signal of interest from other spectral influencing phenomena (Knipling 1970). Airborne hyperspectral remote sensing studies, however, have demonstrated that it is possible to detect vegetation stress at the canopy and subcanopy level (Lawrence and Labus 2003; Sampson et al. 2003).

A single hyperspectral aerial image of vegetation over a shallow CO_2 release experiment showed that vegetation exhibited a stress response to elevated soil CO_2 (Male et al. 2010). This vegetation, however, was exposed to high levels of soil CO_2 for 27 days and was visibly stressed compared to surrounding vegetation. A single date classification of extremely stressed vegetation due to prolonged exposure to elevated soil CO_2 leaves unresolved questions about the efficacy of hyperspectral monitoring and the extent that a CO_2 leak can be detected from an airplane.

Research Objectives

Several years of research has been devoted to investigating potential GCS monitoring techniques, and no single method has clearly demonstrated that it can meet the monitoring demands of a real-world GCS site because of economic and logistical concerns. Land GCS (as opposed to submarine GCS) might encompass a large area that requires a monitoring method with nearly instantaneous data acquisition and large spatial coverage capabilities. We conducted a 2010 aerial imaging campaign with a hyperspectral imager (Resonon Inc.) mounted to a small aircraft to construct a time series of images over a controlled shallow CO_2 release experiment to quantify and characterize the spectral changes to overlying vegetation in response to elevated soil CO_2.

An unsupervised classification was performed to see if locations of known CO_2 leakage could be spectrally distinguished using the ISODATA clustering algorithm. Subsequently, we extracted spectral information from the pixel clusters centrally located over regions known to leak CO_2 at the surface during injection experiments at the ZERT site to develop a new narrow band index that was sensitive to the CO_2 stress signal and could be used to compare pixel cluster index trajectories for the time series imagery. The use of an index has the distinct advantages of removing radiometric variability (i.e. weather and atmospheric differences) between imaging dates, as well as simplifying the complex high dimensionality of hyperspectral data for analytical purposes. The narrow band spectral index was then used to analyze the spectral trajectories as a function of distance from the leak source through time in order to develop a method that could be

emulated to detect a CO_2 leak around a known area of weakness, such as a well bore or geologic fault.

The goal of these analyses was to provide insight into the feasibility of indirectly identifying CO_2 leaks from GCS sites via the detection of plant stress with airborne hyperspectral imaging by elucidating the timing of CO_2 stress signal detection. Additionally, these analyses are potential remote sensing monitoring strategies that could be deployed in a real-world GCS management framework.

Materials and Methods

The Experimental CO_2 Release Site

The Zero Emissions Research and Technology (ZERT) site is a controlled CO_2 release facility located in a 12-ha agricultural field, on the western edge of Montana State University (MSU) in Bozeman, MT (45°39'N, 111°04'W) at an elevation of 1,495 m. The ZERT site is characterized by a buried horizontal release pipe that was developed to simulate a longitudinal CO_2 leak source, such as a geologic fault or a weakness in a geologic capstone atop a subsurface reservoir, in order to study potential monitoring tools for GCS technology. The site is on a relatively flat alluvial plain that consists of thick sandy gravel deposits overtopped by several meters of silts, clays, and topsoil (Mokwa 2006). The buried release pipe is 98-m long with an inner diameter of 10.16-cm and is oriented 45° east of true north. The central 70-m of the pipe is perforated to seep CO_2 during injection. A series of packers were placed within the release pipe to assist in dispersing the gas evenly along the slotted portions of the release pipe (Figure 3.1). The

pipe was buried using a horizontal drilling technique that minimized disturbance to the surface environment, however, the pipe installation was deflected from a perfectly straight path because of cobble in the gravel layer underground. The surface vegetation is primarily composed of a variety of perennial and annual grasses, alfalfa, dandelion, and thistle.

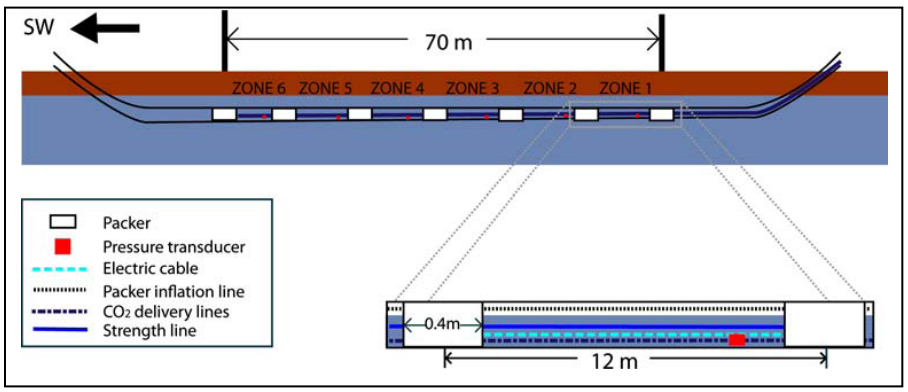

Figure 3.1: A cross-section of the buried release pipe at ZERT (Spangler et al. 2009). Zones 1-3 were injected with CO_2 at a rate of 0.2 ton/day (=34.8 kg/day) from June 3, 13:20 to June 24, 14:25 for the June, 2010 release experiment.

Patterns of CO_2 Movement from a Buried Release Source

Release experiments at the ZERT site have simulated various GCS leak scenarios to investigate different monitoring tools for quantification and characterization of CO_2 leaks since 2006 (Lewicki et al. 2006; Lewicki et al. 2007; Lewicki et al. 2010; Male et al. 2010; Oldenburg et al. 2010; Rouse et al. 2010; Spangler et al. 2009; Strazisar et al. 2009). Research at ZERT has demonstrated that CO_2 injected into the buried release pipe tends to aggregate into local "hot spots" at the surface (Lewicki et al., 2007; Lewicki et al., 2010; Oldenburg et al., 2010). It is theorized that this pattern of movement is caused by small changes in elevation of the release pipe due to immovable cobble in the

subsurface soil and due to soil permeability above the pipe. CO_2 is thought to move from areas of lower to higher elevation within the pipe until the CO_2 is forced upwards by the inserted pipe packers. The CO_2 then follows a path of least resistance to the surface. The CO_2 hotspots have been mapped by accumulation flux chambers (Lewicki et al. 2007; Lewicki et al. 2010; Spangler et al. 2009) and have been detected spectrally (Keith et al. 2009; Male et al. 2010). The original intent of the release experiments was to have a uniform pattern of release, however, the patchy nature of the surface CO_2 might more closely mimic the conditions of real world GCS sites where faults or wellbores would mostly be sealed and escaped CO_2 would follow discrete pathways (Lewicki et al. 2007).

Previous CO_2 flux maps show that the CO_2 hotspots tend to be centered directly over the release pipe and remain relatively unchanged with respect to size and location (Lewicki et al. 2007; Spangler et al. 2009; Lewicki et al. 2010). We assumed, therefore, that these CO_2 flux maps could be used as reference for the 2010 aerial imaging campaign given that no ground data were collected in order to minimize surface disturbance that could bias our analysis. The CO_2 hotspots originated above the pipe packers with the injected CO_2 radiating outward from the center to form areas of pooled CO_2 that are 2 to 5-m in diameter.

2010 Aerial Imaging Campaign

The three-week CO_2 injection experiment commenced on June 3, 2010 at 1320 hours. CO_2 was injected at a rate of 0.2 ton/day (=34.8 kg/day) into zones 1, 2, and 3 in order to mimic a seepage rate less than the 0.01% leak threshold proposed by Benson et al. 2005 (Figure 3.1). Zones 1, 2, and 3 are sections of the perforated release pipe divided

by the first four packers placed at 12 m intervals. The CO_2 injection was terminated on June 24, 2010 at 1425 hours.

We collected eight aerial images with a Pika II hyperspectral imager (Resonon Inc.) mounted above a viewing hole in the fuselage of an airplane. The airborne imaging commenced over the ZERT site before, during, and after the three week CO_2 release (Figure 3.2). Spectral data were collected in 80 bands throughout the visible and near infrared (NIR) wavelengths (424 nm – 929 nm), each with a 6.3-nm channel width. The radiometric resolution of the Pika II sensor was 12-bit quantization at 60 frames per second. The spatial resolution was approximately 0.3 meter from the airplane platform at an approximate imaging altitude of 600 m above ground level.

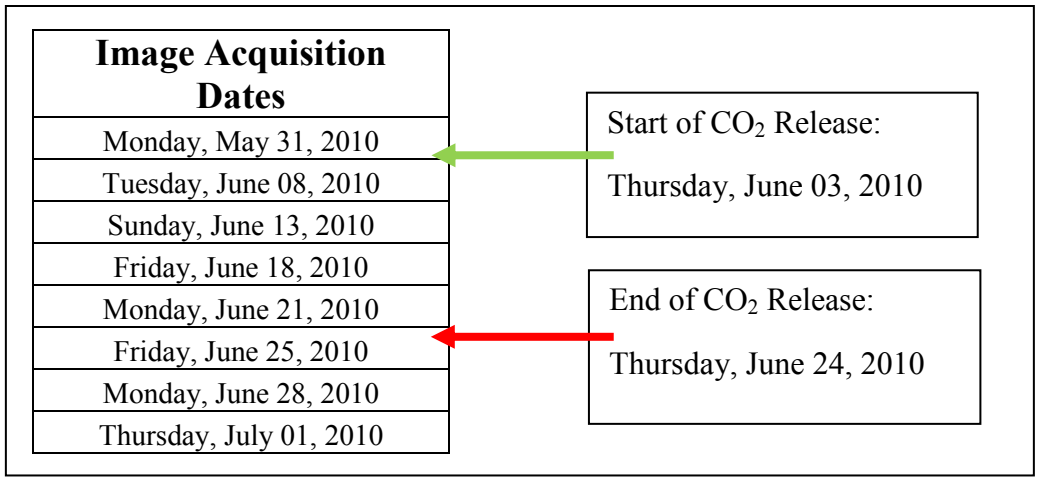

Figure 3.2: Image acquisition dates.

The Pika II was connected to a Resonon PCAQ data acquisition flight computer and an Athena Inertial Navigation System (INS) (Figure 3.3). The flight computer was programmed with the UTM coordinates of the ZERT site, which indicated to the imager

when to begin and end recording. The INS incorporated spatial reference data collected from a Wide Area Augmentation System (WAAS) corrected global positioning system (GPS) and an Inertial Measurement Unit (IMU) to provide geographical position and platform altitude.

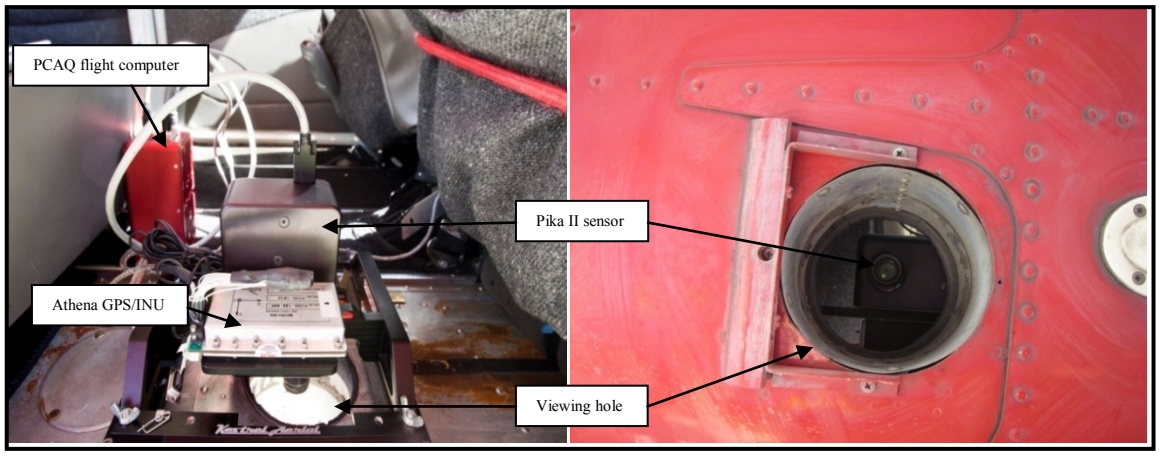

Figure 3.3: Sensor setup in the aircraft.

Image acquisition protocol considered three major factors that determine image quality: (1) the bidirectional reflectance function (BRDF); (2) clouds and particulate matter interference; and (3) image distortions due to turbulence. Morning image acquisition was preferable, given that afternoon thunderstorms, cloud formation, and wind were common obstacles to obtaining quality images. Morning dew consistently covered vegetation at this location, however, which could dramatically affect the spectral characteristics of the imagery. Imagery was collected, therefore, at approximately 1200 hours on each image acquisition day, which allowed the vegetation enough time to dry out and avoided afternoon storm events. Each image was acquired perpendicular to the CO_2 release pipe with a flight approach bearing of 135° SE of true north. This flight

orientation ensured that the sun angle was parallel to the flight path to limit shadowing effects that influence BRDF.

Tropospheric turbulence is known to greatly influence the stability of an aircraft platform. Images can be skewed due to pitch, roll, and yaw of an aircraft, further complicating the geometric correction process of aligning pixels to ground control points. One of the greatest influences of image distortion is due to the roll motion of an airplane (Jensen et al. 2008), therefore, images were collected with a flight orientation that was directly perpendicular to the release pipe to minimize distortions to the linear position of the buried release pipe. The ZERT site was characterized by nearly uniform vegetation cover with few positively identifiable ground points to use for correcting beyond the internal geometric corrections provided by the Athena INS (Figure 3.4). 22 tarps, therefore, were placed at 10-m intervals around the 20-m periphery of the pipe and one more was placed 2 m from the southwest end of the pipe to provide additional identifiable ground control points to aid in geometric correction. The inner two vertices of each tarp (towards the pipe), the pipe ends, and the corners of a semi-permanent storage shed and a temporary scaffolding were geolocated using a survey-grade Trimble R8 GPS receiver with RTK ("real-time kinematic") corrections from the MSU Continuously Operating Reference Station (CORS) to achieve sub-cm accuracy. Several flight passes were made on each image acquisition day to ensure that some cloud shadow-free, full coverage images were obtained for each date. Imagery was collected on May 31, prior to the CO_2 release, to provide a baseline comparison for subsequent imagery of vegetation exposed to elevated soil CO_2. Imagery was also collected after the

termination of the CO_2 release on June 25, June 28, and July 1 to investigate the lingering effects of elevated soil CO_2 and the possibility of a vegetation recovery response.

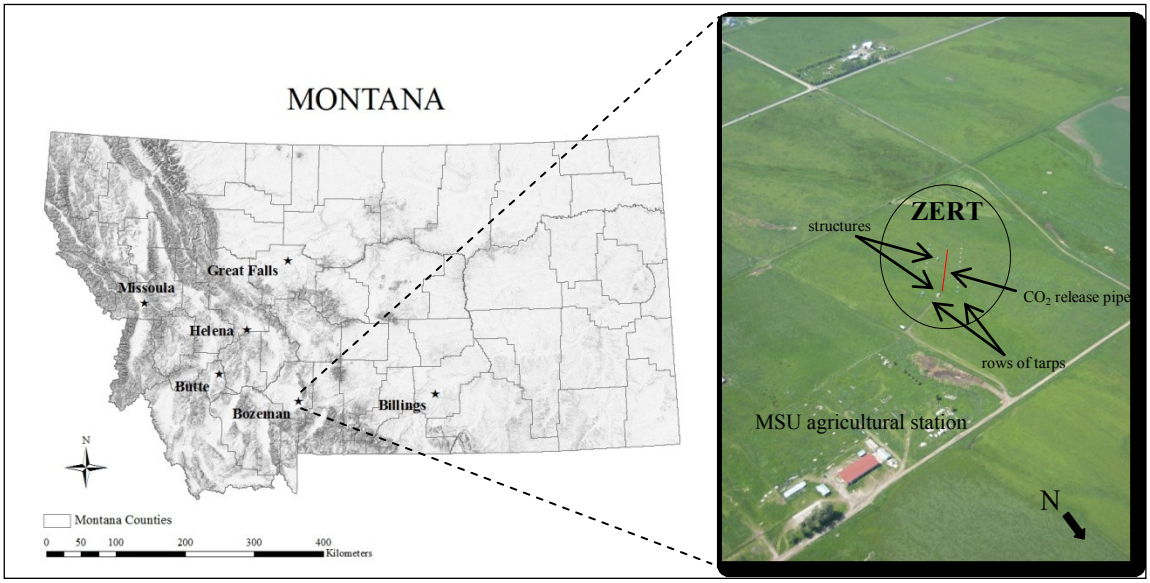

Figure 3.4: Location of the study area in Bozeman, MT, and an aerial view of the ZERT site.

Data Analysis

Image Preprocessing: Acquired raw imagery were filtered to select images that were both cloud and shadow free, as well as contained the entire CO_2 release zone. A single image was chosen for each acquisition date for further analysis. Radiometric corrections were performed by focusing the Pika II sensor into a Gooch & Housego OL Series 455, a National Institute of Standards and Technology (NIST) traceable, calibrated light source that utilizes an integrating sphere to obtain reference spectral response information. Spectral data for every pixel from acquired images were then cross-referenced to the 'radiometric correction cube' to obtain a multiplier used to correct for

the various gain and shutter settings used by the imager on the different image acquisition dates. The resultant spectral data were given in radiance, in units of microflicks (μf).

Images were then geometrically corrected using the Resonon GeoReg processing software for aligning each pixel to geographic longitude and latitude coordinates. The software integrates data collected by the Athena INS for each image, from each flight, to align the imagery with ground coordinates. This process achieved approximately 3-m spatial accuracy. Further geometric correction was performed by referencing a single image (June 25) to the 56 GPS surveyed ground control points. The other images subsequently, were geo-referenced by registering each individual image to the reference image to achieve sub-meter geometric accuracy. All images were corrected using a 1^{st} order polynomial model within ERDAS Imagine using nearest neighbor resampling (Table 3.1).

Each of the images was cropped using an area of interest (AOI) within the tarp boundary to isolate the north end of the pipe where the CO_2 release occurred. The northeast pipe end was masked out to produce images that contained only vegetation pixels. Given the high spatial and spectral resolution of hyperspectral imagery, the image subset reduced computer processing time and produced images that were of the same spatial extent for each acquisition date. The resultant eight cropped images contained a rectangular area that was approximately 52 m long by 35 m wide.

Table 3.1: Summary of each image's spatial resolution and positional error results from the 1st order polynomial geometric correction models using nearest neighbor resampling. GCPs were chosen for accurate identification on both the reference and registered images, therefore, the number of GCPs varied slightly for each date. Each date was resampled using ≥ 50 GCPs.

Reference Image			
Date	**Spatial Resolution (m)**	**# of GCPs**	**Total RMSE (pixels)**
June 25	0.34	56	0.2337
Registered Images			
Date	**Spatial Resolution (m)**	**# of GCPs**	**Total RMSE (pixels)**
May 31	0.37	50	0.2500
June 8	0.34	54	0.9422
June 13	0.33	55	0.6239
June 18	0.36	51	0.5731
June 21	0.33	51	0.4842
June 28	0.36	52	0.4267
July 1	0.34	50	0.4053

Hot Spot Analysis: This study attempted to emulate the steps involved in the detection of a hypothetical leak from a GCS site without knowledge of the precise location of a CO_2 surface leak. GCS will potentially pump many megatons (Mt) of CO_2 into large subsurface geologic features that can range in size up to 200 km^2. Remote sensing has the advantage of being able to monitor large areas with practical cost and time requirements. A GCS site manager might be charged with monitoring these large areas for surface leakage with minimal expert knowledge. Geospatial data might be limited to the location of existing geologic faults and wellbores in the area—the most likely loci for leak occurrence. For these reasons, we attempted to identify regions of plant stress caused by elevated soil CO_2 concentrations by performing an unsupervised classification for each image acquisition date.

The Iterative Self-Organizing Data Analysis Techniques Algorithm (ISODATA) used in the unsupervised classification (ERDAS Imagine®) was performed using a 0.99 convergence threshold and a maximum of 100 iterations to create 20 vegetation clusters for each image. The clusters that contained pixels above the CO_2 release source were further divided by performing a second unsupervised classification to separate healthy and stressed pixels of convoluted clusters. Otherwise the clusters were classified as healthy. The second unsupervised classification used the same thresholding as the first and resulted in 20 final clusters for each image. Each of the resultant 20 clusters was then designated as one of four classes using a qualitative coding scheme. Previous flux maps at ZERT (Lewicki et al. 2007; Lewicki et al. 2010; Spangler et al. 2009) have shown that the CO_2 tends to pool in "hot spots", concentrated areas located above the packers placed in the release pipe to create stratified release zones. It has also been shown that the injected CO_2 does not migrate outside of a 10-m radius from the CO_2 release pipe. Considering this, pixel clusters for each date were coded as the following vegetation classes: severe stress (red) if 100% of the cluster pixels occurred within 2-m of the release pipe; moderate stress (orange) if 100% of the cluster pixels were within 5-m from the pipe; low stress (yellow) if 100% of the cluster pixels were within 10-m of the release pipe; and healthy (not coded) if any of the cluster pixels were further than 10 m away from the release pipe. Spectral information was extracted for all the pixels contained within each of the vegetation stress classes. A companion stratified random subset of healthy vegetation pixels, equal in pixel count to the most severe vegetation stress class coded for that date, within each scene was collected. Spectral information for

each of the 80 Pika II bands was then extracted and averaged for each CO_2 stress class and each companion subset of healthy pixels to compare spectral signatures of healthy and CO_2 stressed vegetation for each image. It was assumed that vegetation within pixel clusters closer to the CO_2 release pipe would exhibit more stress than those clusters that were further away.

A spectral index was developed based on the unsupervised classification results that separated pixel clusters known to be associated with CO_2 leakage and those that were not, to amplify the CO_2 stress signal and to chart plant stress trajectories for the ZERT imaging time series. This index ratioed the peak and trough radiance values of the red edge to create the red edge index (REI), an index sensitive to both chlorophyll absorption in the visible red (the trough) and physical vegetation changes (e.g., leaf area index and canopy geometry) in the near infrared (the peak). The REI, therefore, is a proxy spectral indicator of vegetation stress and allowed for the evolution of the CO_2 stress signal to be evaluated at the ZERT site over the course of the release experiment. The REI for healthy vegetation was expected to be greater than the REI for CO_2 stressed vegetation. The difference in REI ($REI_{\text{healthy vegetation}} - REI_{\text{CO2 stressed vegetation}}$) would be significantly greater than zero (Welch's p-value < 0.05) if elevated soil CO_2 concentrations caused a vegetation stress signal in REI that was statistically distinct from healthy vegetation. Statistical significance is sample size dependent and can be influenced by spatial autocorrelation between pixels that can cause type I error, however. The difference would not be significantly different if the stressed and healthy vegetation were not spectrally distinct and of the same population. Vegetation was expected to exhibit more

stress as the CO_2 injection progressed, that is the difference in REI should increase with longer exposure to injected CO_2, and vegetation should not exhibit further stress after the termination of the CO_2 release, that is the difference in REI should stay the same or decrease once the CO_2 injection ceased.

Proximity Analysis: Plant spectral response was examined as a function of distance from the CO_2 release pipe for the ZERT aerial imagery time series. GCS site managers might have *a priori* knowledge of areas susceptible to potential CO_2 leakage, such as existing wellbores and geologic faults, therefore, the proximity analysis is a relevant methodology for monitoring around these loci. GPS survey points were used in conjunction with the INS data to correct the images to sub-meter positional accuracy on the ground, however, this was insufficient for tracking changes in individual pixels through time. Variable turbulence during image acquisition flights also caused altitude to be inconsistent resulting in different spatial resolutions for each imaging date (Table 1). The REI that was developed from the hotspot analysis was therefore used to assess vegetation stress levels by comparing pixels that were closer to the CO_2 release pipe with pixels that were further away for each image date by using different radius buffer delineations around zones 1-3 of the buried release pipe (Figure 3.5). Mean REI was calculated for the pixels that were inside each buffer radius (closer to the CO_2 release source referred to hereinafter as release zone pixels) and compared with the mean REI of pixels that were outside each buffer boundary (further away from the CO_2 release source referred to hereinafter as healthy zone pixels). Spectral trajectories were then developed

by charting mean REI through time in order to track changes in vegetation stress response to elevated soil CO_2 concentration over the course of the experiment.

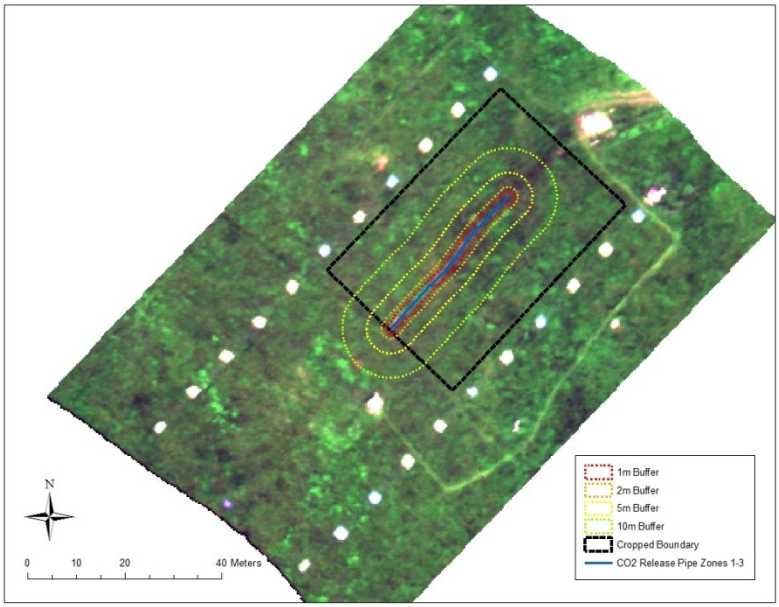

Figure 3.5: Study design of the 2010 ZERT aerial imaging campaign. Aerial hyperspectral image displayed in true color with the cropped boundary of vegetation used in both analyses for all image dates along with the different radius buffer boundaries used in the proximity analysis.

Results

Hot Spot Analysis

The results of the unsupervised classification identified areas of vegetation stress in 7 of the 8 imaging dates (Table 3.2). June 8 was the first image collected after the CO_2 release began and on this day (5 days after the initiation of the CO_2 injection) CO_2 stress in vegetation was classified. July 21 was the final imaging day before the CO_2 release was terminated and it contained the most vegetation stress clusters with 5 of the 20 clusters in the final classification meeting the criteria for moderate and severe vegetation

stress. The July 21 image also contained the largest total area of vegetation stress (16.33 m^2). The CO_2 injection was terminated on June 24. Vegetation stress caused by elevated soil CO_2 concentrations continued to be classified more than 1 week after the CO_2 injection stopped, although the total area shrank to 6.70 m^2 (Table 3.2).

Table 3.2: Number of vegetation stress clusters included within each vegetation stress class and the area (m^2) contained therein from the unsupervised classification results in the hot spot analysis.

VEGETATION STRESS CLASSES				
Date	**Severe Stress Class (Area in m^2)**	**Moderate Stress Class (Area in m^2)**	**Low Stress Class (Area in m^2)**	**Total # of Stress Clusters (Total Area in m^2)**
5/31	0 (0)	0 (0)	0 (0)	0 (0)
6/08	1 (1.73)	1 (6.82)	0 (0)	2 (8.55)
6/13	0 (0)	0 (0)	1 (3.59)	1 (3.59)
6/18	1 (4.02)	0 (0)	0 (0)	1 (4.02)
6/21	2 (3.81)	3 (12.52)	0 (0)	5 (16.33)
6/25	1 (4.39)	0 (0)	1 (6.24)	2 (10.63)
6/28	1 (3.63)	0 (0)	0 (0)	1 (3.63)
7/01	1 (6.70)	0 (0)	0 (0)	1 (6.70)

Visual interpretation of the unsupervised classification results showed that the areas first classified as severe vegetation stress in the June 8 image are the same areas that reappear and persist throughout the time series as severe stress in five of the six subsequent images (Figure 3.6). These areas of severe vegetation stress generally grew in area and remained consistent in location for the duration of the aerial campaign. There was a high degree of spatial correlation between these areas of severe vegetation stress and the mapped CO_2 hotspots (regions of high CO_2 flux) derived from CO_2 flux measurements obtained on the ground from a previous CO_2 release experiment (Figure 3.7).

The mean spectral signatures for each vegetation stress class were compared for each image date and revealed patterns of vegetation spectral response to the CO_2 release over the course of the experiment (Figure 3.8). Radiance increased in the visible portion of the EM spectrum for the severely stressed vegetation classes, while the low and moderately stressed vegetation classes exhibited slightly lower radiance values, as compared to healthy vegetation. All of the stress classes do converge and exhibit a similar response in the near infrared. The red edge was not observed to shift towards shorter wavelengths for CO_2 stressed vegetation. Red edge mean peak radiance decreased and mean trough radiance increased for the severe vegetation stress class as compared to the healthy vegetation class. Severe vegetation stress responses within the peak and trough radiance values of the red edge were inversely related, and therefore, were used to develop an index (Figure 3.9). The REI was a ratio of peak radiance at 750 nm (Pika II band 52) and trough radiance at 674 nm (Pika II band 40) to amplify the vegetation stress signal caused by elevated soil CO_2 concentration (Equation 3.1).

A stress signal was detected after the CO_2 injection began with the difference in REI ($REI_{\text{healthy vegetation}} - REI_{\text{CO2 stressed vegetation}}$) being significantly greater than zero (Welch's *p*-value < 0.001) for all dates that contained a severely stressed vegetation class. The difference in REI increased until the termination of the CO_2 release, after which the difference between the healthy and severely stressed classifications diminished, albeit still spectrally distinguishable (Figure 3.10).

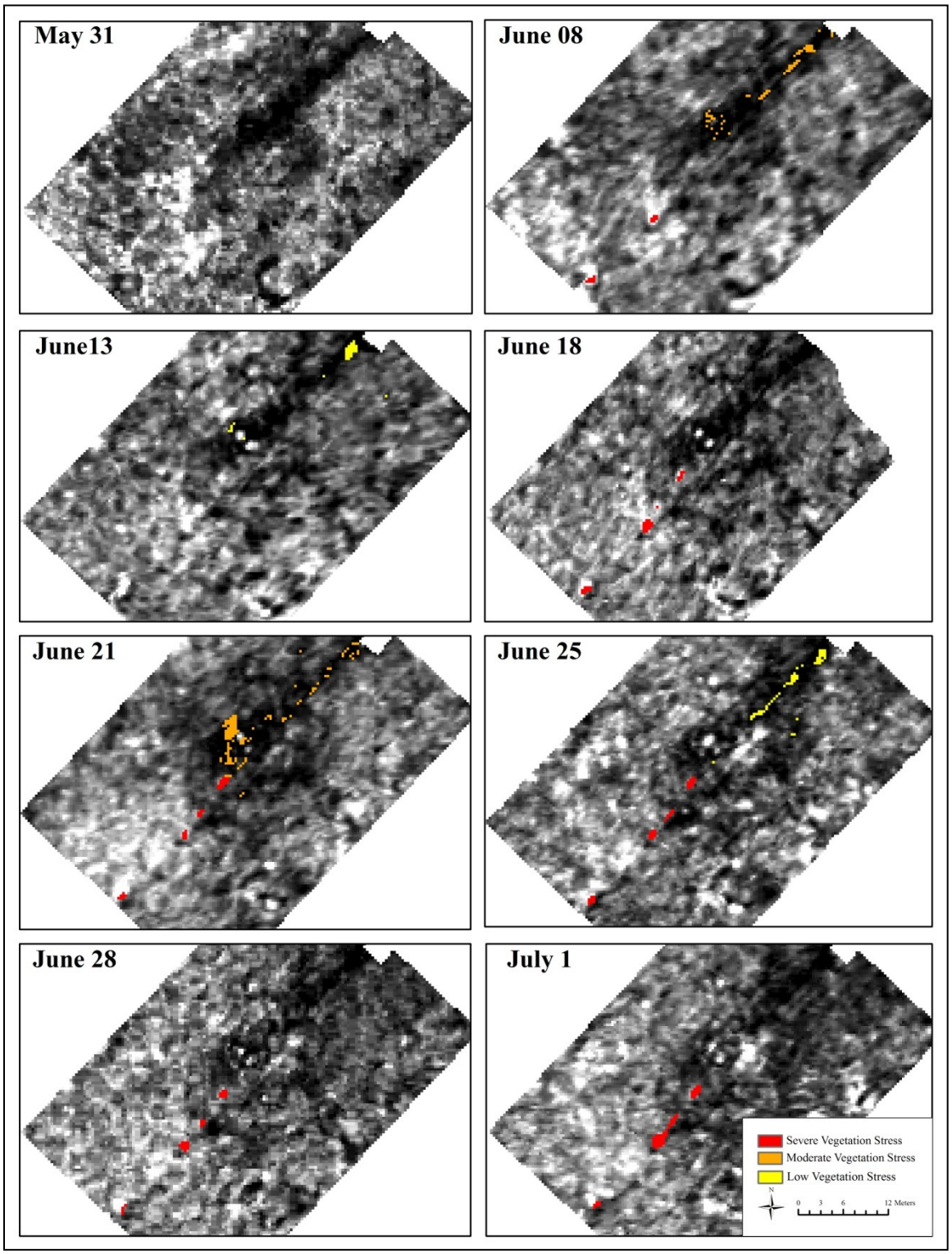

Figure 3.6: Unsupervised classification results for ZERT time series. Images are displayed with a green band (band 21: 552 nm) in grayscale.

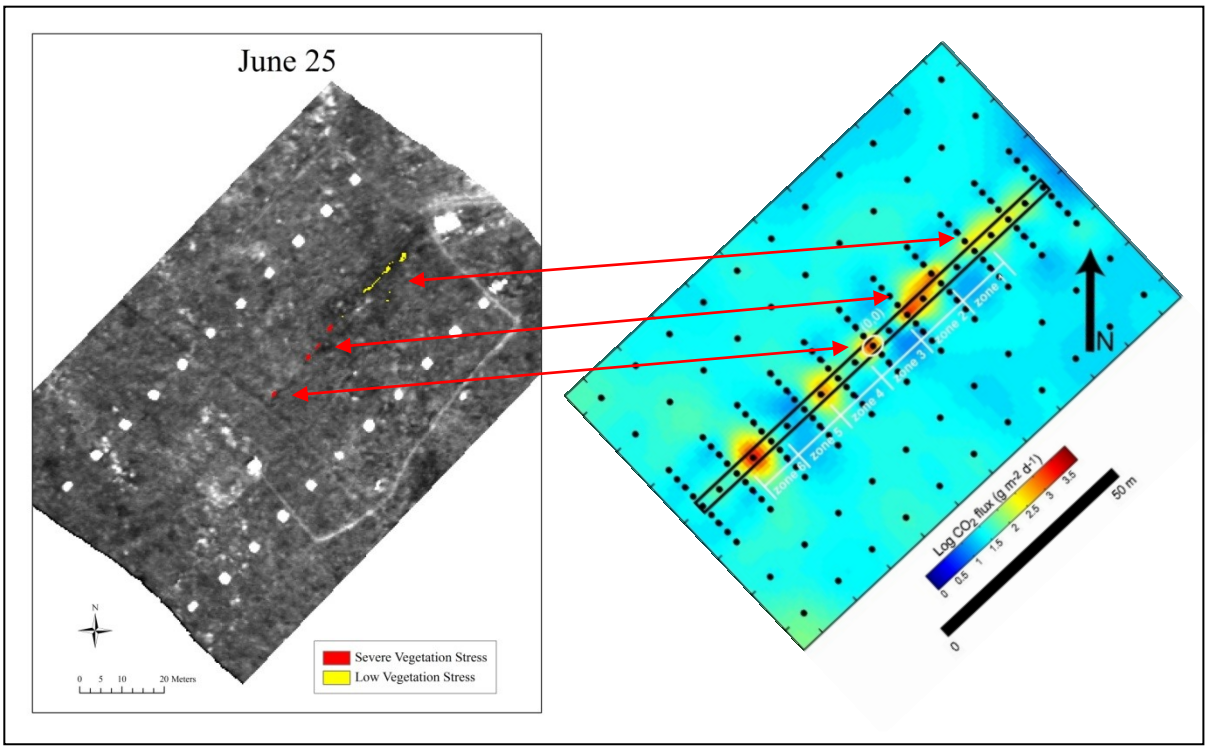

Figure 3.7: Illustration of the high degree of spatial correlation of the hot spot locations between the June 25 unsupervised classification result (left) and a CO2 flux map derived from accumulation chamber ground measurements made on July 30, 2008 at the black dots (right). (Note that the unsupervised classification only included analysis of zones 1-3, whereas the flux map was derived during an injection into zones 1-6. Flux map adapted from Spangler et al. 2009)

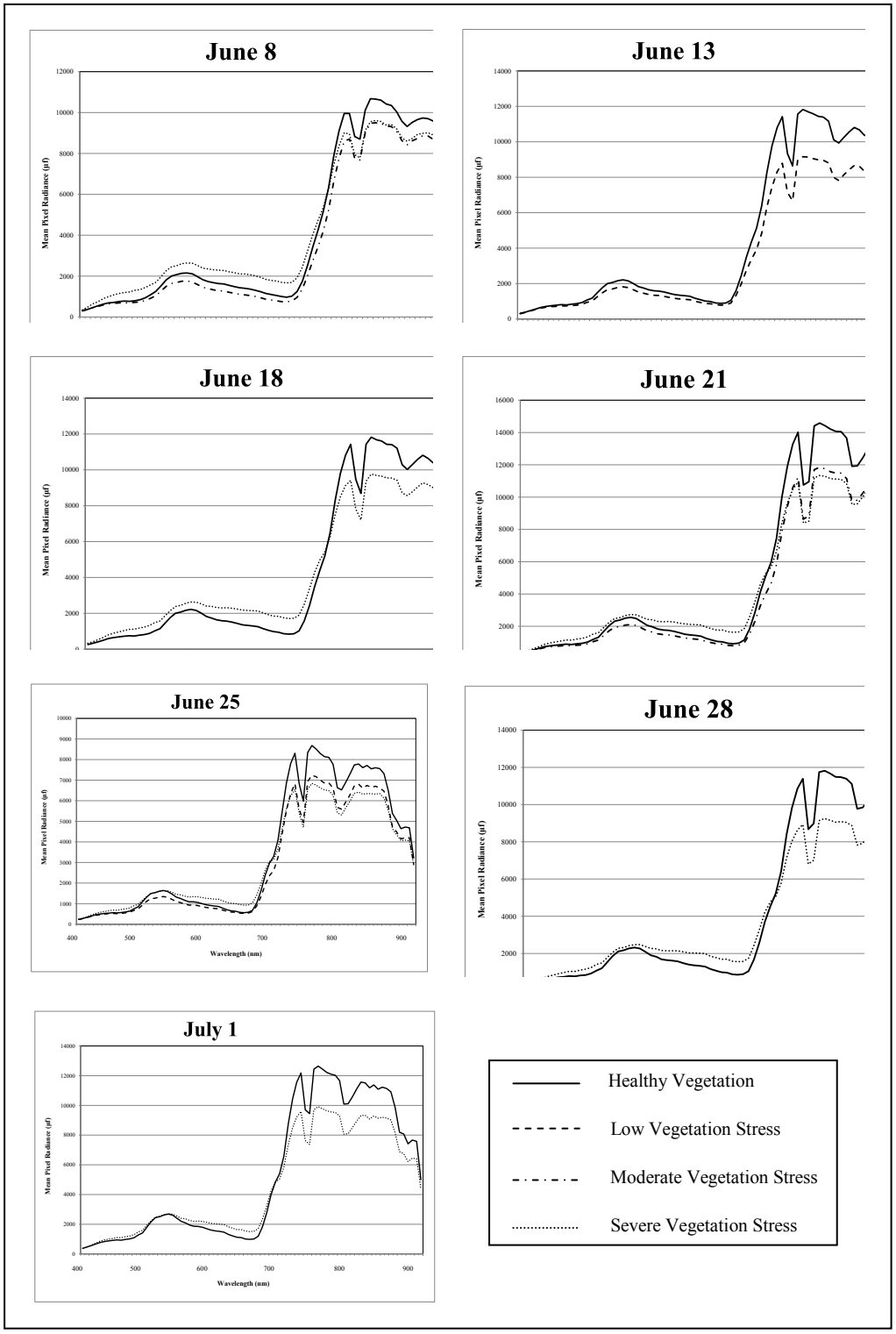

Figure 3.8: Spectral signature comparisons for the unsupervised classification time series. The plotted spectral data is the mean radiance (µf) for each vegetation stress class and the randomly selected pixels classified as healthy for each date.

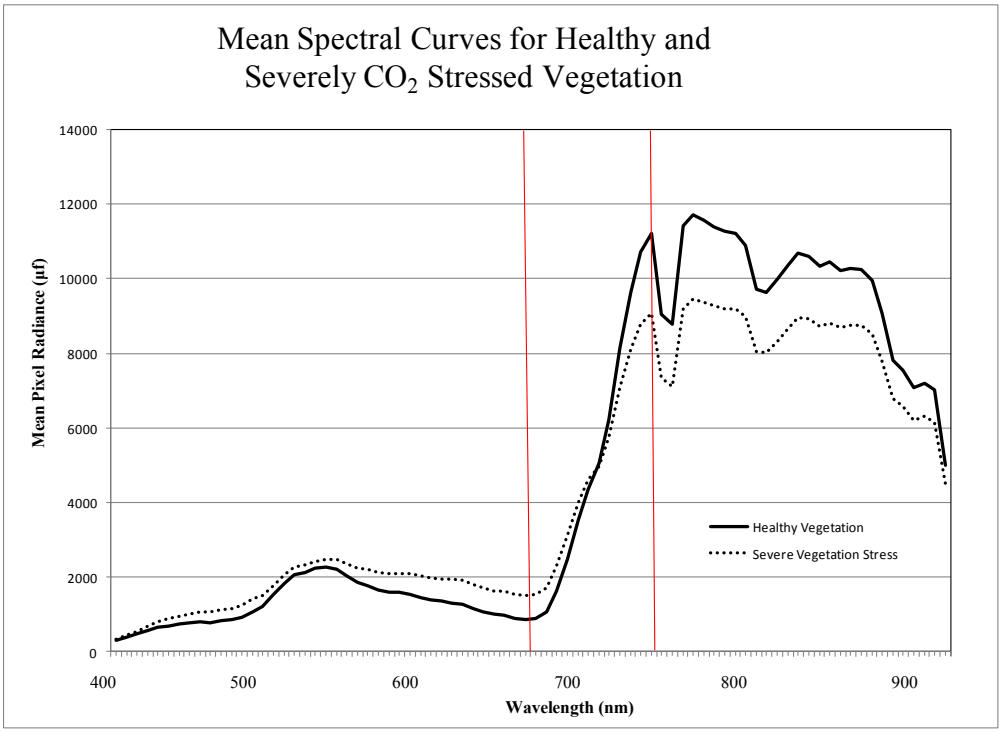

Figure 3.9: Mean spectral signatures for all pixels classified as severe vegetation stress and their randomly selected companion healthy pixels for the ZERT time series imagery in mean radiance (µf). The red lines indicate the peak (674 nm) and trough (750 nm) of the red edge, which were used to develop the spectral index (the REI) used as an indicator of vegetation stress caused by elevated soil CO_2 concentrations.

$$Red\ Edge\ Index = \frac{peak\ radiance\ (nir)}{trough\ radiance\ (red)} = \frac{radiance\ (750\ nm)}{radiance\ (674\ nm)}$$

Equation 3.1: Red Edge Index (REI) equation.

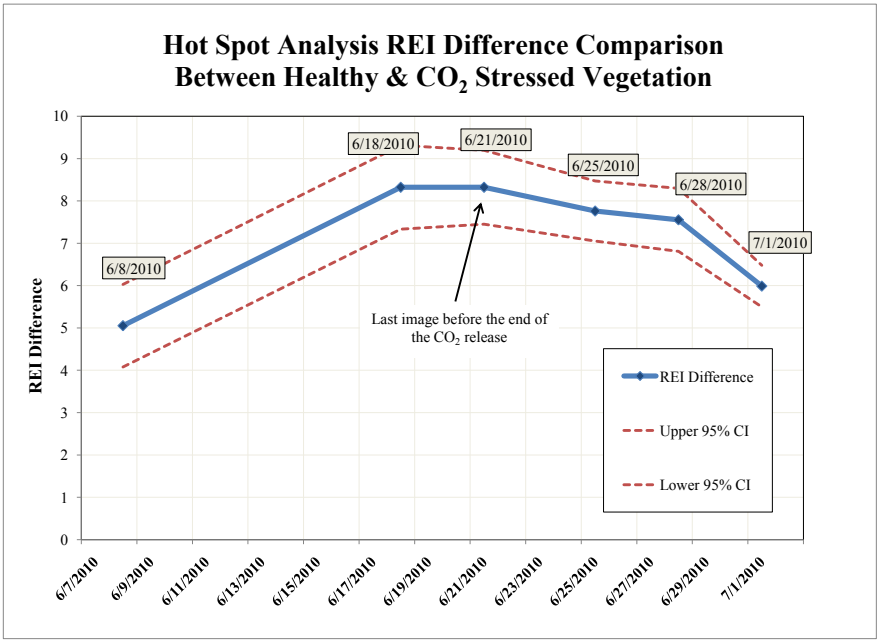

Figure 3.10: Difference in REI (REI $_{\text{healthy vegetation}}$ - REI $_{\text{CO2 stressed vegetation}}$) between healthy and severely stressed vegetation classes from the unsupervised classification hot spot analysis.

Proximity Analysis

The proximity analysis results for each of the different buffers were mostly consistent with our expectations for a vegetation stress response to elevated soil CO_2. The expectation was that the REI should be higher for the healthy zones as compared to their companion release zones, however, this was the case only later in the CO_2 release (Figure 3.11). Prior to CO_2 injection, on May 31, all release zone pixels for all buffers (closer to the buried CO_2 release pipe) actually exhibited a greater REI than the healthy zone pixels. REIs of the vegetation pixels contained within the release zone were significantly lower (Welch's p-value < 0.001) than those outside at the height of the CO_2 release.

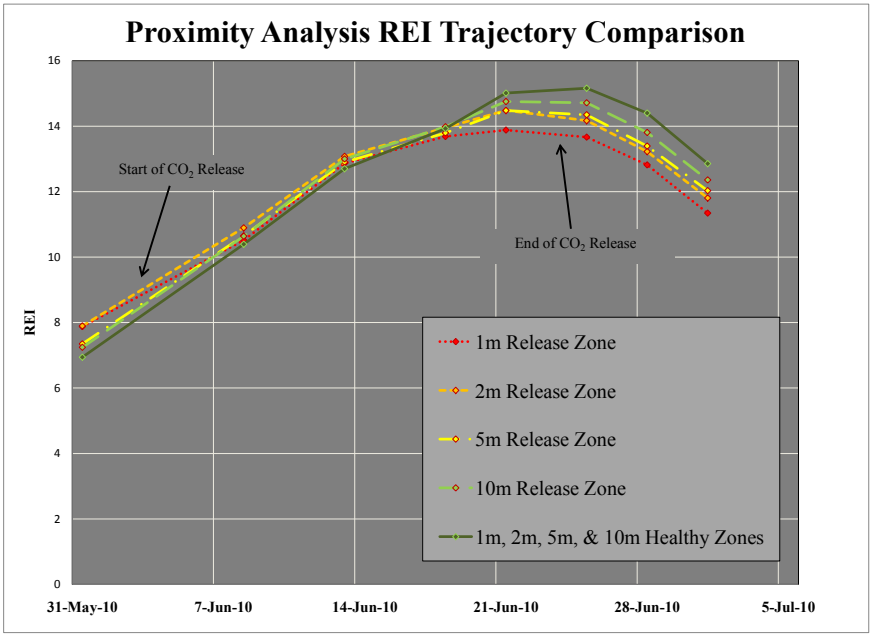

Figure 3.11: REI comparison for the different buffer radii around the CO2 release pipe. Each horizontal distance buffer radius is compared to the surrounding pixels for each image date. Note all of the healthy vegetation (or pixels outside the release zone buffers) overlap, indicating spectral similarity in REI.

The smaller the fixed radius the faster the rate of divergence in REI, indicating that pixels in closer horizontal proximity to the buried CO_2 release source exhibited more vegetation stress (Figure 3.12). The vegetation stress signal caused by the CO_2 release diminished as the buffer radius increased in horizontal distance from the buried CO_2 release source. Even though the regression models show linear upward trends of divergence as a function of time, every buffer radius exhibited a drop in REI difference on July 1.

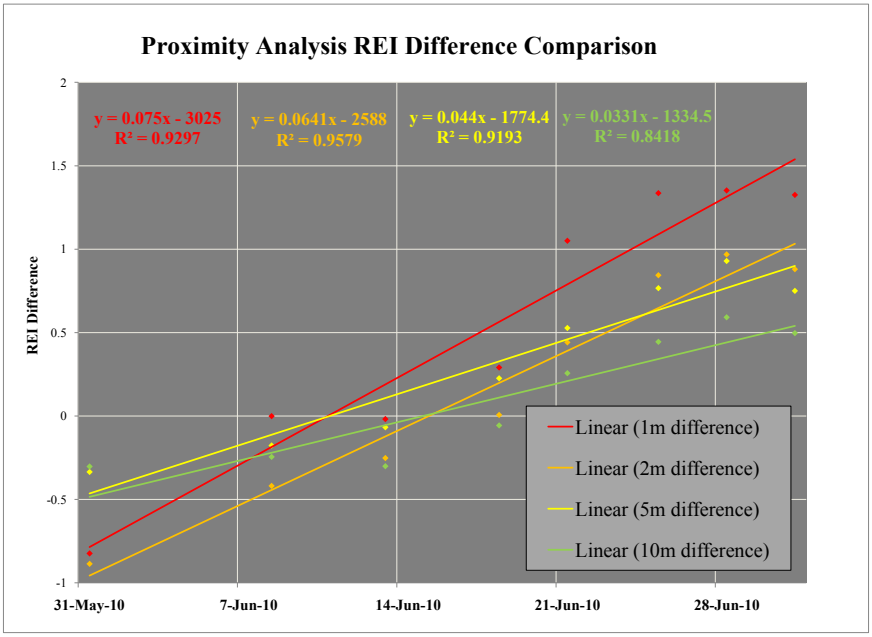

Figure 3.12: Differences in REI between buffer release zones and the corresponding companion healthy zones (pixels outside the buffer). Fitted linear regression models for each buffer distance show trends in slope, indicating rates of health divergence.

Discussion

Hot Spot Analysis

The hot spot analysis of the aerial imagery obtained at the ZERT site demonstrated the ability to detect a buried CO_2 leak expressed as plant stress at the surface even if the exact location is not known *a priori* using an unsupervised classification clustering algorithm. The locations of the severely stressed vegetation class corresponded well with known hot spot locations on previous CO_2 flux maps (Lewicki et al. 2007; Lewicki et al. 2010; Spangler et al. 2009). It is likely that this pattern of CO_2 movement would mimic the movement of CO_2 leaked from a GCS site because the upward migration of injected CO_2 will follow paths of weakness, which will likely be

isolated points of geologic inconsistency given that sequestration sites will be chosen for their geologic integrity (Lewicki et al. 2007).

Analysis of the May 31 image provides a baseline of the pre-release status and overall characterization of the ZERT vegetation before CO_2 injection began. It was important that all subsequent analysis was compared to the initial health of the vegetation above the CO_2 release zones because there was the potential for residual effects from previous CO_2 release experiments that could have influenced vegetation spectral characteristics at the ZERT site. The May 31 image did not contain pixel clusters that qualified for any of the stress classes from the unsupervised classification results because it was obtained prior to the CO_2 release. The June 8 unsupervised classification result discerned severely stressed vegetation at the location of the two major hot spots that have repeatedly been observed above zones 1 and 2 during prior CO_2 release experiments. We did not observe a shift in the red edge towards shorter wavelengths for stressed vegetation, presumably because the 6.3 nm spectral resolution of the Pika II sensor was not fine enough to discern a subtle blue shift of the red edge feature that has been associated with pre-visual plant stress detection (Carter, 1993; Carter and Miller, 1994; Rock et al. 1988). The accurate identification of these hot spots occurred only five days after the CO_2 injection began, however. At this time there were no visible changes to vegetation observed from the airplane over the ZERT site and this was perhaps evidence of pre-visual vegetation stress detection with a hyperspectral imager. The hot spots persisted in the unsupervised classification results from subsequent imagery and increased in size from the time of initial detection, except for the June 13 classification

where the hotspots were confused with a small area of vegetation that was located more than 10-m from the release pipe, and therefore, they were not mapped. This vegetation that caused the confusion was potentially stressed by something other than CO_2, such as human trampling or from deer bedding down at night.

The REI trajectories through the image time series illustrated the initial detection of the CO_2 stress signal on June 8 and the amplification of the CO_2 stress signal as the injection progressed with the hot spots being most discernable after two weeks of elevated soil CO_2 exposure on June 18 and June 21. The REI trajectories also illustrated the subsequent abatement of the CO_2 stress signal in the June 25, June 28, and July 1 images after the termination of the CO_2 injection on June 24, perhaps indicating vegetation recovery. The difference in REI of the randomly selected healthy pixels and the severely stressed pixels for each unsupervised classification result were decreasing with time after the CO_2 injection ceased. This would be consistent with a vegetation recovery, but could be attributed to a synchronous plant senescence event that would cause a disproportionate spectral response in the healthy vegetation pixels. This response would then cause "healthy" pixels to more closely resemble the CO_2 stressed pixels.

Proximity Analysis

The curvilinear time series trend of REI for all of the vegetation pixels demonstrates increasing plant vigor for all pixel groups until June 21, when the REI begins to tail off. This pattern is likely due to both seasonal plant phenological events, as well as responses to local weather. There were only eight rain-free days during the 2010 aerial campaign, and the average daily high temperature at the ZERT site was steadily

climbing throughout the course of the experiment (Figure 3.13a & 3.13b). Due to the relatively wet weather and increasing temperature for Bozeman, MT, this trend in REI was most likely related to vegetation moisture content as the vegetation at ZERT was drying out by the end of June. Although REI is sensitive to plant vigor as well as plant stress, the stress signal might be isolated by comparing the REI of pixels affected by the CO_2 release to those that were either not affected by the CO_2 release or were further from the release pipe.

The proximity analysis of the different radius buffers surrounding the buried CO_2 release pipe at ZERT provided a method that a GCS site manager could use to examine imaged vegetation pixels surrounding potential point or line sources of leakage, such as a well bore or a geologic fault, for CO_2 stress signals. The REI trajectories for the time series were congruent with a comparatively greater stress response for smaller buffer radii as compared to their companion pixels surrounding the buffers, meeting the expectation that pixels closer to the CO_2 release pipe were more spectrally distinct from pixels that were further away. Differences in mean REI between the healthy and stressed pixel groups prior to the CO_2 release was negative, which would imply that the release zone pixels were initially 'healthier' than the healthy zone pixels (Figure 3.12). This difference was most likely attributable to variability in phenological expression and species composition at the ZERT site. The differences in REIs were positive, however, for the 1 m, 2 m, and 5 m buffers beginning June 18, and for the 10 m buffer beginning June 21. More importantly, the differences in REI for the different radii all showed a clear upward linear trend with the smaller radii exhibiting comparatively steeper slopes.

This was indicative of a progressively greater rate of divergence in REI between healthy and release zone pixels. Notwithstanding the non-uniformity of the ZERT vegetation structure, these trends are consistent with a vegetation stress response to elevated soil CO_2. The proximity analysis corroborates the results of the hot spot analysis. The CO_2 stress signal was first detected on June 8, given the immediate upward trend of the differences in REI for all of the different radius buffers. It continued to be registered and increased as the CO_2 injection progressed. All of the different radii exhibited a drop in REI difference between healthy and release zone pixels by July 1, perhaps indicating vegetation recovery after the termination of the CO_2 injection.

These results were consistent with an early remote detection of a CO_2 leak in vegetation that was unmanipulated, in contrast to previous analyses at the ZERT site that characterized CO_2 releases when the vegetation was mechanically mown to uniform height and were evaluated with instruments causing impacts to the surface environment (Male et al. 2010, Spangler et al. 2009). The analysis techniques offered herein present a methodology by which imagery collected from a hyperspectral imaging system mounted to an aircraft could possibly be used to monitor for CO_2 leaks from a GCS site. This proposed monitoring system would provide broad spatial coverage while minimizing costs and labor requirements.

a.

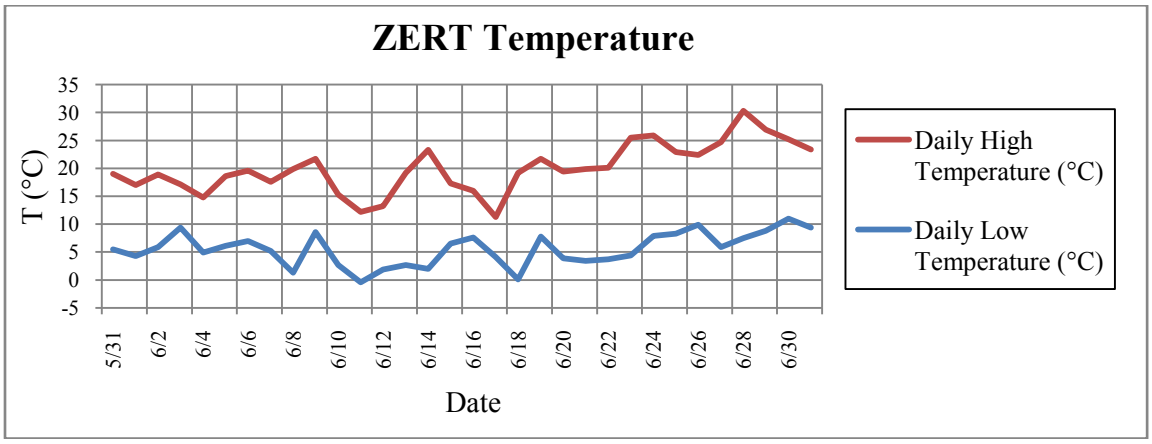

b.

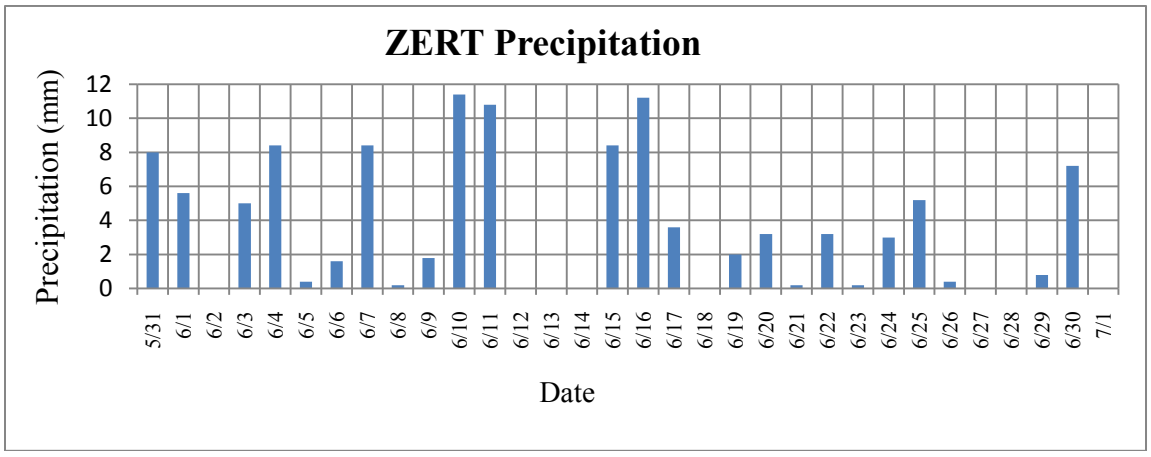

Figure 3.13a & 3.13b: ZERT weather over the course of the 2010 aerial imaging campaign.

Further Research

Although our results provide evidence that hyperspectral remote sensing could be a complimentary monitoring tool that could possibly aid in the detection of CO_2 leaks at GCS sites, further study is required to evaluate several key questions. First, both analyses examined REI trajectories, which only utilized 2 narrow spectral channels (674 nm and 750 nm). These bands were deliberately chosen for their sensitivity to the CO_2 stress signal within the red edge based on the unsupervised classification results that utilized information collected in all 80 Pika II bands. Ground monitoring studies at ZERT, however, have demonstrated that by using a multi-spectral imaging system, utilizing broad spectral channels, detection of CO_2 stress in plants is possible (Rouse et al., 2010). Questions remain as to whether or not a broad band, multi-spectral imager could be used to detect CO_2 stress from an aircraft or if a narrow band, 2-channel imager devoted to REI detection would suffice for monitoring GCS sites. Higher CO_2 leak detection rates might also have been possible if a method was developed that used all of the spectral information afforded a hyperspectral instrument.

The unsupervised classification distinguished a cluster of vegetation pixels in an area of elevated soil CO_2 on June 8, perhaps providing evidence of early, maybe even pre-visual, stress detection from an airplane. Further study is warranted because the vegetation at the ZERT site exhibited signs of a disturbance legacy as a result of repeated CO_2 exposure. Successive release experiments over the past several summers have potentially altered the vegetation community and phenology above the buried release pipe from its original state. It must be assumed that the spectral characteristics of the

vegetation impacted by the CO_2 releases are not consistent with respect to the surrounding vegetation through time. The current response of ZERT vegetation to elevated soil CO_2 stress could be confounded if the distribution of vegetation species and/or vegetation density has changed.

The unsupervised clustering algorithm identified regions classified as severely stressed vegetation throughout the release, whereas, low and moderately stressed vegetation classes were infrequently identified. Further spectral analyses of these clusters, therefore, were not performed. It is worth noting that the pixel clusters classified as low and moderate vegetation stress exhibited lower radiance in the visible portion of the EM spectrum, perhaps due to relatively higher soil moisture concentrations, differences in vegetation, or shadowing effects in these areas. Lower radiance was exhibited in the near infrared compared to healthy vegetation. The low and moderately stressed pixels, thus, behaved like healthy pixels in the visible and like severely stressed pixels in the near infrared. This would be problematic for using the REI to identify regions of low and moderate vegetation CO_2 stress and is a danger to using ratio-based indices because you could get the same index value despite having very different visible and near infrared reflectance for two different spectra. This unexpected result may be due to spatial autocorrelation between the stressed clusters. The question of how subtle or small a CO_2 leak could be detected still remains unanswered by this study.

Another potential limitation of using remote sensing to indirectly monitor for CO_2 leaks at GCS sites is the influence of seasonality. Imaging must commence when

vegetation will exhibit a stress response to elevated soil CO_2 for remote sensing to be a viable monitoring technique. Further investigation is necessary to understand how sensitive plants are to CO_2 stress throughout their growth cycle. This experiment demonstrated that vegetation appears to be sensitive to the CO_2 stress signal during the height of the growing season. Imaging took place when the water table was very high, and during the first couple of weeks over the CO_2 release experiment there was standing water overlying portions of the buried release pipe at ZERT. Knowledge of the spectral influence of vegetation senescence is critical to understanding the limitations of remote sensing of plant stress caused by elevated soil CO_2.

Finally, regarding the sensitivity of vegetation to the CO_2 stress signal, questions remain as to whether or not the CO_2 stress signal is spectrally unique as compared to other plant physiological stressors. For instance, does vegetation that is experiencing stress caused by elevated soil CO_2 look spectrally distinct from trampled vegetation or vegetation experiencing water stress? It will be important to understand whether different sources of physiological plant stress are spectrally discernable in order to properly interpret vegetation stress signals during image analysis. Perhaps the highly dimensional nature of hyperspectral data lends itself to discriminating among different types of vegetation stress.

References

Benson, S.M., Gasperikova, E., Hoversten, G.M. 2005. Monitoring protocols and lifecycle costs for geologic storage of carbon dioxide. In: *Proceedings of the 7th International Conference on Greenhouse Gas Control Technologies (GHGT-7)*. pp. 1259–1266.

Bergfeld, D., Evans, W.C., Howle, J.F., Farrar, C.D. 2006. Carbon dioxide emissions from vegetation-kill zones around the resurgent dome of Long Valley caldera, eastern California, USA. *Journal of Volcanology and Geothermal Research*. 152: 140-156.

Buschmann, C., Nagel, E. 1993. In vivo spectroscopy and internal optics of leaves as basis for remotes sensing of vegetation. *International Journal of Remote Sensing*. 14 (4): 711-722.

Carter, G.A. 1993. Responses of leaf spectral reflectance to plant stress. *American Journal of Botany*. 80: 239-243.

Carter, G. A., Knapp, A.K. 2001. Leaf optical properties in higher plants: linking spectral characteristics to stress and chlorophyll concentration. *American Journal of Botany*. 88: 677-684.

Carter, G.A., Miller, R.L. 1994. Early detection of plant stress by digital imaging within narrow stress-sensitive wavebands. *Remote Sensing of Environment*. 50: 295-302.

Cortis, A., Oldenburg, C.M., Benson, S.M. 2008. The role of optimality in characterizing CO_2 seepage from geologic carbon sequestration sites. *International Journal of Greenhouse Gas Control*. 2: 640-652.

Cuffey, K.M., Vimeux, F. 2001. Covariation of carbon dioxide and temperature from the Vostok ice core after deuterium-excess correction. *Nature*. 412: 523-527.

Demetriades-Shah, T.H., Steven, M.D., Clark, J. A. 1990. High resolution derivative spectra in remote sensing. *Remote Sensing of Environment*. 33: 55-64.

Gitelson, A.A., & Merzlyak, M.N. 1996. Signature analysis of leaf reflectance spectra: Algorithm development for remote sensing of chlorophyll. *Journal of Plant Physiology*. 148: 494-500.

Gitelson, A.A., & Merzlyak, M.N. 1997. Remote estimation of chlorophyll content in higher plant leaves. *International Journal of Remote Sensing*. 18: 2691-2697.

Goetz, A.F.H., Vane, G., Solomon, J.E., Rock, B.N. 1985. Imaging spectrometry for Earth Remote Sensing. *Science*. 228 (4704): 1147-1153.

Hansen, J., Sato, M., Kharecha, P., Beerling, D., Masson-Delmotte, V., Pagani, M., Raymo, M., Royer, D.L., Zachos, J.C. 2008. Target atmospheric CO_2: where should humanity aim? *Open Atmospheric Science Journal*. 2: 217-231.

Hepple, R.P. 2002. Implications of surface seepage on the effectiveness of geologic storage of carbon dioxide as a climate change mitigation strategy. *Lawrence Berkeley National Laboratory (LBNL)*, Paper LBNL-51267.

Hepple, R.P., Benson, S.M. 2005. Geologic storage of carbon dioxide as a climate change mitigation strategy: performance requirements and the implications of surface seepage. *Environmental Geology*. 47: 576-585.

Herzog, H.J. 2001. What future for carbon capture and sequestration? *American Chemical Society.* 35 (7): 148A–153A.

Intergovernmental Panel on Climate Change (IPCC), 2005. *IPCC Special Report on Carbon Dioxide Capture and Storage*. Cambridge University Press, Cambridge, UK.

IPCC Fourth Assessment Report (AR4), 2007. *IPCC Fourth Assessment Report on Climate Change*. Cambridge University Press, Cambridge, UK.

Jensen, R. R., Jackson, M.W., Lulla, V. 2008. Single line correction method to remove aircraft roll errors in hyperspectral imagery. *Journal of Applied Remote Sensing*. 2: 1-10.

Jong, S.M. 1998. Imaging spectrometry for monitoring tree damage caused by volcanic activity in the Long Valley caldera, California. *ITC Journal.* 1-10.

Joos, F., Spahni, R. 2008. Rates of change in natural and anthropogenic radiative forcing over the past 20,000 years. *Proceedings of the National Academy of Sciences (PNAS)*. 105: 1425-1430.

Keith, C.J., Repasky, K.S., Lawrence, R.L., Jay, S.C., Carlsten, J.L. 2009. Monitoring effects of a controlled subsurface carbon dioxide release on vegetation using a hyperspectral imager. *International Journal of Greenhouse Gas Control*. 3: 626-632.

Kling, G.W., Evans, W.C., Tanyileke, G., Kusakabe, M., Ohba, T., Yoshida, Y., Hell, J.V. 2005. Degassing Lakes Nyos and Monoun: Defusing certain disaster. *Proceedings of the National Academy of Sciences*. 102: 14185-14190.

Knauss, K.G., Johnson, J.W., Steefel, C.I. 2005. Evaluation of the impact of CO2, cocontaminant gas, aqueous fluid and reservoir rock interactions on the geologic sequestration of CO_2. *Chemical Geology*. 217: 339–350.

Knipling, E.B. 1970. Physical and physiological basis for the reflectance of visible and near-infrared radiation from vegetation. *Remote Sensing of Environment*. 1 (3): 155-159.

Knott, T. 2008. Capturing carbon dioxide. *Frontiers the BP magazine of technology and innovation*. April: 16-24.

Korbol, R., Kaddour, A. 1995. Sleipner vest CO_2 disposal-injection of removed into the Utsira formation. *Energy Conversion and Management*. 36: 509–512.

Lawrence Berkeley National Laboratory (LBNL), 2000. An overview of geologic sequestration of CO_2. In: *ENERGEX'2000: Proceedings of the 8th International Energy Forum*, Las Vegas, NV

Lawrence, R.L., Labus, M. 2003. Early detection of Douglas-fir beetle infestation with subcanopy resolution hyperspectral imagery. *Westeren Journal of Applied Forestry*. 18: 202-206.

Lawrence, R.L., Ripple, W.J. 1997. Comparisons among vegetation indices and bandwise regression in a highly disturbed, heterogeneous landscape: Mount St. Helens, Washington. *Remote Sensing of Environment*. 64: 91-102.

Lewicki, J.L., Hilley, G.E., Oldenburg, C.M. 2006.An improved strategy to detect CO_2 leakage for verification of geologic carbon sequestration. *Lawrence Berkeley National Laboratory*. http://escholarship.org/uc/item/5cz867jk.

Lewicki, J.L., Hilley, G.E., Dobeck, L., Spangler, L. 2010. Dynamics of CO_2 fluxes and concentrations during a shallow subsurface CO_2 release. *Environmental Earth Sciences*. 60: 285-297.

Lewicki, J.L., Oldenburg, C.M., Dobeck, L., Spangler, L. 2007. Surface CO_2 leakage during two shallow subsurface CO_2 releases. *Geophysical Research Letters*. Vol. 34, L24402, doi:10.1029/2007GL032047.

Lillesand, T. M., Kiefer, R. W., Chipman, J. W. 2008. *Remote Sensing and Image Interpretation 6th Edition*. John Wiley & Sons.

Maček, I., Pfanz, H., Francetič, V., Batič, F., Vodnik, D. 2005. Root respiration response to high CO2 concentrations in plants from natural CO2 springs. *Environmental and Experimental Botany*. 54: 90-99.

Maldal, T., Tappel, I.M. 2004. CO_2 underground storage for Snøhvit gas field development. *Energy*. 29: 1403–1411.

Male, E.J., Pickles, W.L., Silver, E.A., Hoffmann, G.D., Lewicki, J.L., Apple, M., Repasky, K., Burton, E.A. 2010. Using hyperspectral plant signatures for CO_2 leak detection during the 2008 ZERT CO_2 sequestration field experiment in Bozeman, Montana. *Environmental Earth Sciences*. 60: 251-261.

Mingzhe, D., Zhaowen, L., Shuliang, L., Huang, S. 2006. CO_2 sequestration in depleted oil and gas reservoirs-caprock characterization and storage capacity. *Energy Conservation and Management*. 47: 1372–1382.

Mokwa R. 2006. Subsurface exploration for the MSU CO2 injection project-Phase I. Unpublished report, Montana State University, Civil Engineering Department, 2006

Monnin, E., Indermühle, A., Dällenbach, A., Flückiger, J., Stauffer, B., Stocker, T.F.,Raynaud, D., Barnola, J.-M. 2001. Atmospheric CO_2 concentrations over the last glacial termination. *Science.* 291 (5501): 112–114.

National Energy Technology Laboratory (NETL). 2007. *Carbon Sequestration Atlas of the United States and Canada*

National Energy Technology Laboratory (NETL). 2008. *Carbon Sequestration Atlas of the United States and Canada*

Noomen, M.F., Skidmore, A.K. 2009. The effects of high soil CO_2 concentrations on leaf reflectance of maize plants. *International Journal of Remote Sensing*. 30: 481-497.

Noomen, M.F., Smith, K.L., Colls, J.J., Steven, M.D., Skidmore, A.K., Van der Meer, F.D. 2008. Hyperspectral indices for detecting changes in canopy reflectance as a result of underground natural gas leakage. *International Journal of Remote Sensing*. 29: 5987-6008.

Norby, R.J., Luo, Y. 2006. Evaluating ecosystem responses to rising atmospheric CO2 and global warming in a multi-factor world. *New Phytologist*. 162 (2): 281–293.

Oldenburg, C.M., Bryant, S.L., Nicot, J.P. 2009. Certification framework based on effective trapping for geologic carbon sequestration. *International Journal of Greenhouse Gas Control*. 3: 444-457.

Oldenburg, C.M., Lewicki, J.L., Pan, L., Dobeck, L., Spangler, L. 2010. Origin of the patchy emission pattern at ZERT CO_2 release test. *Environmental Earth Sciences*. 60: 241-250.

Pacala, S., Socolow, R. 2004. Stabilization wedges: solving the climate problem for the next 50 years with current technologies. *Science*. 305: 968-972.

Parmeson, C., 2006. Ecological and evolutionary responses to recent climate change. *Annual Review of Ecology, Evolution , and Systematics*. 37: 637-669.

Petit, J.R., Jouzel, J., Raynaud, D., Barkov, N.I., Barnola, J.-M., Basile, I., Bender, M., Chappellaz, J., Davis, M., Delaygue, G., Delmotte, M., Kotlyakov, V.M., Legrand, M., Lipenkov, V.Y., Lorius, C., Pepin, L., Ritz, C., Saltzman, E., Stievenard, M. 1999. Climate and atmospheric history of the past 420,000 years from the Vostok ice core, Antarctica. *Nature*. 399: 429-436.

Pickles, W.L., P.W. Kasameyer, B.A. Martini, D.C., Potts, E.A. Silver. 2001. Geobotanical remote sensing for geothermal exploration. *Geothermal Resources Council Transactions*. 25: 307-312.

Pruess, K. 2008. On CO_2 fluid flow and heat transfer behavior in the subsurface, following leakage from a geologic storage reservoir. *Environmental Geology*. 54: 1677-1686.

Resonon Inc. 2008. Pika II Imaging Spectrometer. www.resonon.com/pika.html

Rock, B.N., Hoshizaki, T., Miller, J.R. 1988. Comparison of *in situ* and airborne spectral measurements of the blue shift associated with forest decline. *Remote Sensing of Environment*. 24 (1): 109-127.

Rouse, J.H., Shaw, J.A., Lawrence, R.L., Lewicki, J.L., Dobeck, L.M., Repasky, K.S., Spangler, L.H. 2010. Multi-spectral imaging of vegetation for detecting CO_2 leaking from underground. *Environ Earth Sci*. 60: 313-323.

Sampson, P.H., Zarco-Tejada, P.J., Mohammed, G.H., Miller, J.R., Noland, T.L. 2003. Hyperspectral remote sensing of forest condition: Estimating chlorophyll content in tolerant hardwoods. *Forest Science*. 49: 381-391.

Schuerger, A.C., Capelle, G.A., Di Benedetto, J.A., Mao, C.Y., Thai, C.N., Evans, M.D., Richards, J.T., Blank, T.A., Stryjewski, E.C. 2003. Comparison of two hyperspectral imaging and two laser-induced fluorescence instruments for the detection of zinc stress and chlorophyll concentration in bahia grass (Paspalum notatum Flugge.). *Remote Sensing of Environment*. 84: 572-588.

Seigenthaler, U., Stocker, T.F., Monnin, E., Lüthi, D., Schwander, J., Stauffer, B., Raynaud, D., Barnola, J.-M., Fischer, H., Masson-Delmotte, V., Jouzel, J. 2005. Stable carbon cycle-climate relationship during the Late Pleistocene. *Science*. 310: 1313-1317.

Shackleton, N.J. 2000. The 100,000-year ice-age cycle identified and found to lag temperature, carbon dioxide, and orbital eccentricity. *Science.* 289: 1897–1902.

Smith, K.L., Steven, M.D., Colls, J.J. 2004. Use of hyperspectral derivative ratios in the red-edge region to identify plant stress responses to gas leaks. *Remote Sensing of Environment*. 92: 207-217.

Smith, K.W., Vogelmann, T.C., DeLucia, E.H., Bell, D.T., Shepherd, K.A. 1997. Leaf form and photosynthesis. *BioScience*. 47:785-793

Spangler, L.H., Dobeck, L.M., Repasky, K.S., Nehrir, A.R., Humphries, S.D., Barr, J.L., Keith, C.J., Shaw, J.A., Rouse, J.H., Cunningham, A.B., Benson, S.M., Oldenburg, C.M., Lewicki, J.L., Wells, A.W., Diehl, J.R., Strazisar, B.R., Fessenden, J.E., Rahn, T.A., Amonette, J.E., Barr, J.L., Pickles, W.L., Jacobson, J.D., Silver, E.A., Male, E.J., Rauch, H.W., Gullickson, K.S., Trautz, R., Kharaka, Y., Birkholzer, J., Wielopolski, L. 2009. A shallow subsurface controlled release facility in Bozeman, Montana, USA, for testing near surface CO_2 detection techniques and transport models. *Environ Earth Sci*. doi:10.1007/s12665-009-0400-2

Strachan, I.B., Pattey, E., Boisvert, J.B. 2002. Impact of nitrogen and environmental conditions on corn as detected by hyperspectral reflectance. *Remote Sensing of Environment*. 80 (2): 213-224.

Strazisar, B.R. , Wells, A.W., Diehl, R.J., Hammack, R.W., Veloski, G.A. 2009. Near-surface monitoring for the ZERT shallow CO_2 injection project. *International Journal of Greenhouse Gas Control*. 3: 736-744.

Vinnikov, K.Y., Grody, N.C. 2003. Global warming trend of mean tropospheric temperature observed by satellites. *Science*. 302: 269–272.

Vogelmann, J.E., Rock, B.N., Moss, D.M. 1993. Red edge spectral measurements from sugar maple leaves. *International Journal of Remote Sensing*. 14: 1563-1575.

Whittaker, S.G. 2004. Geological storage of greenhouse gases: the IEA Weyburn CO_2 monitoring and storage project. *Canadian Society of Petroleum and Geologists Reservoir*. 31 (8): 9.

Wilson, E.J., Friedmann, S.J., Pollak, M.F. 2007. Research for deployment: Incorporating risk, regulation, and liability for carbon capture and sequestration. *Environmental Science & Technology*. 41: 5945-5952.

Xu, T. 2004. CO_2 geological sequestration. Lawrence Berkeley National Laboratory, Paper LBNL-56644 JArt.

Zarco-Tejada, P.J., Miller, J.R., Mohammed, G.H.; Noland, T.L. 2000. Chlorophyll fluorescence effects on vegetation apparent reflectance: I. leaf-level measurements and model simulation. *Remote Sensing of Environment*. 74 (3): 582-595

CHAPTER 4

HYPERSPECTRAL DETECTION OF A CO_2 LEAK IN THE PRESENCE OF WATER STRESSED VEGETATION

Introduction

Geologic Carbon Sequestration

Post-industrial atmospheric carbon dioxide (CO_2) concentration has risen from 280 ppm to over 380 ppm (Cuffey and Vimeux 2001; Masarie and Tans 1995; Monnin et al. 2001; Petit et al. 1999; Scripps 2007; Seigenthaler et al. 2005). Atmospheric CO_2 absorbs and reemits radiation energy from the Earth's surface causing a warming of the surface environment (IPCC AR4 2007). Global warming could drastically reshape the Earth's climate and environment (Parmesan 2006; Hansen et al. 2008; Norby and Luo 2006; Shackleton 2000; Vinnikov and Grody 2003). Geologic carbon sequestration (GCS) is a potential climate change mitigation strategy that captures point source CO_2 emissions from industrial sources and stores them in large sub-surface reservoirs. GCS, conceptually, has the potential to store gigatonnes (Gt) of CO_2 , which would otherwise be released into the atmosphere, into specialized geologic formations for long-term storage (Hepple and Benson 2005; Hepple 2002; Herzog 2001; IPCC 2005; LBNL 2000; Pacala and Socolow 2004; Wilson et al. 2007).

There is a mandate to monitor GCS sites for CO_2 leakage to ensure the efficacy of this technology, given that it is on the brink of commercial-scale deployment (Cortis et al. 2008; Hepple and Benson 2005; Oldenburg et al. 2009; Schuerger et al. 2002; Wilson et al. 2007). Remote sensing is being investigated as a possible cost-effective, large-area

monitoring method to detect surface CO_2 leaks at GCS sites (Keith et al. 2009; Male et al. 2010). A leak from a GCS site would not only compromise the viability of this technology as a climate mitigation strategy, but it could also threaten the safety of the surrounding environment and inhabitants at the surface. The 1986 eruption of CO_2 at Lake Nyos, Western Camaroon, killed over 1,700 people and demonstrated that a large pneumatic CO_2 explosion can have devastating consequences (Kling et al. 2005). Natural sources of CO_2 leakage from the Long Valley Caldera in California have caused extensive forest mortality (Bergfeld et al. 2006; Jong 1998; Pickles 2001).

Elevated CO_2 levels in soil are known to cause anoxic conditions in plant roots (Bergfeld et al. 2006; Maček et al. 2005), thereby interfering with plant respiration and inducing a stress response that could possibly be remotely sensed using aerial imagery (Male et al. 2010). Vegetated areas at GCS sites, presumably, could act as bellwethers to signal operational inefficiencies in hazardous CO_2 leak scenarios. Vegetation status and seasonality will determine when the remote detection of vegetation stress caused by elevated soil CO_2 would be feasible. Soil water availability is highly spatially variable, and water stressed vegetation could appear spectrally similar to vegetation stressed by elevated soil CO_2. Drought is another common environmental occurrence that can have lasting impacts on whole land regions and can be short-lived or persist for years. Regardless of duration and spatial extent, monitoring GCS sites with remote sensing data would require discrimination between water and CO_2 stress to accurately identify CO_2 leaks.

Remote Sensing as a Monitoring Technique for GCS Sites

A variety of monitoring techniques are being investigated for efficiency and accuracy at detecting a CO_2 leak from a subsurface storage reservoir (Spangler 2009). Most methods tend to be expensive and resource intensive, while providing only limited spatial coverage. Remote sensing, alternatively, has the potential to provide near instantaneous monitoring over large swaths of land. Aerial imaging over GCS sites would be relatively inexpensive and might be performed with limited labor requirements. Regions of elevated soil CO_2, if accurately detected with remote sensing equipment, could be further investigated with instruments on the ground to properly diagnose the leak source. Early leak detection would allow site managers to take immediate remediation measures to prevent further CO_2 leakage, while minimizing safety risk and economic loss. GCS monitoring could tolerate false positives, within reason, whereas, a false negative resulting in a missed CO_2 leak could have serious consequences.

Hyperspectral Remote Sensing for Plant Stress Detection

Hyperspectral sensors collect nearly continuous spectral data across narrow channel widths throughout the visible and infrared portion of the electromagnetic (EM) spectrum (400 – 2500 nm). Spectral signatures or spectra can be used to detect subtle patterns in vegetation reflectance to better understand the physiological condition of plants. Plant pigment concentrations, leaf cellular structure, and leaf moisture content can be discerned with hyperspectral data to assess the overall health of vegetation and characterize plant stress (Goetz et al. 1985; Carter 1993).

Hyperspectral remote sensing has been used to detect and characterize numerous types of vegetation stressors within the visible and infrared portion of the EM spectrum. Hyperspectral data have been analyzed to model plant stress caused by elevated soil CO_2 (Noomen and Skidmore 2009),water stress (Peguero-Pina et al. 2008; Penuelas et al. 1997; Suarez et al. 2008), insect and pest invasion (Lawrence and Labus 2003; Pu et al. 2008; Fitzgerald et al. 2004; Muhammed 2005), heavy metal contamination (Schuerger et al. 2002), salinity stress (Naumann et al. 2009), nutrient levels and crop status (Gamon et al. 1997; Strachan et al. 2002); ozone exposure (Meroni et al. 2008); and natural gas leaks (Noomen et al. 2008). Certain spectral regions are known to be especially sensitive, because they relate to the specific chemical and physical responses of plants to stress.

Low reflectance in the visible portion of the EM spectrum (400 – 700 nm) is determined primarily by chlorophyll *a* and *b* pigment abundance and absorption, while high reflectance in the near infrared (NIR) is governed by the structural, spongy mesophyll contained in plant leaves (Carter and Knapp 2001; Goetz 1985; Knipling 1970; Smith et al. 1997; Zarco-Tejada et al. 2000). Chlorophyll absorption is highest in the visible blue (400 – 500 nm) and middle red (near 680 nm), therefore these regions are not sensitive to subtle changes in chlorophyll content, because the spectral signal is saturated (Carter and Knapp 2001; Lichtenthaler 1987). Absorption by chlorophyll pigments is weakest in the visible green – orange (500 – 620 nm) and the far visible red (700 nm), therefore, these wavelengths are sensitive to stress and subtle changes in chlorophyll content (Carter and Knapp 2001; Buschmann and Nagel 1993). Red edge indices are frequently used to detect stress at the boundary of the far red and NIR to

detect changes in chlorophyll content. The red edge is a reflectance spike caused by steep transition from low reflectance in the far red to high reflectance in the NIR, which is used as reference because it is determined by the physical structure of plant leaves. Far red reflectance (near 700 nm) is known to increase as a plant exhibits a physiological stress response of reducing chlorophyll content to down regulate photosynthesis, thereby reflecting proportionally more potentially damaging photosynthetically active radiation compared to healthy vegetation, which can utilize all of that incoming energy. Vegetation stress caused by depleted oxygen concentrations around the roots from natural gas leaks and elevated soil CO_2 has been detected in the red edge region of the EM spectrum (Keith et al. 2009; Male et al. 2010; Noomen et al. 2008; Noomen and Skidmore 2009; Smith et al. 2004). Water stress has also been found to cause reflectance changes related to chlorophyll pigment concentrations in the red edge (Carter 1991, Tucker et al. 1980b).

Shifts of the red edge 5 – 10 nm towards shorter wavelengths, termed the "blue shift", has also been associated with a decline in chlorophyll absorption for stressed vegetation (Carter 1993; Carter and Miller 1994; Noomen and Skidmore 2007; Noomen et al. 2008; Smith et al. 2004a, b; Rock et al. 1988; Vogelmann et al. 1993). This phenomenon has been associated with the early detection of vegetation stress by hyperspectral remote sensing instruments. The sensitivity of hyperspectral instruments to detect vegetation stress early, and perhaps even before it is visible to the human eye, has distinct advantages over conventional monitoring methods, because land managers could

then take quicker ameliorative action to minimize losses to valuable resources (Lawrence and Labus 2003).

Vegetation reflectance in the green portion of the EM spectrum is associated with xanthophyll pigments in addition to chlorophyll. Xanthophyll pigments contained within plants' palisade mesophyll perform photoprotective roles that also influence photosynthetic radiation use efficiency and are sensitive to stress (Gamon et al. 1997; Gamon and Surfus 1999). Vegetation reflectance within the green, therefore, will increase in response to stress to down regulate photosynthetic activity because of both xanthophyll pigment activity and decreases in chlorophyll content. The Photochemical Reflectance Index (PRI) is a narrow-band, hyperspectral index ratioing green reflectance and is known to be sensitive to xanthophyll pigment activity. The PRI has been used as an early indicator of water stress in plants caused by drought conditions (Peguero-Pina et al. 2008; Penuelas et al. 1997; Strachan et al. 2002; Suarez et al. 2008).

Water stress responses in vegetation have also been detected in spectral water absorption features in the shortwave infrared (SWIR) portion of the EM spectrum. Reflectance within the 1300 – 2500 nm wavelengths has been associated with leaf water content and has been observed to increase as a primary response of plants to water stress (Carter 1991). Visible spectrum reflectance has also been shown to increase, but only as a secondary plant response to water stress, in which chlorophyll pigment concentration decreases as a mechanism of down regulating photosynthesis during prolonged dehydration in vegetation (Tucker 1980b; Carter 1991). Spectral measurements of leaf water content in the SWIR, therefore, directly monitors for plant dehydration and would

be a more immediate method of detecting a plant's response to water stress. The primary response of plants to drought within the water absorption bands also could possibly be spectrally distinct from other types of physiological stressors, including stress caused by elevated soil CO_2.

Our greenhouse experiment objectives were (1) to evaluate if elevated soil CO_2 stress can be detected in alfalfa plants using hyperspectral data, and if so how quickly; (2) to determine if CO_2 stress is spectrally distinguishable from water stress since water availability is likely to be spatially variable at GCS sites and water stressed vegetation will likely co-occur with CO_2 stressed vegetation during a CO_2 leak scenario; and (3) to determine if CO_2 stress is distinguishable during drought conditions when all vegetation is water stressed during a CO_2 leak scenario. It is still unknown whether the plant stress signal caused by elevated soil CO_2 is spectrally distinguishable from other forms of plant physiological stress. Water stress or drought conditions in particular, are common natural occurrences that might confound a CO_2 stress signal if both plant physiological stressors coincide. Remote CO_2 leak detection might therefore be problematic in the context of GCS monitoring. Understanding the spectral discernability between stress caused by elevated soil CO_2, water stress, and their interaction is important for determining the appropriate times and conditions in which remote sensing image acquisition should commence over GCS sites.

Materials and Methods

Data Collection

Alfalfa (*Medicago sativa*) seeds were planted on June 1, 2010, to obtain 40 mature plants for this greenhouse experiment. Each alfalfa seedling was transplanted into a 45 cm tall, 9.6-l tree pot (Stuewe & Sons, Inc.). These tree pots were modified in several ways prior to planting in order to facilitate CO_2 injection into each individual plant pot and to best emulate a CO_2 leak scenario from a GCS site. The drainage holes at the bottom of each pot were sealed using plastic wrap, silicone, and Gorilla tape to minimize injected CO_2 from readily escaping through the bottom of the pots. The pots were then filled with 1.0 l of pea-sized gravel placed on top of a layer of gauze cotton cloth that covered drain holes at the bottom of each pot. A 0.6-cm diameter tube was inserted into each plant pot above the bottom 5-cm layer of gravel. The tube terminated in a 5-cm long, ceramic air stone (Top Fin®) intended to disperse the CO_2 gas radially, as opposed to being released from a single point source. The embedded air stone plumbing was topped with an additional l of gravel to assist in the dispersion of the CO_2 gas throughout each pot and to allow for adequate water drainage from the soil (Figure 4.1).

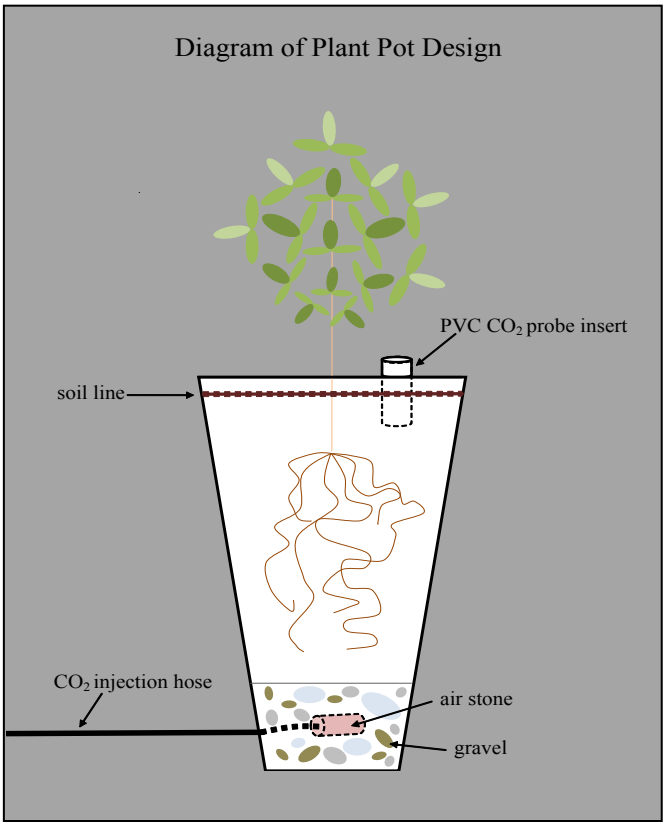

Figure 4.1: Diagram of a plant pot for the greenhouse experiment.

Soil was placed on top of another layer of gauze above the gravel to keep the media separate. The soil used in the pots was a mixture of equal parts loam, washed concrete sand, and Canadian Sphagnum peat moss. Additionally, AquaGro 2000 wetting agent was blended into the soil at a ratio of 0.5 kg/m^3 soil mix. The soil mix was pasteurized with aerated steam at 70° C for 60 minutes. A 10 cm long piece of 2.54 cm diameter PVC pipe was inserted 5 cm down into the surface of the soil of every plant to allow for immediate access for soil CO_2 concentration measurements with a Vaisala GMP221 probe to verify injection. The alfalfa plants were watered with approximately 300 ml of water at 0800 hours every Monday, Wednesday, and Friday. They were

fertilized twice a week with a $^{1\ gm}/_{0.5\ l}$ dilution of NPK fertilizer (20-10-20) every Wednesday and Friday until CO_2 injection began. The greenhouse temperature averaged 21.25 ± 1.60°C over the course of the experiment. Sixteen hours a day of supplemental artificial lighting was provided using 1000 watt metal halide growth bulbs (GE Multi-Vapor MVR 1000/C/U) from 0500 to 2100 hours. Greenhouse integral photosynthetic photon flux measured within each of the treatment blocks ranged from 9.41 to 15.79 mol/m^2/day on peak sunny days and 0.09 to 0.11 mol/m^2/day on cloudy days (Apogee Instruments Line quantum sensors).

Five treatment blocks were developed, containing eight plants each (two replicates of each of four treatment groups per block). The four treatment groups included: (1) CO_2 injection (I); (2) water stress (WS); (3) an interaction group that was subjected to both water stress and CO_2 injection (WSI); and (4) adequate water and no CO_2 injection (C). Each treatment block contained two plants from each treatment group. CO_2 gas was delivered to the plant pots through a plumbing manifold that used equal lengths of tubing between each of the injected plants and a 2-stage pressure reducing regulator (Smith®) at the CO_2 tank, which maintained constant pressure and did not require adjustment as the pressure within the CO_2 storage cylinder decreased over time. The gas was delivered from cylinders containing 50 lbs. liquid CO_2 at a constant pressure of 15 psig.

Alfalfa plants were randomly assigned to treatment blocks and to discrete positions within each block using a random number generator. Treatments within the blocks were randomly assigned using a stratified randomization developed to maintain

equal lengths tubing between the injected plants (Figure 4.2). The plants that received water continued on the same watering regiment of 300 $^{ml}/_{day}$, while the water-stressed plants were not given any water in order to mimic drought conditions once CO_2 injection began.

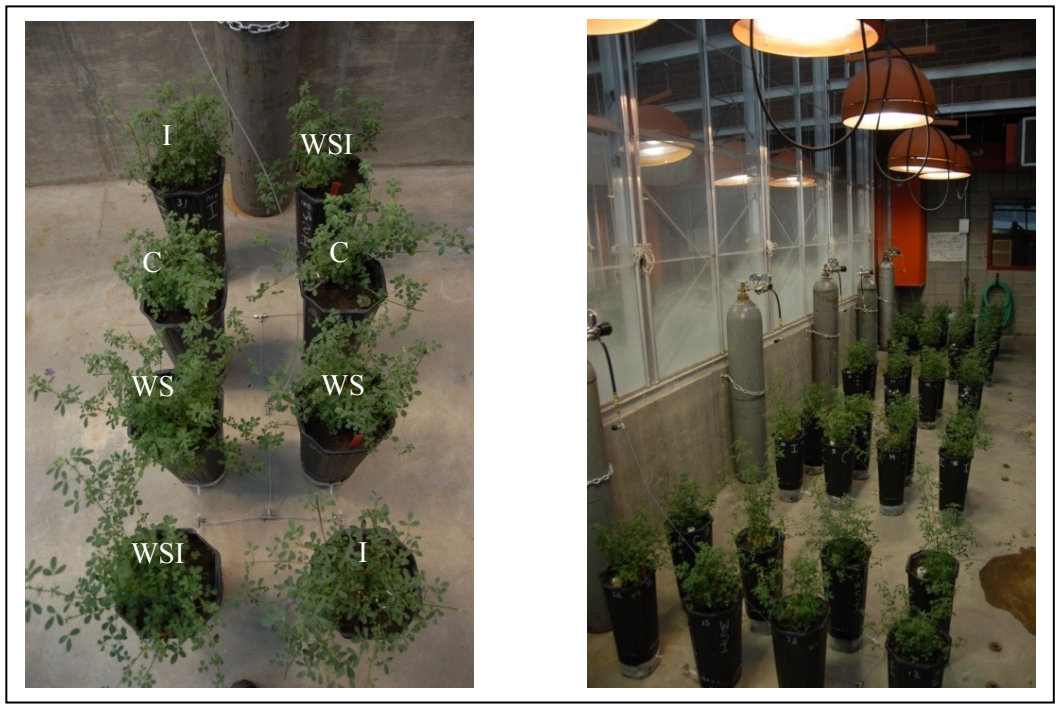

Figure 4.2: Single treatment block shown with plumbing and labeled treatments shown in white for each plant (left). Four of five treatment blocks are shown within the greenhouse (right).

Each alfalfa plant was scanned three times a week for three weeks, and all 40 alfalfa plants were sampled twice to obtain two spectral measurements per plant on each scanning date using an ASD Field Spec Pro 350. The ASD is a 16-bit spectrometer that has a spectral range of 350 – 2500 nm. The spectral resolution is 3 nm at 700 nm, 8.5 nm at 1400 nm, and 6.5 nm at 2100 nm. The sampling interval for the instrument is 1.4 nm at 350 – 1000 nm and 2 nm at 1000 – 2500 nm. The instrument takes a scan every 100

ms (ASD Inc.). A single sample consisted of two clipped alfalfa leaves, each containing three leaflets, from a randomly selected stem, determined by the roll of a 4-sided die. Each selected stem was clipped off at the bottom of the sixth node and spectral scans were taken from the four largest leaves on the cut stem. This sampling design intended to measure leaves from both the lower and upper canopy of each alfalfa plant to ensure that stress was not exhibited in one more than the other. The first sample consisted of the upper two biggest leaves and the second was taken from the lower two largest leaves of each cut stem. The leaves were dissected, meaning each leaflet was clipped from each sampled leaf (the leaves were left entire for ease and maximum coverage of the viewing spot later in the experiment, when samples had leaves that were too desiccated and brittle to dissect). The three leaflets from the bottom leaf of the top sample were placed in parallel on a spectralon target overlapped by the three leaflets of the upper leaf from the same sample to achieve total leaf surface coverage of the ASD fiber optic sensor viewing spot, the region from which spectral information is collected. The process was repeated for the lower set of leaves from the same plant for the second sample. These protocols were implemented both to preserve the spatial relationship among the leaf samples, as well as to keep the orientation of the leaves relative to the plant consistent to best simulate what a remote sensing instrument from an airborne platform would view (Figure 4.3).

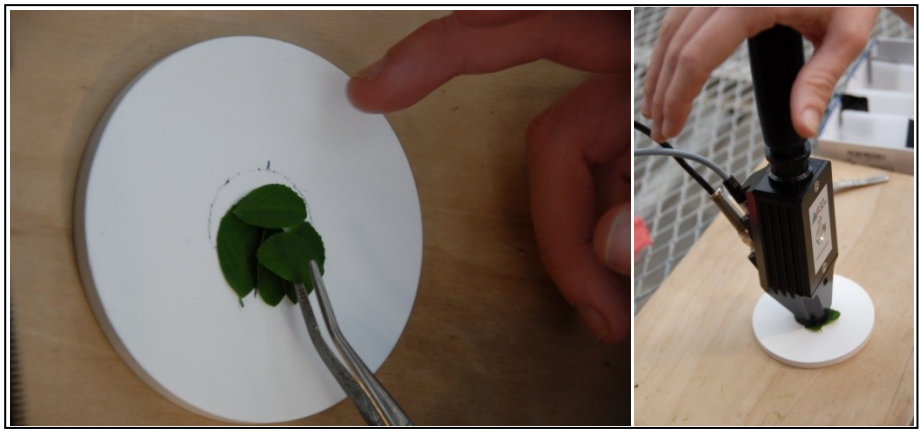

Figure 4.3: Two dissected alfalfa leaves on the spectralon target (left). The ASD fiber optic and plant probe assembly (right).

The fiber optic cable of the ASD was equipped with a plant probe accessory for leaf-level spectral measurements. The plant probe was 10 in. long and contained an internal, low-intensity halogen bulb, which produces little heat, for collecting spectral scans from vegetation. The viewing geometry of the mounted fiber optic cable created a 10 mm by 13 mm oval viewing spot from which spectral information was collected. Initial spectral readings were taken for all 40 plants at 1000 hours on February 7, 2011, as a baseline before treatments were applied. CO_2 injection began at 1400 hours on February 7, 2011. A Vaisala soil probe was used to monitor CO_2 concentrations over time and to confirm successful injection into the individual plant pots. A Swagelok G2 model variable area flowmeter also was used to measure CO_2 flux at the quick-connect union for each plant. Injection rates ranged from 0.25 to > 5 l/hr for all injected plants. All 40 plants were spectrally scanned on Monday, Wednesday, and Friday for three weeks. Each plant was sampled and scanned on nine dates, except one plant, which was only scanned on eight dates because it was discovered on February 9 that a plant was not receiving CO_2 injection for some unknown reason. The plant therefore, was swapped

out. A total of 18 scans were acquired for all plants, except for the exchanged plant, which had 16 scans. The injection was terminated on February 25, 2011, upon the completion of scanning all the plants earlier that day.

All spectral measurements were in reflectance and were a derived average of 25 individual scans. The instrument was calibrated to set gains and off-sets by an optimization process in the RS^3 software (ASD Inc.). A dark current was collected subsequently and the sensor was white referenced using a spectralon target. The ASD instrument was periodically recalibrated on each scanning date to ensure accurate and repeatable spectral measurements. A new white reference and dark current reading was made after the acquisition of both spectral scans for a single plant. The ASD was re-optimized upon the completion of acquiring data for an entire treatment block—eight plants.

Data Analysis

We developed a classification tree model for each individual scanning date to determine the timing and extent to which the different treatment groups were spectrally distinguishable. Classification tree analysis is a non-parametric statistical modeling method that has been successfully used to discriminate vegetation stress classes using hyperspectral data because it can utilize different band combinations to distinguish each class (Lawrence and Labus 2003). Classification trees use recursive, decision-based rules that can be interpreted by an analyst. This is important when trying to ascertain how and where the different plant physiological stressors are spectrally distinguished.

Although the ASD contained spectral data within the ultraviolet portion (350 – 400 nm) of the EM spectrum, these data were removed from further analysis because they were noisy and airborne hyperspectral sensors generally do not collect data at these wavelengths. The ASD measurements for the 400 – 2500 nm spectral range were output in an ascii format and exported into an Excel spreadsheet. TIBCO Spotfire S+ statistical software package was used to fit classification tree models to each scanning date's data using treatment group as the response variable and the ASD bands as explanatory (predictor) variables. Additionally, a factor variable indicating the relative position (upper or lower) of each leaf sample was included as a possible predictor variable in case sample location had an influence on treatment response. Cross-validation trees within S+ were used to prune the classification tree models for each date, so that they were unbiased and not over fit (Venables and Ripley 1997). A standard 10-fold cross-validation was performed to determine the appropriate number of terminal nodes to lower deviance among samples, except that, given the small sample size, a script was written in S+ to take a random sample of scans stratified on treatment type (I, WS, WSI, or C) for each cross-validation tree to ensure that a balanced sample for each treatment group was withheld for validation purposes. This process was repeated five times, taking a different stratified random sample for each successive cross-validation tree and the plurality determined the appropriate size for pruning each classification tree. The spectral locations (wavelengths) used to distinguish between treatment groups for each of the binary nodes within each pruned classification tree model were examined to elucidate the

spectral regions that best discerned between water stress and stress caused by elevated soil CO_2 in plants.

A random forest classification (Breiman 2001) also was performed on the individual scanning dates to evaluate the levels of prediction accuracy that could be achieved in discerning water and CO_2 stress agents. The algorithm is a "bagging" method that takes a bootstrap sample from the data observations to develop a classification tree by using a random subset of all possible explanatory variables (spectral bands) at each binary split (Breiman 2001). This is done iteratively to form hundreds of classification trees (the forest) and then each observation is classified on the resultant plurality vote of the forest. Random forest models were derived with an ensemble of 500 classification trees with 45 randomly selected explanatory variables (of the possible 2100 spectral bands or the categorical variable indicating relative leaf position in the canopy) to be tried at each binary split within each tree. Variable importance plots from the random forest models were used to highlight the spectral regions used in distinguishing between the different treatment classes. Hyperspectral data have been modeled using random forest to greatly increase classification accuracies, as compared to other methods, as well as provide an unbiased, reliable internal estimate of accuracy for mapping land cover (Gislason et al. 2006) and invasive plants (Lawrence et al. 2006). A disadvantage of random forest is the inability to ascertain the relevance of individual explanatory variables and make meaningful interpretations of the model. Since hundreds of individual trees contribute to a random forest model, the classification results are essentially determined inside a "black box" that is effective for the purpose of prediction,

but not for interpreting the decision-based rules that determine those predictions (Prasad et al. 2006).

The lack of replicates in this study forced us to rely on internal measurements of predictive accuracy to evaluate spectral distinguishability. No data were withheld in the construction of the individual classification trees and the random forest classifier withheld approximately one third of each date's data as a bootstrap (out-of-bag) sample for internal validation within each of the 500 constructed trees. The random forest classifier has proved itself as a robust classification tool that contains an unbiased internal accuracy assessment that does not require a separately withheld dataset for validation (Lawrence et al. 2006). Overall classification accuracies, Kappa statistics (a more robust estimate of classification accuracy because it takes into account chance agreement by differencing the observed accuracy from that of a total random assignment), and individual user's (mapping errors of commission) and producer's accuracies (mapping errors of omission) were used to assess predictive capabilities for the class distinctions through time (Congalton and Greene 2009).

Results

Examination of the individual sample spectral signatures for the different treatment groups illustrated the spectral regions that were critical in their distinction and accurate classification (Figure 4.4). Sample spectra for each of the treatment groups appeared to exhibit similar reflectance properties throughout the EM spectrum before treatments were applied, on February 07. Spectral deviations were due to natural inherent variability between alfalfa plants. Spectral separation occurred after treatment

application and stressed sample spectra appeared to exhibit increased reflectance in the visible spectrum, especially within the visible green, as compared to the C class on February 21, at the height of spectral distinction among treatment groups. Water stressed samples exhibited increased reflectance in the SWIR as compared to the C and I classes. The WSI class predominantly exhibited higher reflectance in the visible and SWIR regions compared to all other samples. The red edge spectral boundary shifted towards shorter wavelengths (the "blue shift") for stressed samples after four days of treatment application, however, visual symptoms of stress were also observed on this day. The blue shift was not uniquely expressed among stressed treatment groups.

Classification Tree Analysis

Cross-validation results determined that four terminal nodes were appropriate for February 21 and 23, otherwise the classification trees were pruned smaller to ensure they were not over fit (Table 4.1). Only the February 21 and 23 classification tree models, therefore, distinguished among all four treatment groups. A decision split or node was not justified for the classification tree models during the first week of the experiment. Not until February 14 were two or more terminal nodes warranted (Figure 4.5). The categorical variable indicating relative leaf sample position within each alfalfa canopy was never used as a splitting rule for any of the classification trees.

WS and WSI classes exhibited greater reflectance than the C and I classes within the water absorption bands near the 1400, 1900, and 2500 nm wavelengths. These distinctions in the SWIR infrared regions began on February 14 and persisted until the end of the experiment. Second level distinctions (decisions in trees with three or more

terminal nodes) were made within the red edge at the 717 nm wavelength, where greater reflectance was exhibited by leaf samples from the I class as compared to the C class. The I class also exhibited greater reflectance in the visible green-visible orange at the 545, 621, and 541 nm wavelengths as compared to the C class. The WSI interaction group exhibited compound stress effects with greater reflectance as compared to the WS class in the water absorption bands at 1429 nm and 1901 nm.

Table 4.1: Number of terminal nodes determined by the cross-validation results for the single date classification tree models. The plurality of the five cross-validation trials determined the appropriate size of the final trees.

Cross-Validation Tree Results						
Date	**x1**	**x2**	**x3**	**x4**	**x5**	**Plurality**
2/7	1	1	1	1	1	1
2/9	1	1	1	1	1	1
2/11	1	1	2	2	1	1
2/14	2	1	2	2	1	2
2/16	3	3	3	3	2	3
2/18	2	2	5	2	2	2
2/21	4	4	4	4	4	4
2/23	4	4	4	4	4	4
2/25	3	2	2	3	3	3

Confusion early in the experiment, from February 14-18, occurred almost exclusively between (1) I and C classes, and (2) WSI and WS classes (Table 4.2). The C class was accurately distinguished by the second week of stress treatment application (user's and producer's accuracies $\geq$ 91%). Spectral differentiation between treatment groups was greatest on February 21 and February 23 (after two weeks of treatment application) with overall classification accuracies of 90% (Kappa of 0.87) and 81% (Kappa 0.75), respectively. Confusion during maximum spectral distinction primarily occurred (1) with I samples being classified as WS, and (2) WS being classified as WSI.

Producer's accuracies for the I class were 80% and 55%, while the WSI class had perfect producer's accuracies (100%) on both February 21 and 23. Overall classification accuracy dropped to 66% (Kappa of 0.55) on the last scanning date, February 25.

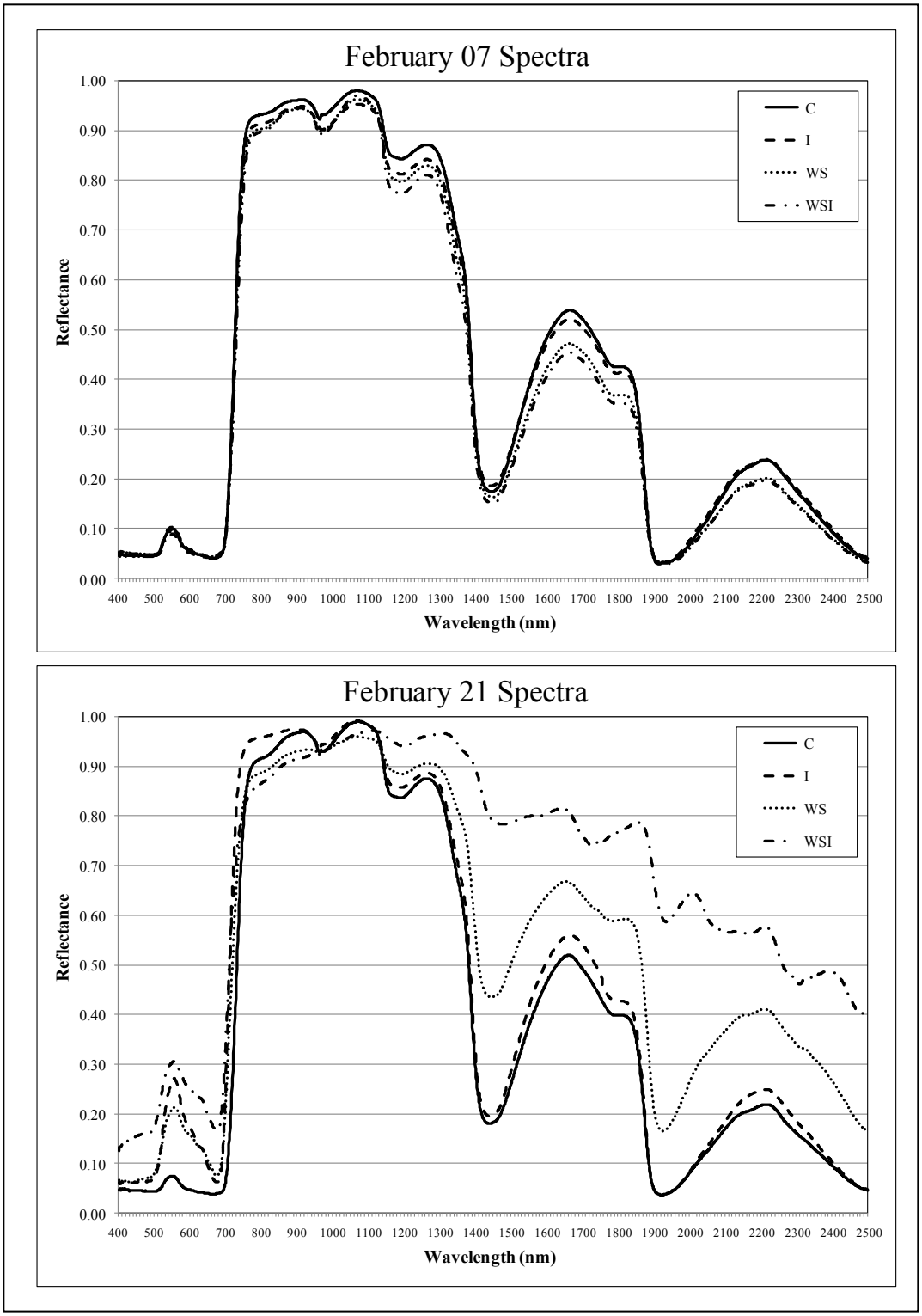

Figure 4.4: Sample reference class spectra for each of the four treatment groups from February 07 (before treatment application) and February 21 (when spectral distinction was greatest between treatment groups).

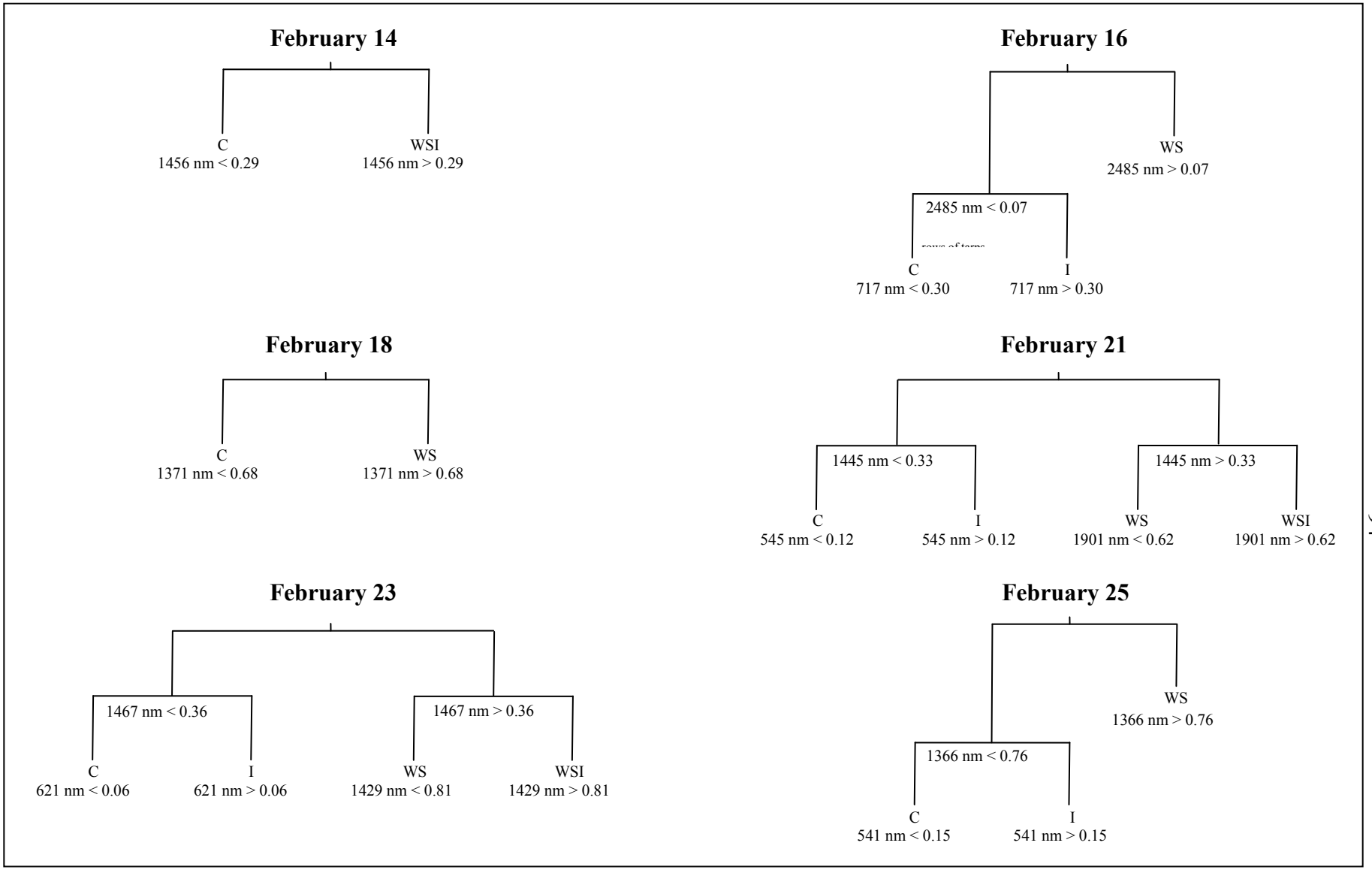

Figure 4.5: Pruned single date classification trees show the utilized spectral bands (by central band wavelength) and reflectance levels for each splitting rule. Splitting rules apply to the left branches of the tree. C = control class; I = CO_2 injection class; WS = water stress class; and WSI = water stress and CO_2 injection interaction class.

Table 4.2: Internal classification accuracies and Kappa statistics for each single date classification tree model containing at least two terminal nodes. Treatment group columns represent the reference data while the rows represent the classified data.

February 14, 2011	C	I	WS	WSI	User's Accuracy
C	20	20	6	3	41%
I	0	0	0	0	na
WS	0	0	0	0	na
WSI	0	0	14	17	55%
Producer's Accuracy	100%	0%	0%	85%	Overall Accuracy 46%
Kappa Statistic	0.28				

February 16, 2011	C	I	WS	WSI	User's Accuracy
C	16	0	0	0	100%
I	4	19	0	0	83%
WS	0	1	20	20	49%
WSI	0	0	0	0	na
Producer's Accuracy	80%	95%	100%	0%	Overall Accuracy 69%
Kappa Statistic	0.58				

February 18, 2011	C	I	WS	WSI	User's Accuracy
C	20	20	0	0	50%
I	0	0	0	0	na
WS	0	0	20	20	50%
WSI	0	0	0	0	na
Producer's Accuracy	100%	0%	100%	0%	Overall Accuracy 50%
Kappa Statistic	0.33				

February 21, 2011	C	I	WS	WSI	User's Accuracy
C	20	0	0	0	100%
I	0	16	0	0	100%
WS	0	4	16	0	80%
WSI	0	0	4	20	83%
Producer's Accuracy	100%	80%	80%	100%	Overall Accuracy 90%
Kappa Statistic	0.87				

February 23, 2011	C	I	WS	WSI	User's Accuracy
C	20	2	0	0	91%
I	0	11	0	0	100%
WS	0	6	14	0	70%
WSI	0	1	6	20	74%
Producer's Accuracy	100%	55%	70%	100%	Overall Accuracy 81%
Kappa Statistic	0.75				

February 25, 2011	C	I	WS	WSI	User's Accuracy
C	20	1	0	0	95%
I	0	13	0	0	100%
WS	0	6	20	20	43%
WSI	0	0	0	0	na
Producer's Accuracy	100%	65%	100%	0%	Overall Accuracy 66%
Kappa Statistic	0.55				

Random Forest Analysis

The trend in accuracy of the random forest models throughout the time series was similar to that of the classification tree models (Figure 4.6). Out-of-bag accuracy predominantly exhibited a curvilinear trend with increasing out-of-bag accuracy from 25% (Kappa of 0) on February 7 (before treatments were applied) to peak classification accuracy of 83%, (Kappa of 0.77) on February 21. Subsequently, classification accuracy decreased. By February 25 out-of-bag accuracy had dropped to 65% (Kappa of 0.53). The C treatment group was best distinguished with user's and producer's accuracy ≥ 80% after one week of treatment application (Table 4.3). Most class confusion existed between WSI and WS treatment groups, once overall out-of-bag accuracy was ≥ 65% (February 14-25). I class producer's accuracy was ≥ 65% from February 14 onward. WSI class producer's accuracy was 90% for February 21 and 23, but was much lower on other dates.

The variable importance plots provided a visual display of the spectral regions that were the most influential in single date random forest model prediction (Figure 4.7). The variable importance plots were very noisy before there was spectral discernability among treatment groups. Spectral regions became more clearly defined as classification accuracies increased. The red edge region (700-750 nm) was shown to be the most important on February 14 and 16. On February 18, variable importance was predominantly placed on the spectral wavelengths centered on approximately 1400 nm. During maximum spectral distinction among treatment groups, variable importance was placed (1) in the visible green-yellow portion of the EM spectrum centered at approximately 550 nm; (2) the red edge (700-750 nm); and (3) the three water absorption

features centered at approximately 1400, 1900, and 2500 nm. On February 25, the last scanning date, more emphasis was placed on the visible and NIR spectral regions rather than the water absorption features. The categorical variable indicating relative leaf sample position within each alfalfa canopy was never deemed important in any of the random forest classification models (variable importance < 0.01).

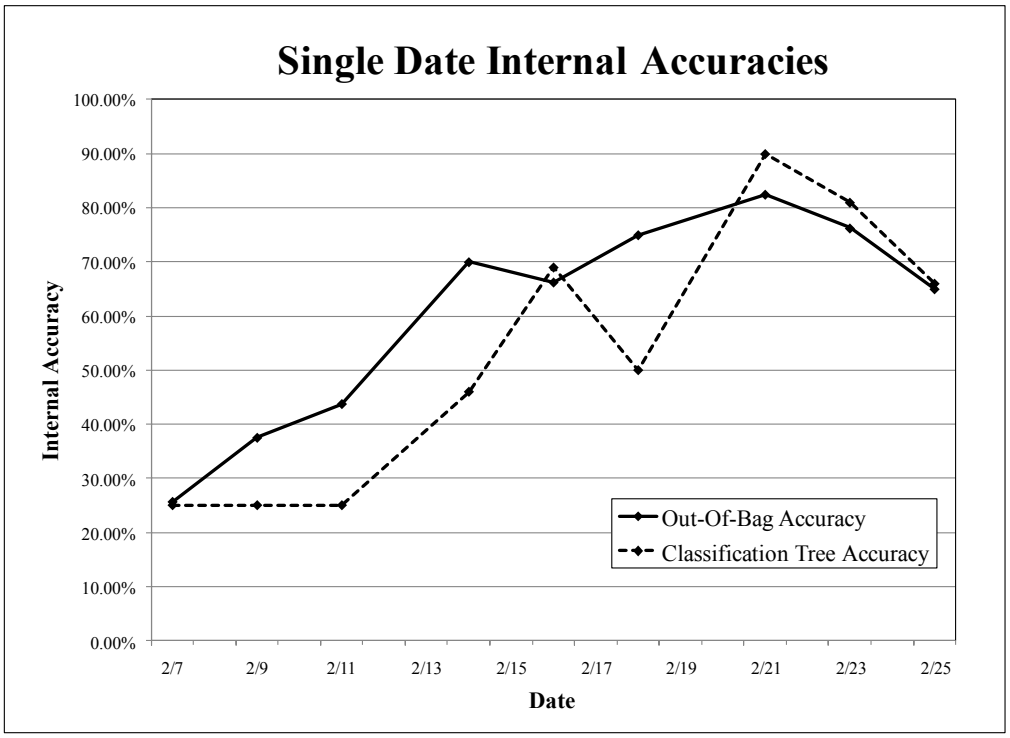

Figure 4.6: Overall internal accuracies for each random forest and classification tree model over the course of the experiment. (Note that the February 7-11 classification trees did not contain ≥ two terminal nodes)

Table 4.3: Out-of-bag accuracies and Kappa statistics for each single date random forest model. Treatment group columns represent the reference data while the rows represent the classified data.

February 7, 2011	C	I	WS	WSI	User's Accuracy
C	5	2	3	5	33%
I	3	4	6	2	27%
WS	4	6	5	7	23%
WSI	8	6	6	6	23%
Producer's Accuracy	25%	22%	25%	30%	Overall Accuracy 26%
Kappa Statistic	0				

February 9, 2011	C	I	WS	WSI	User's Accuracy
C	9	2	4	2	53%
I	4	9	6	8	33%
WS	3	4	7	5	37%
WSI	4	5	3	5	29%
Producer's Accuracy	45%	45%	35%	25%	Overall Accuracy 38%
Kappa Statistic	0.17				

February 11, 2011	C	I	WS	WSI	User's Accuracy
C	9	10	2	3	38%
I	10	7	3	3	30%
WS	0	2	10	5	59%
WSI	1	1	5	9	56%
Producer's Accuracy	45%	35%	50%	45%	Overall Accuracy 44%
Kappa Statistic	0.25				

February 14, 2011	C	I	WS	WSI	User's Accuracy
C	17	2	2	0	81%
I	2	13	1	2	72%
WS	1	2	12	4	63%
WSI	0	3	5	14	64%
Producer's Accuracy	85%	65%	60%	70%	Overall Accuracy 70%
Kappa Statistic	0.6				

February 16, 2011	C	I	WS	WSI	User's Accuracy
C	16	4	0	0	80%
I	4	15	1	1	71%
WS	0	1	13	10	54%
WSI	0	0	6	9	60%
Producer's Accuracy	80%	75%	65%	45%	Overall Accuracy 66%
Kappa Statistic	0.55				

February 18, 2011	C	I	WS	WSI	User's Accuracy
C	17	4	0	0	81%
I	3	14	1	0	78%
WS	0	2	14	5	67%
WSI	0	0	5	15	75%
Producer's Accuracy	85%	70%	70%	75%	Overall Accuracy 75%
Kappa Statistic	0.67				

February 21, 2011	C	I	WS	WSI	User's Accuracy
C	19	1	0	0	95%
I	1	16	2	0	84%
WS	0	3	13	2	72%
WSI	0	0	5	18	78%
Producer's Accuracy	95%	80%	65%	90%	Overall Accuracy 83%
Kappa Statistic	0.77				

February 23, 2011	C	I	WS	WSI	User's Accuracy
C	19	2	0	0	90%
I	1	14	3	0	78%
WS	0	4	10	2	63%
WSI	0	0	7	18	72%
Producer's Accuracy	95%	70%	50%	90%	Overall Accuracy 76%
Kappa Statistic	0.68				

February 25, 2011	C	I	WS	WSI	User's Accuracy
C	19	2	1	0	86%
I	1	15	2	0	83%
WS	0	1	8	10	42%
WSI	0	2	9	10	48%
Producer's Accuracy	95%	75%	40%	50%	Overall Accuracy 65%
Kappa Statistic	0.53				

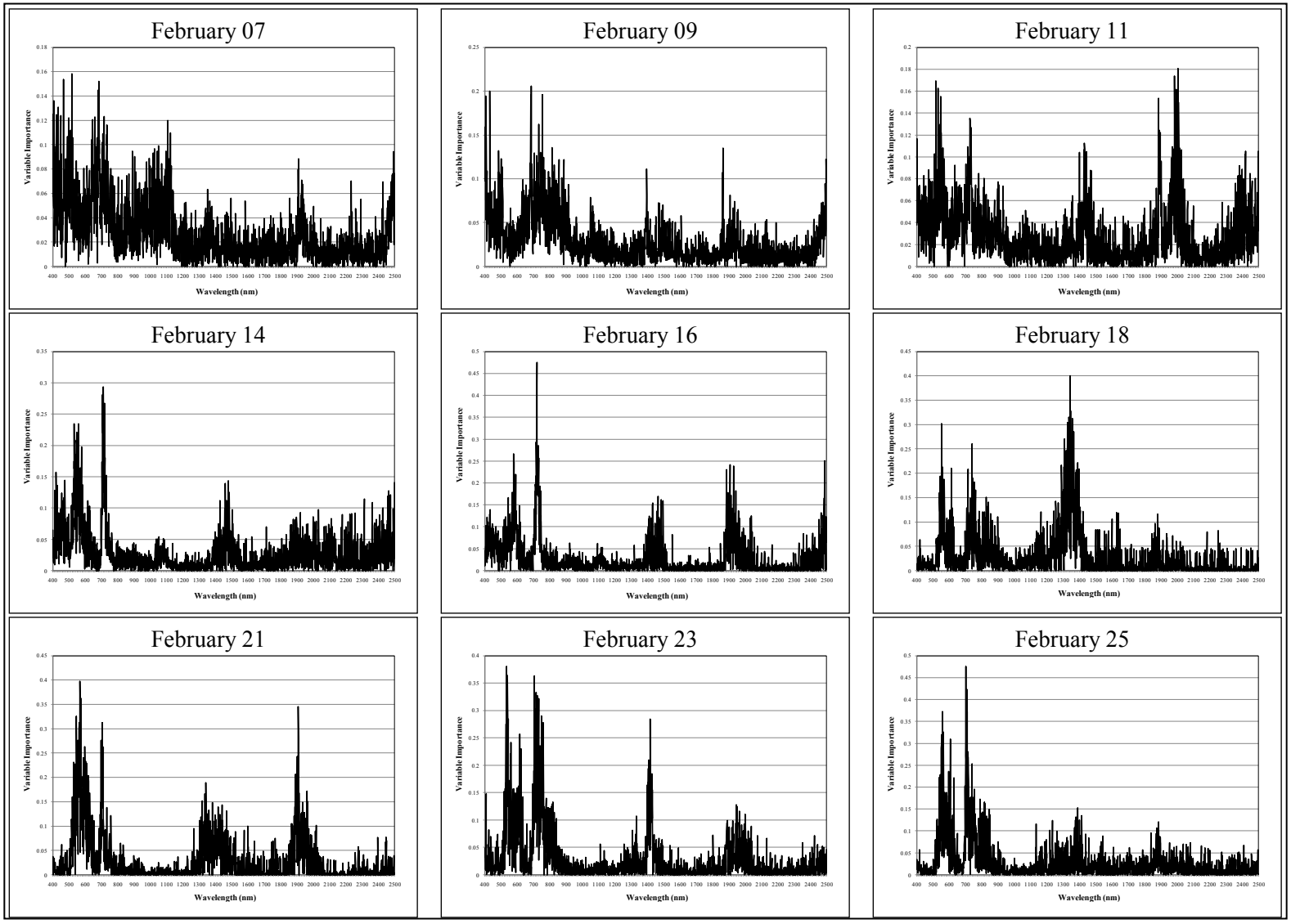

Figure 4.7: Variable importance plots for the single date random forest models, excluding the leaf position categorical variable.

Discussion

Our analyses demonstrated that hyperspectral spectrometry could distinguish between CO_2 stressed and healthy alfalfa leaves (I v. C). Furthermore, the spectral distinction of plant stress caused by elevated soil CO_2, water stress conditions, and their interaction was possible at certain times during the greenhouse experiment. Those findings have significant implications for the use of hyperspectral imaging to monitor GCS sites for CO_2 leaks given that water stress is a prevalent environmental condition and could be a confounding factor. Remote sensing monitoring of CO_2 leaks amid a landscape of patchy, water stressed vegetation would most likely require differentiation of CO_2 and water stress (I v. WS), whereas during widespread drought, vegetation stressed by both CO_2 and water stress would need to be spectrally distinct from surrounding vegetation (WSI v. WS).

Confusion predominantly occurred between (1) I and C classes, (2) I and WS classes, and (3) WSI and WS classes, which could be problematic for CO_2 leak detection in a GCS monitoring context. Mapping errors of omission (low producer's accuracy) for CO_2 stressed vegetation (I and WSI) would be less acceptable from a hyperspectral monitoring standpoint, while mapping errors of commission (low user's accuracy) would be more tolerable, since a CO_2 leak would be less likely to go unidentified. High commission error and low omission error would result in the overestimation of CO_2 leaks, perhaps wasting labor resources for ground verification, however, CO_2 leaks would less likely be missed.

CO_2 Leak Detection When Water Is Not Limiting

Hyperspectral monitoring of GCS sites when water stressed vegetation is not present would consider the spectral discrimination between I and C classes. Spectral distinctions in the red edge, visible green, and visible orange regions were used to distinguish I from C classes. Decision rules within the individual classification trees discerned increased green reflectance within the I class multiple times near 550 nm, a spectral region sensitive to xanthophyll pigment activities associated with photosynthetic efficiency (Gamon et al. 1997; Gamon and Surfus 1999) and changes to chlorophyll content (Carter and Knapp 2001). Additionally, increased reflectance at the 620 nm and 717nm wavelengths distinguished I from C classes. These are also spectral regions that are known to be highly sensitive to chlorophyll *a* content and absorption (Carter 1993). The primary spectral response of the I class to elevated soil CO_2 was increased reflectance within the visible green–orange spectrum.

The I class was distinguished from all treatment groups with user's and producer's accuracies $\geq$ 70% beginning February 16, after ten days of CO_2 injection. Classification accuracies of the I class remained high until the end of the experiment, suggesting that a detectable stress signal caused by a CO_2 leak could persist for a substantial period of time. Some of the I class confusion likely occurred because CO_2 injected alfalfa plants received comparatively higher injection flux rates, therefore higher soil CO_2 concentrations, due to minor differences in gas flow dynamics influenced by plant pot plumbing geometry and soil compaction. Severity and timing of stress caused by CO_2 injection therefore, varied. Healthy C class plants also appeared to be

disproportionately targeted by a two-spotted spider mite infestation, which possibly caused a stress response that was most spectrally similar to stress caused by elevated soil CO_2 given that the insects (thrips and two-spotted spider mites) caused a discoloration in the leaves most similar to the chlorosis observed in the alfalfa plants receiving CO_2 injection. The two-spotted spider mites were treated with numerous pesticides and biological controls, however, they probably remained an influential stress factor for healthier alfalfa plants. The results of the random forest classification demonstrated that stressed and non-stressed vegetation were accurately distinguished after one week of treatment application (C class accuracies $\geq$ 80%). Spectral differentiation among the stress classes was more difficult and time dependent, however.

It was noteworthy that the I treatment group sample spectra exhibited comparatively higher reflectance in the NIR as compared to the other treatment groups, including the control. Higher NIR reflectance could indicate a proportionately higher density of spongy mesophyll or a lower density of palisade cells that contain chloroplasts within CO_2 stressed leaves. Leaflets of the CO_2 injected alfalfa plants were visually observed to stand comparatively more erect. This might have been evidence of a localized ambient CO_2 fertilization effect that resulted in structural tissue growth within the injected alfalfa plants' leaves. The NIR spectral region was not discretely used in any of the individual classification trees to discern CO_2 stress, nor was it among the more important spectral regions in the development of the single date random forest models.

CO_2 Leak Detection When Soil Moisture Is Spatially Variable

Identification of a CO_2 leak would likely require water stress to be spectrally distinguished from stress caused by elevated soil CO_2 because soil moisture availability is highly variable across most landscapes (Baier 1969; Denmead and Shaw 1962). Increased reflectance within the water absorption regions near 1400 and 2500 nm was the most important characteristic that distinguished water stressed classes (WSI and WS) from C and I classes. The primary spectral response of leaf dehydration occurs within the water absorption regions (near 1400, 1900, and 2500 nm) that are sensitive to leaf water content (Carter 1991).

Patterns of variable importance for each of the random forest models identified discrete spectral regions that were particularly useful in discriminating among treatment groups. The red edge and the visible green-visible orange spectral regions were at least as important as the water absorption bands for distinguishing among the different classes. However, the "black box" nature of the random forest classifier did not allow for specific interpretation of the spectral distinctions made by the model (Prasad et al. 2006). It is possible that the variable importance within the visible and NIR wavelengths was related to distinguishing between the I and C classes given that these two treatment groups appeared to be spectrally similar in the SWIR region, while the water stress classes were likely separated by distinctions in the water absorption regions. Eventually increased reflectance in the visible, NIR, and SWIR regions can be exhibited by all stressed plants regardless of the cause, however (Carter 1991).

Alfalfa plants of the I treatment group exhibited visual stress predominantly as chlorosis (yellowing of plant leaves due to lack of chlorophyll production), although some CO_2 injected plants' leaves did become desiccated by the end of the experiment, suggesting leaf water loss. Leaves of the WS treatment group generally exhibited a lack of vigor (leaves were droopy) early in the experiment, and eventually, they became desiccated and brittle as the water stress severity increased. Overall these classes were distinguished reasonably well. Only minor confusion occurred probably because of similar reflectance properties in the visible wavelengths due to eventual chlorophyll loss to water stressed samples and due to eventual leaf moisture loss, expressed as increased reflectance in the water absorption bands of I class samples (Carter 1991; Carter et al. 1992).

CO_2 Leak Detection During Drought Conditions

Remote monitoring of GCS sites could require CO_2 leaks to be spectrally distinguished during drought conditions when all vegetation is subjected to water stress. Elevated soil CO_2 would thereby have to interact with water stress to cause a compound stress response in vegetation that was spectrally discernable. Greater reflectance in the water absorption bands near 1400 nm was used to distinguish WSI from WS classes, perhaps in response to diminished water-use-efficiency caused by comparatively faster leaf moisture loss or reduced water uptake at the root level. This was consistent with a compound stress interaction being exhibited by the WSI class. Treatment class accuracies indicated that alfalfa plants that went without water for one week exhibited water stress that became spectrally discernable on February 14. The confusion existed

primarily *between* them and not with the other classes. Individual WS and WSI class accuracies, therefore, were low. This was consistent with a water stress signal that was more easily discerned because of the discrete water absorption features where leaf reflectance is directly related to leaf moisture content. Spectral distinction of the WSI class remained relatively convoluted with the WS class throughout the experiment. The WSI class was distinguished with high producer's accuracies (low omission error) on February 21 and 23, perhaps suggesting that vegetation could exhibit stress in response to a CO_2 leak that could be distinguished during drought conditions, albeit a narrow time window.

The plant leaves of the water stressed treatment groups became desiccated and brittle as the experiment progressed. These plants eventually began to die. Spectral distinction within the water absorption bands was probably difficult due to the extreme leaf moisture loss caused by severe drought by the end of the experiment. Little variable importance was placed on the water absorption features in the last classification date (February 25), where the water stressed treatment groups were poorly distinguished (accuracies $\leq 50\%$), while the I and C treatment groups were classified with reasonable accuracy (accuracies $\geq 75\%$). This was evidence that the alfalfa plants' response to severe drought surpassed a stress threshold that rendered the CO_2 stress signal spectrally indistinguishable.

Pre-visual Plant Stress Detection

Pre-visual stress detection would be a critical attribute and an advantage to using hyperspectral remote sensing for early CO_2 leak detection at a GCS site. February 11

was the first day that subtle visual evidence of stress to some of the WSI and I treatment group plants was evident. Early visual symptoms of stress (i.e., chlorosis and languid leaves) were confined to older leaves located lower on the stems within the alfalfa plant canopies. Visible stress was most prominent within the WSI treatment group, which exhibited the compound effects of both CO_2 injection and lack of water. The accurate classification of the WSI samples did not occur until February 14, one week into the experiment, even though visual stress was noted for some of the WSI plants three days before that time. Differences in CO_2 injection flux rates prevented simultaneous stress responses for injected plants, resulting in visible or spectral stress responses in only some of the plants. This would have precluded an accurate WSI classification on February 11. The blue shift of the red edge towards shorter wavelengths has been associated with the pre-visual detection of plant stress (Carter 1993; Carter and Miller 1994; Rock et al. 1988), and was observed for some sample spectra by February 11. Blue shift spectral characteristics were similar in depth and slope for all of the stressed classes and, therefore, could not be used to distinguish among stress agents. This experiment provided no evidence that the pre-visual detection of plant stress was possible with hyperspectral data.

Summary

The primary conclusions that can be drawn from this greenhouse experiment are (1) that plant stress caused by elevated soil CO_2 was spectrally detected, probably in the visible spectrum, after approximately one week of CO_2 injection through the end of the experiment (random forest I class accuracies $\geq$ 65%). Potentially, this is evidence that a

spectral stress signal caused by elevated soil CO_2 could persist for a substantial period of time; (2) CO_2 and water stress were spectrally distinguishable; and (3) Elevated soil CO_2 appeared to cause a compound stress response detected in plants that were already water stressed, however, there was a relatively narrow time window when the WSI class was spectrally distinguished from the WS class. This was indicative of a time-dependent compound stress response caused by the interaction of elevated soil CO_2 and drought.

These results suggest that remote sensing may be used to monitor GCS sites for CO_2 leaks. Detection of a CO_2 leak when the availability of soil water is highly variable across space might be possible even if there are co-occurring patches of water stressed vegetation. Plants appear to hit a stress threshold, however, that renders spectral detection of a CO_2 leak unlikely during severe drought conditions. Regardless, this research demonstrated the necessity for remote sensing instruments to be spectrally sensitive to SWIR reflectance in order to accurately distinguish CO_2 and water stress.

Even though pre-visual stress detection was not possible at the leaf-scale, the early detection of stress caused by elevated soil CO_2 was achieved. Hyperspectral imaging has been demonstrated to be effective for early stress detection at broader spatial scales (Lawrence and Labus 2003). Monitoring for CO_2 leaks at GCS sites will possibly require large area coverage, which will only be possible from an airborne platform. Hyperspectral instruments with high spatial resolution optics for canopy-level monitoring at altitude, therefore, might be important for the early detection of CO_2 leaks. Additional research is warranted to understand the extent to which elevated soil CO_2 stress could be detected at the canopy-level using airborne remote sensing, especially when water stress

conditions exist. Spectral differentiation between CO_2 and water stressed vegetation would likely include spectral distinctions within the water absorption features. Spectral data acquired within the water absorption regions from an airborne remote sensing platform would likely be attenuated by atmospheric water vapor, perhaps further confounding CO_2 leak detection (Knipling 1970; Tucker 1980b). Snow cover and drought are going to limit the applicability of remote sensing data in temperate climates, therefore hyperspectral monitoring will need to be used in conjunction with other monitoring methods to obtain adequate temporal coverage of GCS sites. Improved understanding of vegetation spectral responses to stress caused by plant senescence will also be critical in determining the seasonal timing in which remote sensing data are appropriate for the detection of plant stress caused by an underground CO_2 leak.

References

Baier, W. 1969. Concepts of soil moisture availability and their effect on soil moisture estimates from a meteorological budget. *Agricultural Meteorology*. 6: 165-178.

Bergfeld, D., Evans, W.C., Howle, J.F., Farrar, C.D. 2006. Carbon dioxide emissions from vegetation-kill zones around the resurgent dome of Long Valley caldera, eastern California, USA. *Journal of Volcanology and Geothermal Research*. 152: 140-156.

Breiman, L., 2001. Random Forests. *Machine Learning*. 45:5-32.

Buschmann, C., Nagel, E. 1993. In vivo spectroscopy and internal optics of leaves as basis for remotes sensing of vegetation. *International Journal of Remote Sensing*. 14 (4): 711-722.

Carter, G.A. 1993. Responses of leaf reflectance to plant stress. *American Journal of Botany*. 80: 239-243.

Carter, G. A., Knapp, A.K. 2001. Leaf optical properties in higher plants: linking spectral characteristics to stress and chlorophyll concentration. *American Journal of Botany*. 88: 677-684.

Carter, G.A., Miller, R.L. 1994. Early detection of plant stress by digital imaging within narrow stress-sensitive wavebands. *Remote Sensing of Environment*. 50: 295-302.

Congalton, R. G., Green, K. 2009. *Assessing the accuracy of remotely sensed data: principles and practices Second edition*. Taylor and Francis Group.

Cortis, A., Oldenburg, C.M., Benson, S.M. 2008. The role of optimality in characterizing CO_2 seepage from geologic carbon sequestration sites. *International Journal of Greenhouse Gas Control*. 2: 640-652.

Cuffey, K.M., Vimeux, F. 2001. Covariation of carbon dioxide and temperature from the Vostok ice core after deuterium-excess correction. *Nature*. 412: 523-527.

Denmead, O, T, Shaw, R.H. 1962. Availability of soil water to plants as affected by soil moisture content and meteorological conditions. *Agronomy Journal*. 54: 385-390.

Fitzgerald, G.J., Maas, S.J., Detar, W.R. 2004. Spider mite detection and canopy component mapping in cotton using hyperspectral imagery and spectral mixture analysis. *Precision Agriculture*. 5: 275-289.

Gamon, J.A., Serrano, L., Surfus, J.S. 1997. The photochemical reflectance index: an optical indicator of photosynthetic radiation use efficiency across species, functional types, and nutrient levels. *Oecologia*. 112: 492-501

Gamon, J.A., Surfus, J.S. 1999. Assessing leaf pigment content and activity with a reflectometer. *New Phytologist*. 143: 105-117.

Gislason, P.O., Benediktsson, J.A., Sveinsson, J.R. 2006. Random Forest for land cover classification. *Pattern Recognition Letters*. 27: 294-300.

Goetz, A.F.H., Vane, G., Solomon, J.E., Rock, B.N. 1985. Imaging spectrometry for Earth Remote Sensing. *Science*. 228 (4704): 1147-1153.

Hansen, J., Sato, M., Kharecha, P., Beerling, D., Masson-Delmotte, V., Pagani, M., Raymo, M., Royer, D.L., Zachos, J.C. 2008. Target atmospheric CO_2: where should humanity aim? *Open Atmospheric Science Journal*. 2: 217-231.

Hepple, R.P. 2002. Implications of surface seepage on the effectiveness of geologic storage of carbon dioxide as a climate change mitigation strategy. *Lawrence Berkeley National Laboratory (LBNL)*, Paper LBNL-51267.

Hepple, R.P., Benson, S.M. 2005. Geologic storage of carbon dioxide as a climate change mitigation strategy: performance requirements and the implications of surface seepage. *Environmental Geology*. 47: 576-585.

Herzog, H.J. 2001. What future for carbon capture and sequestration? *American Chemical Society.* 35 (7): 148A–153A.

Intergovernmental Panel on Climate Change (IPCC), 2005. *IPCC Special Report on Carbon Dioxide Capture and Storage*. Cambridge University Press, Cambridge, UK.

IPCC Fourth Assessment Report (AR4), 2007. *IPCC Fourth Assessment Report on Climate Change*. Cambridge University Press, Cambridge, UK.

Jong, S.M. 1998. Imaging spectrometry for monitoring tree damage caused by volcanic activity in the Long Valley caldera, California. *ITC Journal.* 1-10.

Keith, C.J., Repasky, K.S., Lawrence, R.L., Jay, S.C., Carlsten, J.L. 2009. Monitoring effects of a controlled subsurface carbon dioxide release on vegetation using a hyperspectral imager. *International Journal of Greenhouse Gas Control*. 3: 626-632.

Kling, G.W., Evans, W.C., Tanyileke, G., Kusakabe, M., Ohba, T., Yoshida, Y., Hell, J.V. 2005. Degassing Lakes Nyos and Monoun: Defusing certain disaster. *Proceedings of the National Academy of Sciences*. 102: 14185-14190.

Knipling, E.B. 1970. Physical and physiological basis for the reflectance of visible and near-infrared radiation from vegetation. *Remote Sens. Environ*. 1: 155-159.

Lawrence Berkeley National Laboratory (LBNL), 2000. An overview of geologic sequestration of CO_2. In: *ENERGEX'2000: Proceedings of the 8th International Energy Forum*, Las Vegas, NV.

Lawrence, R.L., Labus, M. 2003. Early detection of Douglas-fir beetle infestation with subcanopy resolution hyperspectral imagery. *Westeren Journal of Applied Forestry*. 18: 202-206.

Lawrence, R.L., Wood, S.D., Sheley, R.L. 2006. Mapping invasive plants using hyperspectral imagery and Breiman Cutler classifications (RandomForest). *Remote Sensing of Environment*. 100: 356-362.

Lawrence, R.L., Wright, A. 2001. Rule-based classification systems using classification and regression tree (CART) analysis. *Photogrammetric Engineering & Remote Sensing*. 67: 1137-1142.

Lewicki, J.L., Hilley, G.E., Dobeck, L., Spangler, L. 2010. Dynamics of CO_2 fluxes and concentrations during a shallow subsurface CO_2 release. *Environmental Earth Sciences*. 60: 285-297.

Lewicki, J.L., Oldenburg, C.M., Dobeck, L., Spangler, L. 2007. Surface CO_2 leakage during two shallow subsurface CO_2 releases. *Geophysical Research Letters*. Vol. 34, L24402, doi:10.1029/2007GL032047.

Lichtenthaler, H.K. 1987. Chlorophylls and carotenoids: pigments of photosynthetic biomembranes. *Methods in Enzymology*. 148: 350-382.

Maček, I., Pfanz, H., Francetič, V., Batič, F., Vodnik, D. 2005. Root respiration response to high CO2 concentrations in plants from natural CO2 springs. *Environmental and Experimental Botany*. 54: 90-99.

Male, E.J., Pickles, W.L., Silver, E.A., Hoffmann, G.D., Lewicki, J.L., Apple, M., Repasky, K., Burton, E.A. 2010. Using hyperspectral plant signatures for CO_2 leak detection during the 2008 ZERT CO_2 sequestration field experiment in Bozeman, Montana. *Environmental Earth Sciences*. 60: 251-261.

Masarie, K., Tans, P.T. 1995. Extension and integration of atmosphere carbon dioxide data into a globally consistent measurement record. *Journal of Geophysical Research*. 100: 11593-11610.

Meroni, M., Rossini, M., Picchi, V., Panigada, C., Cogliati, S., Nali, C., Colombo, R. 2008. Assessing steady-state fluorescence and PRI from hyperspectral proximal sensing as early indicators of plant stress: The case of ozone exposure. *Sensors*. 8: 1740-1754.

Merzlyak, M.N., Gitelson, A.A., Chivkunova, O.B., Rakitin, V.Y. 1999. Non-destructive optical changes during leaf senescence and fruit ripening. *Physiologia Plantarum*. 106: 135-141.

Monnin, E., Indermühle, A., Dällenbach, A., Flückiger, J., Stauffer, B., Stocker, T.F.,Raynaud, D., Barnola, J.-M. 2001. Atmospheric CO_2 concentrations over the last glacial termination. *Science.* 291 (5501): 112–114.

Muhammed, H.H. 2005. Hyperspectral crop reflectance data for characterizing and estimating fungal disease severity in wheat. *Biosystems Engineering*. 91: 9-20.

Naumann, J.C., Young, D.R., Anderson, J.E. 2009. Spatial variations in salinity stress across a coastal landscape using vegetation indices derived from hyperspectral imagery. *Plant Ecology*. 202: 285-297.

Noomen, M.F., Skidmore, A.K. 2009. The effects of high soil CO_2 concentrations on leaf reflectance of maize plants. *International Journal of Remote Sensing*. 30: 481-497.

Noomen, M.F., Smith, K.L., Colls, J.J., Steven, M.D., Skidmore, A.K., Van der Meer, F.D. 2008. Hyperspectral indices for detecting changes in canopy reflectance as a result of underground natural gas leakage. *International Journal of Remote Sensing*. 29: 5987-6008.

Norby, R.J., Luo, Y. 2006. Evaluating ecosystem responses to rising atmospheric CO_2 and global warming in a multi-factor world. *New Phytologist*. 162 (2): 281–293.

Oldenburg, C.M., Bryant, S.L., Nicot, J.P. 2009. Certification framework based on effective trapping for geologic carbon sequestration. *International Journal of Greenhouse Gas Control*. 3: 444-457.

Oldenburg, C.M., Lewicki, J.L., Pan, L., Dobeck, L., Spangler, L. 2010. Origin of the patchy emission pattern at ZERT CO_2 release test. *Environmental Earth Sciences*. 60: 241-250.

Pacala, S., Socolow, R. 2004. Stabilization wedges: solving the climate problem for the next 50 years with current technologies. *Science*. 305: 968-972.

Parmeson, C., 2006. Ecological and evolutionary responses to recent climate change. *Annual Review of Ecology, Evolution , and Systematics*. 37: 637-669.

Peguero-Pina, J.J., Morales, F., Flexas, J., Gil-Pelegrin, E., Moya, I. 2008. Photochemistry, remotely sensed physiological reflectance index and de-epoxidation state of the xanthophyll cycle in Quercus coccifera under intense drought. *Oecologia.* 156: 1-11.

Penuelas, J., Llusia, J., Pinol, J., Filella, I. 1997. Photochemical reflectance index and leaf photosynthetic radiation-use-efficiency assessment in Mediterranean trees. *International Journal of Remote Sensing*. 18: 2863-2868.

Petit, J.R., Jouzel, J., Raynaud, D., Barkov, N.I., Barnola, J.-M., Basile, I., Bender, M., Chappellaz, J., Davis, M., Delaygue, G., Delmotte, M., Kotlyakov, V.M., Legrand, M., Lipenkov, V.Y., Lorius, C., Pepin, L., Ritz, C., Saltzman, E., Stievenard, M. 1999. Climate and atmospheric history of the past 420,000 years from the Vostok ice core, Antarctica. *Nature*. 399: 429-436.

Pickles, W.L., P.W. Kasameyer, B.A. Martini, D.C., Potts, E.A. Silver. 2001. Geobotanical remote sensing for geothermal exploration. *Geothermal Resources Council Transactions*. 25: 307-312.

Prasad, A.M., Iverson, L.R., Liaw, A. 2006. Newer classification and regression tree techniques: Bagging and random forests for ecological prediction. *Ecosystems*. 9: 181-199.

Pruess, K. 2008. On CO_2 fluid flow and heat transfer behavior in the subsurface, following leakage from a geologic storage reservoir. *Environmental Geology*. 54: 1677-1686.

Pu, R., Kelly, M., Anderson, G.L., Gong, P. 2008. Using CASI hyperspectral imagery to detect mortality and vegetation stress associated with a new hardwood forest disease. *Photogrammetric Engineering & Remote Sensing*. 74: 65-75.

Rock, B.N., Hoshizaki, T., Miller, J.R. 1988. Comparison of *in situ* and airborne spectral measurements of the blue shift associated with forest decline. *Remote Sensing of Environment*. 24 (1): 109-127.

Rouse, J.H., Shaw, J.A., Lawrence, R.L., Lewicki, J.L., Dobeck, L.M., Repasky, K.S., Spangler, L.H. 2010. Multi-spectral imaging of vegetation for detecting CO_2 leaking from underground. *Environ Earth Sci*. 60: 313-323.

Schuerger, A.C., Capelle, G.A., Di Benedetto, J.A., Mao, C.Y., Thai, C.N., Evans, M.D., Richards, J.T., Blank, T.A., Stryjewski, E.C. 2003. Comparison of two hyperspectral imaging and two laser-induced fluorescence instruments for the detection of zinc stress and chlorophyll concentration in bahia grass (Paspalum notatum Flugge.). *Remote Sensing of Environment*. 84: 572-588.

Scripps CO_2 program (Scripps). 2007. Monthly average carbon dioxide concentration. http://scrippsco2.ucsd.edu/graphics_gallery/mauna_loa_record/mauna_loa_record.html, Scripps Institute of Oceanography.

Seigenthaler, U., Stocker, T.F., Monnin, E., Lüthi, D., Schwander, J., Stauffer, B., Raynaud, D., Barnola, J.-M., Fischer, H., Masson-Delmotte, V., Jouzel, J. 2005. Stable carbon cycle-climate relationship during the Late Pleistocene. *Science*. 310: 1313-1317.

Shackleton, N.J. 2000. The 100,000-year ice-age cycle identified and found to lag temperature, carbon dioxide, and orbital eccentricity. *Science.* 289: 1897–1902.

Smith, K.L., Steven, M.D., Colls, J.J. 2004a. Use of hyperspectral derivative ratios in the red-edge region to identify plant stress responses to gas leaks. *Remote Sensing of Environment*. 92: 207-217.

Smith, K.L., Steven, M.D., Colls, J.J. 2004b. Spectral responses of pot-grown plants to displacement of soil oxygen. *International Journal of Remote Sensing*. 25: 4395-4410.

Smith, K.W., Vogelmann, T.C., DeLucia, E.H., Bell, D.T., Shepherd, K.A. 1997. Leaf form and photosynthesis. *BioScience*. 47:785-793.

Strachan, I.B., Pattey, E., Boisvert, J.B. 2002. Impact of nitrogen and environmental conditions on corn as detected by hyperspectral reflectance. *Remote Sensing of Environment*. 80 (2): 213-224.

Suarez, L., Zarco-Tejada, P.J., Sepulcre-Canto, G., Perez-Priego, O., Miller, J.R., Jimenez-Munoz, J.C., Sobrino, J. 2008. Assessing canopy PRI for water stress detection with diurnal airborne imagery. *Remote Sensing of Environment*. 112: 560-575.

Thomas, J.R., Gausman, H.W. 1977. Leaf reflectance vs. leaf chlorophyll and carotenoid concentrations for eight crops. *Agronomy Journal*. 69: 799-802.

Tucker, C.J. 1980a. Remote sensing of leaf water content in the near infrared. *Remote Sens. Environ*. 10: 23-32.

Tucker, C.J., Elgin, J.H., McMurtrey, J.M. 1980b. Relationship of red and photographic infra-red spectral data to alfalfa agronomic values. *International J Remote Sens*.

Venables, W.N., and B.D. Ripley. 1997. Modern Applied Statistics with S-Plus, Second Edition. Springer-Verlag, New York, NY, 548 p.

Vinnikov, K.Y., Grody, N.C. 2003. Global warming trend of mean tropospheric temperature observed by satellites. *Science*. 302: 269–272.

Vogelmann, J.E., Rock, B.N., Moss, D.M. 1993. Red edge spectral measurements from sugar maple leaves. *International Journal of Remote Sensing*. 14: 1563-1575.

Wilson, E.J., Friedmann, S.J., Pollak, M.F. 2007. Research for deployment: Incorporating risk, regulation, and liability for carbon capture and sequestration. *Environmental Science & Technology*. 41: 5945-5952.

Zarco-Tejada, P.J., Miller, J.R., Mohammed, G.H.; Noland, T.L. 2000. Chlorophyll fluorescence effects on vegetation apparent reflectance: I. leaf-level measurements and model simulation. *Remote Sensing of Environment*. 74 (3): 582-595.

CHAPTER 5

CONCLUSION

Subsurface geologic formations that are capable of retaining megatons of condensed CO_2 are very large and can cover hundreds of square kilometers. Monitoring these sites will require techniques with broad area coverage that can discern a subtle CO_2 stress signal within natural background variability. Remote sensing could potentially be a monitoring method that could offer broad-scale, large area coverage from an airborne platform that would be much less expensive and resource intensive compared to other ground-based methods. Previously, only a single aerial image that contained severely stressed vegetation subjected to elevated soil CO_2 for nearly three weeks has been successfully classified to show vegetation stress caused by elevated soil CO_2 detected from the air (Male et al. 2010).

The development of low-cost, high spatial resolution, hyperspectral instruments and advances in computers are allowing for the diverse application of these technologies in a wide range of investigations. Former caveats in instruments and software are now being resolved, which grants the processing of very large data sets with complex data mining tools in a time efficient manner. The Pika II proved to be a compact, relatively low-cost hyperspectral imager that was capable of detecting plant stress caused by elevated soil CO_2. Time series image analysis from the 2010 aerial campaign demonstrated that the aerial detection of a CO_2 leak is possible before it was clearly visible to the human eye from an airplane. After approximately one week of CO_2

injection, CO_2 stress was detected in hyperspectral imagery acquired from an approximate altitude of 2000' above ground level. Single date identification of CO_2 stressed vegetation with the unsupervised classification ISODATA clustering algorithm was a valuable detection technique when ground reference data was not available and *a priori* knowledge of areas of elevated soil CO_2 are not known. The "hot spot" clusters of pixels identified in the unsupervised classification coincided with areas of high CO_2 flux during previous release experiments conducted at ZERT.

Derived from the spectral signatures of the CO_2 stressed pixel clusters identified in the unsupervised classification, the Red Edge Index (REI) was developed to analyze the spectral health trajectories of pixels near and far from the zones of CO_2 injection. The red edge is a spectral feature that occurs at the boundary of the near infrared, which is determined by physical plant structure, and the visible red, which is determined by chlorophyll content and absorption (Carter and Knapp 2001). The REI ratioed peak radiance (at 750 nm) and trough radiance (at 674 nm) of the red edge. The REI, therefore, amplified the stress signal by considering both the physical and chemical responses of vegetation to CO_2 stress. The CO_2 stress signal was detected throughout the experiment with maximum distinction in REI between healthy and stressed vegetation occurring at the height of the CO_2 release. Subsequently, the REI signal began to abate once CO_2 injection ceased, possibly suggesting vegetation recovery.

It is known that areas of CO_2 leakage from a GCS site are most likely going to be confined to improperly sealed well-bores, weaknesses in the GCS cap rock, or geologic fault zones (Cortis et al. 2008). The "proximity analysis", which calculated mean REI for

the image time series data obtained at ZERT, provided a method for detecting vegetation stress caused by a CO_2 leak around a buried linear source, similar to a geologic fault. Proximity buffers were used around the known CO_2 leak source in order to delineate pixel zones that were closer and further away. Mean REI trajectories were then compared as a function of distance from the buried release pipe. As expected, areas closer to the CO_2 leak source exhibited more stress than those further away and maximum distinction occurred during the height of the CO_2 release.

Water stress is frequently experienced by vegetation because soil moisture availability is highly variable across space and drought is a common environmental occurrence. The greenhouse experiment demonstrated that water and CO_2 stress agents are spectrally distinguished in alfalfa plants after approximately one week of treatment application. Classification tree and random forest models showed that after two weeks of water stress and CO_2 injection, the different treatment groups were most spectrally distinguishable with overall accuracies of 90% (Kappa statistic of 0.87) for the classification tree model and 83% (Kappa statistic of 0.77) for the random forest classifier. Subsequently, classification accuracies decreased as the water stressed plant's leaves became totally desiccated and the plants themselves began to die.

The short-wave infrared water absorption features near the 1400, 1900, and 2500 nm wavelengths were most important in distinguishing water stressed plants from each other and the other treatment groups. The visible green - visible orange spectral region (520 - 620 nm) appeared to most distinguish CO_2 stressed plants from healthy alfalfa plants. Variable importance from the single date random forest models indicated that the

visible green - visible orange wavelengths (520 - 620 nm), the red edge wavelengths (~700 - 750 nm), and the water absorption features near 1400 and 1900 nm were the most influential spectral regions in the construction of the ensemble of decision based trees.

Early in the experiment, on treatment day four, the red edge was also observed to shift towards shorter wavelengths (the "blue shift") in some stressed samples, which has been associated with early stress detection (Carter and Miller 1994). Subtle visual symptoms of stress were observed within confined areas on individual alfalfa plants on this same day that 5-10 nm blue shifts were seen in some spectral scans. The early visual evidence of stress included chlorosis (yellowing of plant leaves) within CO_2 stressed plants and languid leaves within alfalfa canopies of water stressed plants. Reasonable classification of stressed samples in the greenhouse did not happen until alfalfa plants were subjected to one week of stress application. This evidence precludes the idea that pre-visual detection of stress at the leaf-level is possible with hyperspectral data. However, from the aerial perspective (the ZERT imagery), where remote sensing of CO_2 leaks would have the greatest advantage over other GCS monitoring methods because of the broad coverage capabilities of airborne remote sensing, early CO_2 stress detection appears possible with no visual evidence from the air.

These experimental results suggest that aerial detection and characterization of a CO_2 leak is feasible using hyperspectral imaging. High spatial resolution optics might be necessary for the early identification of stress from an airborne remote sensing platform. The spectral distinction between CO_2 and water stress agents is only possible with sensors that collect data in the shortwave infrared. The distinction between CO_2 and

water stress appears to be possible when soil water availability is highly variable and during periods of moderate drought. Severe drought, however, will likely cause all of the vegetation within a scene to become extremely desiccated, which will likely render the spectral discernment of stress caused by elevated soil CO_2 impossible. These results indicate that when using remote sensing to monitor GCS sites for CO_2 leaks, not only will snow cover in temperate climates limit temporal coverage, but drought events will also influence the time appropriateness of the remote detection of CO_2 stress in vegetation. Additional investigation of the spectral differentiation between CO_2 and water stress from airborne remote sensing platforms is required given that the difficulty of plant stress detection increases when scaling up data from the ground to the air, especially when using water absorption features that become attenuated due to atmospheric water vapor interference (Knipling 1970; Tucker 1980).

Further investigation is warranted to understand if other common occurring vegetation stress events confound stress signals caused by elevated soil CO_2, such as seasonal vegetation senescence and physical trampling of vegetation. Spectral distinction between stress agents has important implications for the temporal application, as well as for the limits of remote sensing to be used for GCS monitoring purposes. Further research is needed to investigate CO_2 leak migration from a deeper storage source to better understand the spatial extent of CO_2 stress expressed in vegetation at the surface. Although the ZERT site has provided many insights for GCS monitoring during preliminary experiments, a more realistic subsurface CO_2 storage facility is needed for deeper inquiry. Concerns remain that a vegetation legacy left behind as a result of

repeated CO_2 release experiments over the past few years has reshaped the vegetation community above and around the release pipe, thereby limiting the scope of any findings there.

References

Carter, G. A., Knapp, A.K. 2001. Leaf optical properties in higher plants: linking spectral characteristics to stress and chlorophyll concentration. *American Journal of Botany*. 88: 677-684.

Carter, G.A., Miller, R.L. 1994. Early detection of plant stress by digital imaging within narrow stress-sensitive wavebands. *Remote Sensing of Environment*. 50: 295-302.

Cortis, A., Oldenburg, C.M., Benson, S.M. 2008. The role of optimality in characterizing CO_2 seepage from GCS sites. *International Journal of Greenhouse Gas Control*. 2: 640-652.

Male, E.J., Pickles, W.L., Silver, E.A., Hoffmann, G.D., Lewicki, J.L., Apple, M., Repasky, K., Burton, E.A. 2010. Using hyperspectral plant signatures for CO_2 leak detection during the 2008 ZERT CO_2 sequestration field experiment in Bozeman, Montana. *Environmental Earth Sciences*. 60: 251-261.